JPL PUBLICATION 85-14

Water Vapor Radiometry Research and Development Phase Final Report

G.M. Resch
M.C. Chavez
N.I. Yamane
K.M. Barbier
R.C. Chandlee

April 1, 1985

National Aeronautics and
Space Administration

Jet Propulsion Laboratory
California Institute of Technology
Pasadena, California

JPL PUBLICATION 85-14

Water Vapor Radiometry Research and Development Phase Final Report

G.M. Resch
M.C. Chavez
N.I. Yamane
K.M. Barbier
R.C. Chandlee

April 1, 1985

National Aeronautics and
Space Administration

Jet Propulsion Laboratory
California Institute of Technology
Pasadena, California

The research described in this publication was carried out by the Jet Propulsion Laboratory, California Institute of Technology, under a contract with the National Aeronautics and Space Administration.

PREFACE

The work described in this report is the result of several years of research activity involving the use of microwave frequencies for measuring the delay caused by atmospheric water vapor in the RF path of a microwave system. The original motivation for this work was to support the application of radio interferometry for precision geodesy. A total of seven developmental microwave radiometers were constructed and deployed to very long baseline interferometer sites that are part of the NASA Crustal Dynamics Project. These instruments are now being retrofitted to improve operability and reliability in the field. This initial research has led to a second-generation development, which is in its testing and evaluation phase at JPL.

N. A. RENZETTI, MANAGER
JPL GEODYNAMICS PROGRAM

ACKNOWLEDGEMENT

The authors wish to acknowledge Mr. T. L. Fischetti of NASA Headquarters for his support and foresight in funding water vapor radiometry research and development activities at JPL. The calibration of path delay due to atmospheric water vapor is fundamental to the successful employment of microwave measurement systems in the field of precision geodesy.

It is a pleasure to acknowledge also the assistance of colleagues who, at various times, have contributed to this task. Pete MacDoran, Don Trask, and Jim Johnston provided support and encouragement at critical times. Bruce Gary and Joe Waters have generously shared their insight into the techniques of remote sensing. Bob Clauss has made valuable comments regarding both the real and the theoretical behavior of the instrumentation. Al Banisch handled the engineering on the first WVR (Unit R01). Dave Peterson has helped with everything from fabrication to calibration. Rick McKinney performed a valuable service with his part of the testing and the fix for some of the problems that were uncovered. Bill Sinclair wrote the first two versions of the controller software and helped with some of the system support software. Kwok Ong wrote the nucleus of the data acquisition software and helped with system support and data analysis. At different times, Scott Claflin, Robin Hastings, and Henry Fliegel provided much needed help with algorithm development. Bob Miller helped with software development and hardware testing and calibration.

ABSTRACT

This report describes the research and development phase for eight dual-channel water vapor radiometers constructed for the Crustal Dynamics Project at the Goddard Space Flight Center, Greenbelt, Maryland, and for the NASA Deep Space Network.

These instruments were developed to demonstrate that the variable path delay imposed on microwave radio transmissions by atmospheric water vapor can be calibrated, particularly as this phenomenon affects very long baseline interferometry measurement systems. Water vapor radiometry technology can also be used in systems that involve moist air meteorology and propagation studies.

CONTENTS

CONTENTS (Contd.)

Figures

Figures (Contd.)

Tables

SECTION I

INTRODUCTION

This document is a final report on the research and development of eight prototype dual-channel microwave radiometers that were constructed for the Crustal Dynamics Project and the NASA Deep Space Network. The Crustal Dynamics Project is managed by the NASA Goddard Space Flight Center, Greenbelt, Maryland, and the NASA Deep Space Network is managed and operated by the Jet Propulsion Laboratory of the California Institute of Technology.

These instruments, known as water vapor radiometers (WVR), are intended to demonstrate that the variable path delay imposed by atmospheric water vapor on microwave tracking and distance measuring systems can be calibrated. This technology can also be used in other systems that involve moist air meteorology and propagation studies. The eight instruments have been installed at various stations and observatories that participate in very long baseline interferometry (VLBI) experiments, including the Deep Space Network Complexes in California, Spain, and Australia.* Figure 1-1 is a photograph of a typical water vapor radiometer. This report reviews the overall design and development of these instruments and describes the major components, testing and calibration, and the algorithms used to estimate the variable path delay.

*The worldwide Deep Space Network provides the Earth-based communications systems for all of NASA's interplanetary spacecraft.

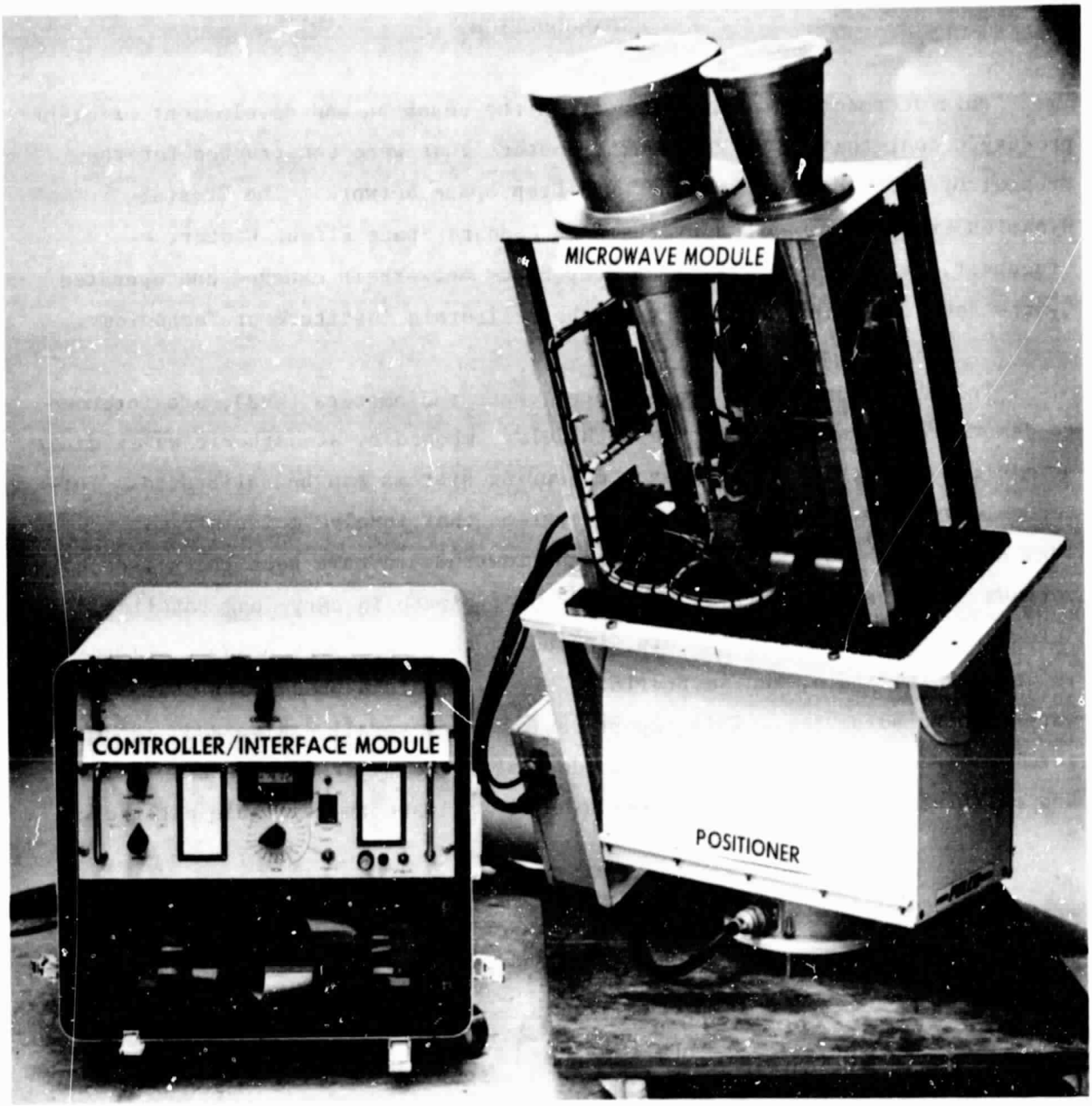

Figure 1-1. Photograph of a Water Vapor Radiometer With the Three Basic Modules Identified.

SECTION II

TASK BACKGROUND

A. INTRODUCTION

Microwave very long baseline interferometry (VLBI) was initially developed by radio astronomers for studying the fine structure of extra-galactic radio sources. With its introduction in the middle 1960s, members of the Earth sciences immediately recognized that the VLBI technique could also be used to investigate a wide variety of geodetic and geophysical phenomena (Ref.1). The basic instrumentation appeared capable of measuring vector baselines 1000 to 2000 km long with centimeter level precision. The strengths and limitations of the technique were thoroughly investigated by Shapiro and Knight (Ref.2). Their analysis pointed out that the overall accuracy of VLBI would be limited by system error sources. Of these, the variable path delay imposed by tropospheric water vapor would probably be the most intractable error source.

B. ARIES

In 1972, the Jet Propulsion Laboratory initiated a research task named ARIES (Astronomical Radio Interferometric Earth Surveying) under the leadership of P. F. MacDoran. The objective was to demonstrate that VLBI could be used to survey short to medium length baselines that might provide useful information about crustal deformation in active earthquake zones. The plan was to form an interferometer using a transportable 9-meter-diameter antenna in conjunction with the stationary Deep Space Stations at Goldstone and the radio telescope at the Caltech Owens Valley Radio Observatory (OVRO). If the transportable station were moved around a network of geophysically interesting sites in southern California, it would be possible to compile a time history of three-dimensional baseline vectors that would be useful in understanding the dynamics of crustal deformation in this tectonically complex region. The accuracy goal was to measure three-dimensional vector baselines up to 1000 km in length with 3- to 5-cm precision in each component and 1- to 2-cm precision in length. Starting in late 1973, Ong, et al. (Ref.3) demonstrated that the

ARIES instrumentation was capable of 3-cm precision by measuring an independently surveyed 300-m baseline between the ARIES antenna and the stationary 64-m antenna Deep Space Station at Goldstone. By the middle of 1974, work on the reduction of internal error sources gave promise that three-dimensional baseline accuracy of a few cm could be achieved in a few years, if a major external error source - variable path delay due to tropospheric water vapor - could be accurately measured and calibrated.

C. RADIO WAVE PATH DELAY

It takes longer for a radio wave to traverse an atmospheric path L relative to the time it would take to traverse the same path in a vacuum. The electrical path length L_e is just the integral of the refractive index of the atmosphere along the path. The difference ΔL between the electrical path length and the physical path length is simply,

$$\Delta L = 10^{-6} \int N \, ds \qquad (2\text{-}1)$$

where N is the refractivity at the point s along the path. The refractivity for the atmosphere as given by Smith and Weintraub (Ref.4) is composed of two terms. The first and largest term is called the dry term and is proportional to the integrated dry air density. For most purposes it is sufficient to "weigh" the atmosphere at the zenith with a barometer in order to estimate the "dry" delay ΔL_d and then scale this zenith quantity to the line-of-sight using a cosecant elevation law. The second term contributing to the refractivity is a function of the atmospheric water vapor. The excess path delay in centimeters for this term of the refractivity is of the form,

$$\Delta L_v = 0.1723 \int (\rho_v / T) \, ds \qquad (2\text{-}2)$$

where ρ_v is the vapor density in g/m^3, T is the temperature in kelvin, and s is in meters. Unfortunately (for our applications) atmospheric water vapor is a highly variable and not well-mixed atmospheric constituent. As a result it is impossible to estimate the path delay in Eq. (2-2) with any high degree of accuracy from surface measurements alone.

In interferometric systems, the primary observable is the differential time-of-arrival of a radio wave at the stations comprising the interferometer. The presence of atmospheric water vapor along the signal path will impose an additional delay between 3 to 60 cm, depending on how much vapor is in the atmosphere and the elevation angle of the observations. Typically, the baseline is derived from observations at several different elevation angles so that the mapping of a propagation effect error into the baseline is rather complex. The water vapor molecule emits spectral radiation at a frequency of 22.235 GHz; the intensity is approximately proportional to the number of molecules (or the delay) along the line of sight. The presence of liquid water complicates the measurement problem as it contributes significantly to the intensity of the atmospheric emission but contributes very little to the excess path delay.

In general, to achieve a system accuracy better than 10-12 cm, the vapor along the signal path must be measured. Of the several techniques that could be employed to measure line-of-sight vapor delay, a cost effective one is passive remote sensing using a dual-channel microwave radiometer. The second channel makes it possible to separate the vapor and liquid effects in all but the most severe weather conditions.

D. INITIAL DELAY EXPERIMENTS

During the summer of 1974, J. W. Waters and R. Longbothum of JPL compared a spacecraft prototype microwave radiometer with radiosondes launched at the El Monte, California, Airport in an experiment to determine atmospheric delay using the technique of passive remote sensing. Their regression analysis against radiosonde data indicated a level of agreement better than 2 cm (units of excess path delay). Later work by Winn et al. (Ref. 5) and Moran and Penfield (Ref. 6) extended this basic result. It was clear that this device, which became known as a water vapor radiometer (WVR), could be used to calibrate vapor-induced delay along the line of sight of a nearby antenna. If the water vapor delay along the line of sight at each station could be calibrated to 2 cm, then 3- to 5-cm VLBI system accuracy could very well be possible.

During this same period, a VLBI data acquisition system was under development at the Northeast Radio Observatory Corporation`s Haystack facility. The system was selected for ARIES and thereby established the requirements for an ARIES WVR. It would need to operate as an integral part of this fully automated VLBI data acquisition system. It would need to operate unattended with a minimum of operator attention. It must be well calibrated, stable, ruggedized, able to operate in all but the most severe weather conditions, and provide a vapor path correction accurate to better than 2 cm. There was also a need to understand the random and systematic error budget of the WVR and to develop an inversion algorithm to convert the WVR observable (brightness temperature) to path delay correction.

E. FUNDING, INITIAL DESIGN, AND DEVELOPMENT

The initial design and development began with an informal WVR working group of three people. The task of specifying the requirements for a small, portable, ruggedized WVR turned out to be relatively easy compared to the effort required to locate adequate funding. In late 1976, with the help of E. J. Johnson of JPL, the WVR working group was able to borrow an engineering model of a spacecraft radiometer from the JPL Nimbus E Microwave Scanner Project (NEMS). A low-key effort was begun to modify and repackage this instrument for VLBI applications. In 1977, a group at Goddard Space Flight Center (GSFC), which was also involved in the development of VLBI systems, purchased two commercially available microwave receivers with the intention of building a dual-channel WVR for their VLBI experiments. Both ARIES and the GSFC VLBI group had selected the Owens Valley Radio Observatory (OVRO) as a base station. Both groups recognized a rare opportunity to work together in mutual self-interest by cooperating in the development of a dual-channel WVR for installation at OVRO. ARIES funding to purchase one of the microwave receivers was obtained from the Caltech President`s Fund; GSFC was able to provide funding for the second channel and for two commercially available positioners for mounting and pointing the WVR. The ARIES WVR group agreed to use these various components to assemble three reasonably compatible WVRs, with the intention that they would be used for research and development. Based on this experience, subsequent units with an improved design would be

built for operational use. In early 1978, the ARIES WVR group, with support from the Goddard VLBI group, received partial funding to package three WVRs. A few months later, directions were received to construct two additional WVRs for the GSFC Crustal Dynamics Project, which was then coming into existence. The ARIES WVR group decided it would be less expensive and faster to construct the two added WVRs "in house" and immediately initiated procurement of long-lead-time parts. In the fall of 1978, the Deep Space Network requested the construction of two more radiometers. A year later ARIES requested a second WVR, making a grand total of eight. The units were given serial numbers R01 through R08, representing the order in which work was begun on a unit. The "R" designation was meant to emphasize the R & D nature of the work.

What had started out as a relatively small and informal R & D effort involving three WVRs had grown into a rather complex, time-sensitive, replication activity. There were some parts for building three WVRs, directions to construct an additional five WVRs, and only limited funding. JPL management also directed that the design and construction of these eight WVRs be consistent with the needs of both JPL and non-JPL users. This presented an additional challenge in that parts for assembling the first three radiometers were already on hand, and the funding limitations dictated the use of off-the-shelf components in the design and construction of the five additional units. The approach chosen was to maintain the original purpose and intention of the ARIES WVR group: to build research tools that were capable of demonstating that vapor delay in VLBI measurements could be satisfactorily calibrated. To keep within budget and time constraints, there would be no research into basic radiometer design and construction. The established "safe" design of a Dicke switched instrument taken largely from the existing spacecraft WVR design would be used. It was decided to standardize on two frequencies, 20.7 and 31.4 GHz, and use doubly stabilized Dicke radiometers. The cold load calibration system used with the two GSFC-supplied microwave receivers would be discarded because (1) the load was inaccurate, (2) keeping it filled with liquid nitrogen was operationally difficult, and (3) the packaging problem was extremely difficult.

It was decided that the WVR would be mounted off the antenna on a positioner that would point the instrument in azimuth and elevation. The choice was made on the assumption that if the WVR was used for some application other than VLBI, it would not tie up the VLBI antenna. Second, the procedure used to establish and check the temperature scale calibration (i.e., the tipping curve) becomes awkward and time-consuming when performed on a large antenna. Third, preliminary analysis suggested that the only difference between the broad-beam WVR and the narrower beam radio telescope would be in the short-period fluctuations caused by water vapor. Since most VLBI observations are the result of incoherently averaging up to 15 minutes of data, it effectively smoothes the rapid but small fluctuations caused by water vapor. To simplify the operational interface, a microcomputer controller was added to allow the user to remotely control WVR operations.

During construction of the first three instruments, several areas were located where minor improvements could be made in design, assembly, and/or construction. Changes that were finally incorporated in units R04 through R08 were essentially dictated by the requirement that all WVRs appear identical to the user at the controller interface. Unfortunately it proved to be impractical to remove all of the differences between the different units. The most obvious remaining difference is that the vapor frequency of WVR-R02 and R03 is centered at 21 GHz (compared to 20.7 GHz for all other units) and the slew rate is approximately a factor of 4 slower than the other radiometers. Thus the eight radiometers that have been deployed consist of three different microwave packages, two different positioners, and three slightly different microcomputer controllers. However, the software that resides in the microcomputer makes these differences largely transparent to the user. The current plan is to mount units R01 and R07 on the edge of the antenna they are intended to calibrate and to use the fast mounts from these units to retrofit units R02 and R03.

In July 1979, unit WVR-R03 was delivered to the Haystack facility in Massachusetts. According to the original agreement with GSFC (now manager of the Crustal Dynamics Project), the WVRs would only be benched-tested at JPL before shipment. Each user was responsible for functional testing and

calibration of the unit it received. The agreement, however, proved to be impractical. Consequently, in late 1979, at the request of the Crustal Dynamics Project, the ARIES WVR working group agreed to functionally test and calibrate each WVR prior to shipment. In addition, the group would assist with installation of the WVR when requested by the observatory, maintain a stock of spare parts, assist with maintenance, provide a minimum level of documentation consistent with R & D instruments, provide the algorithm necessary to convert WVR output into a delay correction, and provide a backup vapor calibration capability as well as a comparison check on WVR performance. For the backup capability, the group also agreed to construct, test, and calibrate a solar hygrometer to accompany each WVR. These increased responsibilities proved to be more time-consuming than originally anticipated. WVR-R02 was installed at OVRO in September 1980; unit R05 was installed at the Haystack facility in January 1981; unit R06 was installed on the ARIES electronics van (Mobile Van-2) also in January; unit R04 was installed at DSS 13 in February; unit R01 was delivered to ARIES (Mobile Van-1) in May; and unit R08 was installed at Ft. Davis, Texas, in June, 1981.

F. COST PERFORMANCE AND FUTURE DEVELOPMENT

Table 2-1 summarizes the hardware costs and time expended on the WVR research and development phase. Hardware costs are referred to epoch October 1981 and, for the most part, must be inflated to the current date. An exception to this is the microprocessor hardware where many components are being reduced in price. The hardware, assembly, testing, and calibration costs are listed on a per unit basis. The development of the algorithm, microprocessor control software, and the data acquisition software is summarized as a total effort. The final accounting of hardware cost and assembly time was very close to our original estimates for this task in spite of severe price inflation. This was due largely to the fact that we were more efficient in assembly than originally estimated. Having several WVRs under construction meant that some jobs could be done on a "production-line" basis and there were always lots of little jobs that kept everyone busy.

The software part of the WVR task cost a great deal more than originally estimated. There were essentially three reasons for this overrun. First,

Table 2-1. Cost Summary

A. Cost per radiometer (as of Oct. 1981)

COMPONENTS	K$
Ferrite switches	7.3
LO/mixer/I.F.	8.5
Horn antennas	3.1
Waveguide components	1.
Power supply	1.7
Detectors	0.1
Temp sensors & control	0.4
Enclosure (microwave)	0.6
Misc. comp.	1.2
Control panel	0.8
Microprocessor	4.5
Positioner	2.8
Cables & connectors	0.5
	$32,500

TASKS	WORKMONTH
Fabrication	3
Assembly & wiring	4
Bench testing	3
Engineering tests	0.8
Calibration	2
	12.8

B. Support Tasks

TASK	WORKYEARS
Controller software (3 versions)	0.2
System support	0.8
Data acquisition S/W	1.0
Environmental test	0.2
Algorithm development	2.0
	5.2

purchase and delivery of the JPL MK III Data Acquisition System were delayed, which forced the purchase of additional software for host computers other than the MK III computer. These additional microcomputers were intended to serve as "host" machines and were not in the original budget. The budget crimp forced the purchase of some less than optimum hardware, which resulted in equipment problems that required schedule slips and more money to be spent later on for maintenance. The second reason for the software overrun was simply due to underestimation of the amount of system level support needed to keep several development systems running. The third and major reason for the overrun was software development personnel turnover. Over the three years of the task, eight people worked on the software and algorithm development. All worked part time and five left after several months on the job.

Had it been realized at the start that the task would grow to involve constructing eight WVR instruments instead of three, the conventional Dicke design would not have been selected. One can imagine a spectrum of design possibilities that range from a fully compensated Dicke radiometer utilizing full digital control and data acquisition to a single horn total power instrument. The goal in any redesign effort should be to lower the parts count, thereby decreasing the hardware cost, reducing assembly time, reducing weight, size, and power requirements, and increasing instrument stability. At some point in the design spectrum one is inevitably faced with the possibility of cost/performance tradeoffs that can limit the applicability of the instrument. It is our educated guess that the cost of the WVR could be reduced 15-30% by simply re-engineering the current design, but keeping the same overall characteristics of the current instruments. Potential cost reductions by a factor of two are possible but entail some technical risk that would require a design study at the least and possibly the construction and testing of a prototype.

SECTION III
DESIGN CONSIDERATIONS AND REQUIREMENTS

A. INTRODUCTION

In response to a directive from the JPL Program Office for the Crustal Dynamics Project a design team was formed to review the design specifications for a water vapor radiometer. The conclusions and recommendations of this team were issued as a JPL internal report, which was written very early in the development stage and became the engineering specifications document. Table 3-1 summarizes these specifications.

As discussed in Ref. 7, the analysis of VLBI error sources suggests that baseline accuracies of 3 to 5 cm are possible if the line-of-sight water vapor effects can be calibrated to ± 2 cm. At the 2-cm level there are several comparable error sources so that it simply does not make sense to invest a large amount of resources in the reduction of any single error source. Keep in mind that the 2-cm vapor delay accuracy refers to a differential measurement so that the accuracy of an individual measurement should be $2/\sqrt{2}$ cm. We would like the precision of the vapor measurement to be a factor of 3 or 4 better in the hope that the increased precision can be used to spot systematic effects. Hence, the overall system requirement for the WVR is that it measures vapor delay with an accuracy of ± 1.5 cm and precision of ± 0.4 cm. The problem in 1978 was to convert this system performance requirement into a set of general design specifications.

B. PHYSICAL CHARACTERISTICS AND ENVIRONMENT

Since a stock of existing parts was to be used, the physical characteristics of the WVR were mostly predetermined. The characteristics of units R01 and R04 to R08 are listed in Table 3-1. Units R02 and R03 have slightly larger volume but are essentially the same physically. The environmental factors were specified by the meteorological conditions for both the mobile and fixed antenna sites that were under consideration by the Crustal Dynamics Project. At temperatures below -10°C it was felt that the atmospheric vapor content

Table 3-1. Water Vapor Radiometer Specifications

1) Physical Characterictics

	Weight (kg)	Volume (m^3)	Power (watt)
Microwave package	45	.12	300-600
Positioner	34	.074	0-450
Control module	26	.15	120

2) Environmental

Operating Range

Ambient Temperature:	-10^{o} to $+50^{o}$C
Wind Speed:	up to 65 km/h
Relative Humidity:	0 to 95% or until liquid water precipitates onto the horn cover

Survivability

Ambient Temperature:	-40^{o} to $+60^{o}$C
Wind Speed:	up to 160 km/h in stowed position
Relative Humidity:	100%, sealed from rain and dust

3) Microwave Module

Operating Frequencies:	20.7 & 31.4 Ghz
Frequency Stability:	$\pm$12 Mhz over operating range
RF Bandwidth:	200 Mhz
IF Bandwidth:	100 Mhz
Integration Time:	software selectable in steps of 0.1 s
Signal Range:	3 to 400 K
Antenna Beamwidth:	7^{o} (full width at half power)
Beam Efficiency:	>99.9% for $\pm 15^{o}$ around beam center
Calibration:	supplied by two waveguide terminations held at fixed temperatures and supplemented with tip curve obervations
Base Load:	315 K
Hot Load:	370 K
Temperature stability:	$\pm$0.1 K/minute

4) Positioner

Coordinates:	Azimuth & Elevation
Range:	0 to 355^{o} in Az, 5 to 175^{o} in El
Slew Rate:	>1.5 deg/s (both axis)
Position Accuracy:	1^{o} both axes
Readout Accuracy:	0.1^{o} both axes

Table 3-1. Water Vapor Radiometer Specifications (Contd.)

5) Control and Interface Module

Operating Modes	
(i) Local:	all data and control lines available for monitoring by built-in digital voltmeter
(ii) Remote	
Interface:	RS-232, twisted pair of cables
Baud Rate:	110 to 19200 baud, selectable by software and hardware jumpers
Protocol:	compatible with MAT* bus
Data Storage:	temporary storage only, mass storage is the responsibility of the host computer

* - MAT = Microprocessor ASCII Transceiver used as the control/communicator standard in the Haystack/GSFC Mark III data acquisition system.

would be very small and hence there would be little need for the vapor correction. The WVRs will survive temperatures as low as -40°C, but below -10°C it becomes increasingly difficult for the internal heaters to thermally stabilize the electronics. Similarly, at wind speeds above 65 km/h the VLBI antenna normally shuts down. At wind speeds higher than 95 km/h it is recommended that the WVR be stowed in the horizontal position to present the minimum surface to wind loading. An additional environmental problem that was not solved was dew accumulation on the cover of the horn antennas.

C. OPERATING FREQUENCIES

One of the most critical specifications in the WVR design is the choice of operating frequencies. This is because the water vapor line centered at 22.235 GHz is pressure broadened. Thus, the line profile will depend on the altitude distribution of the vapor. A given amount of vapor concentrated at low altitude will produce a wide, flat profile relative to the same amount of vapor concentrated at high altitude. Most of the vapor signal is produced at 22.235 GHz; this is also the frequency that is most sensitive to the shape of the line. However, if a frequency is chosen on the wing of the line, e.g., between 20 and 21 GHz, this sensitivity to vapor height (Ref. 8 and 9) can be minimized. The radiometer (unit RO1) obtained from the JPL Nimbus E Microwave Scanner Project (NEMS) operated at 22.2 and 31.4 GHz, while the two GSFC-supplied radiometers (units RO2 and RO3) were designed to operate at 21.0 and 31.4 GHz. Preliminary bench tests indicated that the NEMS components could possibly be used as low as 20.7 GHz. There is a decided advantage in having all WVRs operate at identical frequency pairs; consequently, the design team decided to standardize on 20.7 GHz as the vapor sensitive channel for all follow-on WVRs and attempt to modify and retune the existing components.

D. FREQUENCY STABILITY

The specification of frequency stability is important because the vapor channel operates on that part of the emission line where the rate of change of brightness temperature with respect to frequency is largest. The frequency will change because the Gunn diode local oscillator is temperature sensitive

and the WVR enclosure does not act as a perfect oven. The sensitivity is approximately 3 MHz/^{o}C and since temperature changes of $\pm 4^{o}$C inside the WVR are possible, this implies frequency shifts of ± 0.012 GHz. At a volumnar vapor content of 2 g/cm^{2}, the rate of change of brightness temperature with respect to frequency is 3.3 K/GHz, so that 0.04 K errors are possible in the presence of moderate amounts of vapor. These errors are below the quantization level of the A/D converter for most observing conditions.

E. BANDWIDTH AND INTEGRATION TIME

The bandwidth specification like the operating frequency of 20.7 GHz was governed by the equipment in-hand. Both the NEMS unit and the two GSFC-supplied units are double sideband receivers with an IF passband from 10 to 110 MHz. The Dicke switch rate is 1000 Hz on all of the radiometers. The minimum integration time is set by a low-pass filter on the output of the synchronous detector whose characteristics were based on three considerations. First, the time constant should be long enough to span many cycles of the Dicke switch and thereby average out transients and any short-term dithering in the switch reference frequency. Second, the time constant should be large enough to reduce the random noise fluctuations to a value that is several times the quantization level of the analog-to-digital converter. Third, the time constant should not be so large as to impose tedious wait states between changes of the input. The design team chose a low-pass filter with an equivalent time constant of 100 ms and thereby average 100 cycles of the Dicke switch. The rms fluctuation level is approximately 0.4 K compared to a quantization level of 0.1 K. The wait state after a mode change is determined by the time it takes the previous level to decay to less than the quantization level, which for our design is 9 time constants or 0.9 s. This delay is enforced in the controller software - the WVR simply will not respond for 0.9 s after a mode change. The effective integration time can be lengthened by software averaging techniques.

F. ANTENNA BEAMWIDTH

Ideally, one would like the antenna beamwidth of the WVR to be comparable to the beamwidth of the radio telescope that is to be calibrated.

However, as indicated previously, this restricts the use of the WVR in other applications. In addition, a comparable WVR beam would entail considerable cost either as hardware or in development in that it would mean a WVR aperture whose diameter is comparable to that of the radio telescope with all of the attendant problems of pointing, spillover, etc. These problems are solvable given enough time and money but did not require solution in this application.

A horn antenna with a relatively broad beamwidth (7 degrees, full width at half maximum) was chosen for three reasons: (1) it has virtually no sidelobes, (2) the dimensions could be easily scaled to give the same beamwidth at both operating frequencies, and (3) the temporal/spatial resolution of the broad beam was more than sufficient for the application. The horn beam pattern shown in Figure 3-1 is taken from Ref. 10. In order to have a WVR beam that was comparable to that of the 64-m antenna operating at 3.8 cm, a 16-m aperture would be required. To achieve this, a separate 16-m paraboloid could be employed with the WVR or the WVR could be mounted in a way that would utilize some or all of the 64-m aperture. In either case, considerable engineering effort would have to be devoted toward minimizing the problems of sidelobes and spillover that produce serious systematic errors in the delay determination. Furthermore, since a variety of radio telescopes is used in VLBI applications, a custom WVR aperture or feed would be required for each installation. Clearly this would be impractical; if eight WVRs are needed, a single design is most cost effective. However, if a composite design is used, how does one relate the output of the WVR to the output of the radio telescope when they have unequal beams?

Formally, there is an important distinction between the antenna temperature (which is what the WVR measures) and the sky brightness temperature (which is what we wish to measure). The antenna temperature T_a (neglecting losses) is given by a convolution of the brightness temperature distribution $T_b(\theta, \phi)$ with the antenna beam pattern $P(\theta, \phi)$ as,

$$T_a \sim \int T_b(\theta, \phi)\, P(\theta - \theta_o, \phi - \phi_o)\, d\Omega \qquad (3\text{-}1)$$

where θ, ϕ are spherical coordinates and (θ_o, ϕ_o) is the pointing direction. If the beam pattern has unwanted responses in directions other

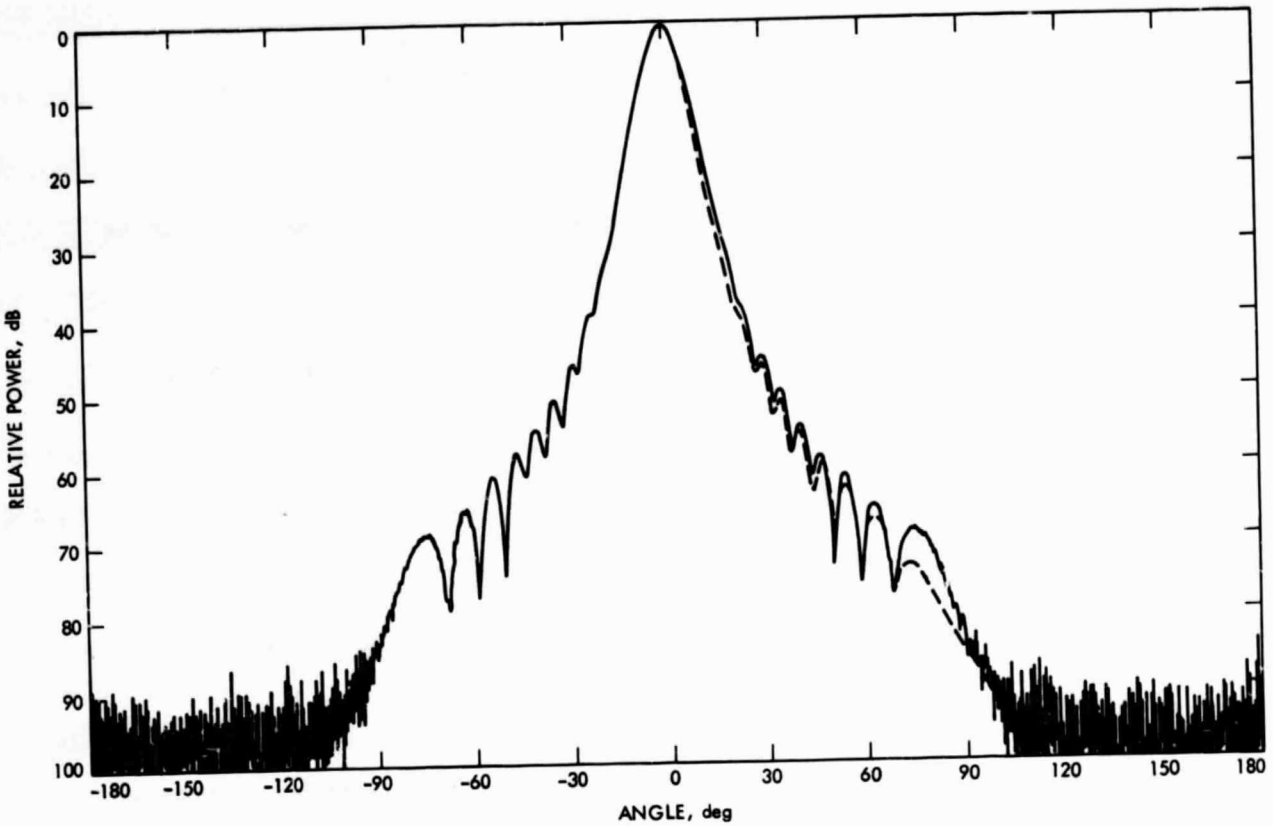

Figure 3-1. WVR Horn Antenna Beam Pattern

than the pointing direction then we must correct for them. A typical sky brightness temperature of 30 K would be considerably corrupted by a 100 K cloud or the 300 K earth in a sidelobe even if the sidelobe response were 20 dB down from the main beam. The virtue of having an antenna beam with no sidelobes (i.e. very high main beam efficiency) is that the antenna temperature can be equated to the brightness temperature (except for a small pointing correction) and a great deal of data "massaging" can be eliminated.

To understand how the vapor affects a large radio telescope, it must be kept in mind that the beam of the radio telescope takes a relatively large distance to form. The extent of the near field of an aperture is

$$L_{nf} \simeq D^2/\lambda \qquad (3\text{-}2)$$

where D is the diameter of the aperture and λ is the observing wavelength. This quantity is tabulated in Table 3-2 for some of the antennas used in this application. Since the scale height of water vapor is typically 2 km, this means that most of the vapor is in the near field of a large radio telescope. Thus, fluctuations in phase for the radio telescope are determined by the vapor inhomogeneities that pass through a cylindrical column of length L_{nf} and diameter D. Let us assume that the water vapor exists in the form of "blobs" that are randomly distributed in size. If we sample equal volumes of atmosphere containing N_1, N_2, blobs, etc., then we would expect to find N blobs on the average with an RMS variation of $\sqrt{N}$. We would obviously expect less variation if we sampled a large volume as compared to sampling a small volume. If we normalize N to be the number of blobs per unit area, then the average value will be independent of the sampling volume, but the RMS variations about the average will be a function of the sampling volume. Thus, we can roughly estimate the difference in fluctuation between the WVR and radio telescope by simply computing the average vapor contained in the two beams. If we assume that on the average the water vapor is exponentially distributed with scale height H_o, and the WVR beam is approximated by a cone of full-width β, then it is straightforward to calculate the ratio R of the volume of vapor in the WVR beam to the volume of vapor in the near field of the radio telescope,

Table 3-2. Extent of the Near-Field and Beam Volume Ratios for WVR and Radio Telescope

Diameter (meter)	Frequency (Ghz)	L_{nf} (km)	R	$\sqrt{R}$
64	8.4	108	29.2	5.4
64	2.3	32		
40	8.4	42	74.8	8.6
40	2.3	12.3		
25	8.4	16.4	191.5	13.8
25	5.0	10.4		
25	2.3	4.8		
9	8.4	2.1	1477.9	38.4
9	2.3	0.6		
4	8.4	0.4		
4	2.3	0.01		

$$R = V_{wvr}/V_{cyl} = 8[H_o/D) + \tan(\beta/2)]^2 \qquad (3\text{-}3)$$

This ratio is shown in Table 3-2 using the 7-deg beamwidth of the WVR. If we neglect instrumental noise then we would expect the ratio of the WVR fluctuations to the fluctuations from the radio telescope to vary as the square root of R. The WVR, since it samples a larger volume, will vary less; but on the average, it will determine the correct delay for the radio telescope.

An alternate way to view this problem is to note that equation 3-1 is a function of time. The brightness temperature describes the two dimensional projection of an assemblage of water vapor inhomogenieties that are constantly rearranged by winds aloft. Thus, the quantity T_a is really a time series. If we had a pencil beam, i.e. $P(\theta, \phi)$ were a delta function, then the time variations of T_a and T_b would be identical. The fact that we have a beam of finite width that is convolved with T_b implies that the antenna acts as a low-pass filter by spatially averaging the details of the sky brightness distribution. Therefore, we expect the output of the WVR to be a smoothed representation of the output from the radio telescope. On very short timescales the radio telescope may exhibit fluctuations that the WVR will not detect.

The calculation of the time scale that relates the WVR to radio telescope fluctuations is quite complex, involving the geometry and the three dimensional spectrum of vapor inhomogeneities. We shall resort to a more intuitive approach. Consider that at the zenith the width of the WVR beam is approximately

$$D_w = 2H \tan(\beta/2) \qquad (3\text{-}4)$$

where H is the height. For a height of 2 km (the nominal scale height of water vapor) and a beamwidth of 7 deg, we calculate D_w=244 m or roughly 10 times the near field width from a 25-m radio telescope. For a given blob diameter D, and radio telescope diameter D_R, we can distinguish three different regimes. Regime 1: $D<D_R$, the ratio of the time that the blob spends in the WVR beam to the time it spends in the radio telescope beam is $T \sim D_w/D_R$. Regime 2: $D_R < D < D_w$, the time scale is $T \sim D_w/D$.

Regime 3: $D>D_w$, the ratio of the times becomes $T \sim 1$. Thus, in this example the very small blobs of vapor will spend about 10 times longer in the WVR beam than in the radio telescope beam, but as the size of the blob grows the ratio of time spent in the two beams approaches unity. If we further assume that the horizontal and vertical dimensions of the blob are roughly equivalent then it follows that the small blobs will cause small phase perturbations and large blobs will cause large perturbations. The WVR will not "see" the short period fluctuations in the radio telescope output that are due to water vapor but it can detect the larger long-term effects. In reality nature is not nearly so simple and all that can be safely said is that there is a rough equivalence between the spatial averaging of the WVR and temporal averaging from the radio telescope.

G. CALIBRATION

The WVR requires two types of calibration in order to produce accurate path delay estimates. Instrument calibration is necessary to ensure that the observed brightness temperatures are referenced to an absolute temperature scale and algorithm calibration is required to ensure that the inversion algorithms produce reliable path delay estimates that are free of bias.

Some degree of stabilization is provided by operating the receiver as a Dicke radiometer. However, the Dicke load is at approximately room temperature and hence normal operation is not fully stabilized. Additional instrumental calibration is accomplished by including internal waveguide loads that can be substituted for the antenna at the user's discretion. If the user observes the output of the radiometer in 1) the hot load position, 2) the ambient (base) load position, 3) the antenna position, and knows the physical temperature of the loads, the antenna temperature can be inferred. Since the antenna temperatures are generally much less than the load temperatures, the inference represents an extrapolation and small errors in the temperature of the hot load or losses in the waveguide or switches can cause large errors in the antenna temperature. To first order, most instrumental loss terms can be corrected by assuming a small correction to the hot load which can then be determined from a "tip curve." In a tip curve we rely on the fact that the

cosmic blackbody background temperature is well determined (2.9 K) and that the atmosphere is approximately stratified. We observe the sky brightness temperature at several values of airmass and solve for the value of the hot load correction that yields 2.9 K at zero airmass and solve for the zenith opacity as well.

Algorithm calibration requires comparing the WVR with some independent method of measuring path delay. Several techniques can be used to refine the instrumental calibration, but the only reasonably cost effective and independent method for estimating the path delay that is currently available uses radiosondes (i.e., an instrument package carried aloft by balloon) to profile the vertical structure of pressure, temperature, and humidity. One must numerically integrate the profile in order to obtain the path delay. The accuracy of the comparison is limited by the accuracy of the radiosonde sensors.

H. TEMPERATURE CONTROL

The quantity that correlates most strongly with gain variations is temperature so that it is important that the WVR have enough thermal inertia to resist sudden changes in temperature. Conversely, the gain should be monitored on time scales shorter than the time scale for real temperature changes. The important specification is the restriction that the physical temperature of any load must not change by more than the quantization level during the time it takes to measure the gain. Thus, the specification $\pm 0.1^{\circ}C$/minute assumes that it will never take longer than one minute to measure the gain.

Almost all of the microwave components are thermally connected to a large aluminum mounting plate. A mercury thermostat controls strip heaters attached to this plate and regulates its temperature to $43^{\circ}C$. A small fan circulates air around the few components that are not attached to the plate. The entire microwave package is enclosed by a sheet metal box that is lined with styrofoam and provides a thermal attenuation of approximately 6-7 dB. The box is attached to the positioner with a base plate made from a thermally insulating material. Thermal baffles are mounted on stand-offs on the four sides of the box that expose the largest area. These baffles are covered with a paint that has high reflectivity in the infrared. These baffles were found to be necessary for summer operation in desert-type environments.

Figures 3-2 and 3-3 show the warmup characteristics of the two waveguide terminations (i.e. the hot and base loads). Typically, the hot load requires 1.5 to 2 hours to thermally stabilize and will remain constant to $\pm 0.2^{\circ}C$ thereafter. The base load, which is representative of the remainder of the electronics package, takes up to 3 hours to reach quasi-equilibrium. Figure 3-4 shows the typical diurnal variation of the enclosure temperature, which correlates very well with the gain variations.

I. POINTING SYSTEM

The specifications for the pointing system followed from the requirement that the WVR point along the same line-of-sight as the radio telescope being calibrated. This is most easily done with an Az/El mount and conversions from right ascension/declination done in software if necessary. Due to the 7-deg bandwidth of the horn antennas, a capability for tracking was not included - only pointing. The commercially manufactured positioner provided by GSFC has a pointing capability of ± 1.0 deg, but is modified to provide a readout precision of ± 0.1 deg. Analysis of the pointing sensitivity indicates that positioning errors of ± 0.1 deg will give worst case errors of 0.5 K in brightness temperature and 3 mm in the path delay in high opacity/low elevation angle conditions. In a typical VLBI experiment, the positioner is pointed to within ± 1 deg of the radio telescope line of sight, keeping 10 deg away from obstructions. Along with the WVR data necessary to calculate the path delay, the indicated position of the WVR must be noted so that the path delay can be correctly mapped to the line of sight by assuming a cosecant elevation angle.

The slew rate of the commercial positioner is generally much faster than the associated radio telescope. This allows the possibility of more complex observing strategy with the WVR than simply following along behind the radio telescope. Details of the operation of the positioner are given in Section IV.

J. WVR CONTROL AND INTERFACE

A primary requirement for WVR control and data acquisition was that the user input controls and the data outputs were to be identical regardless of any nonuniform WVR hardware configurations. The computer interface for the

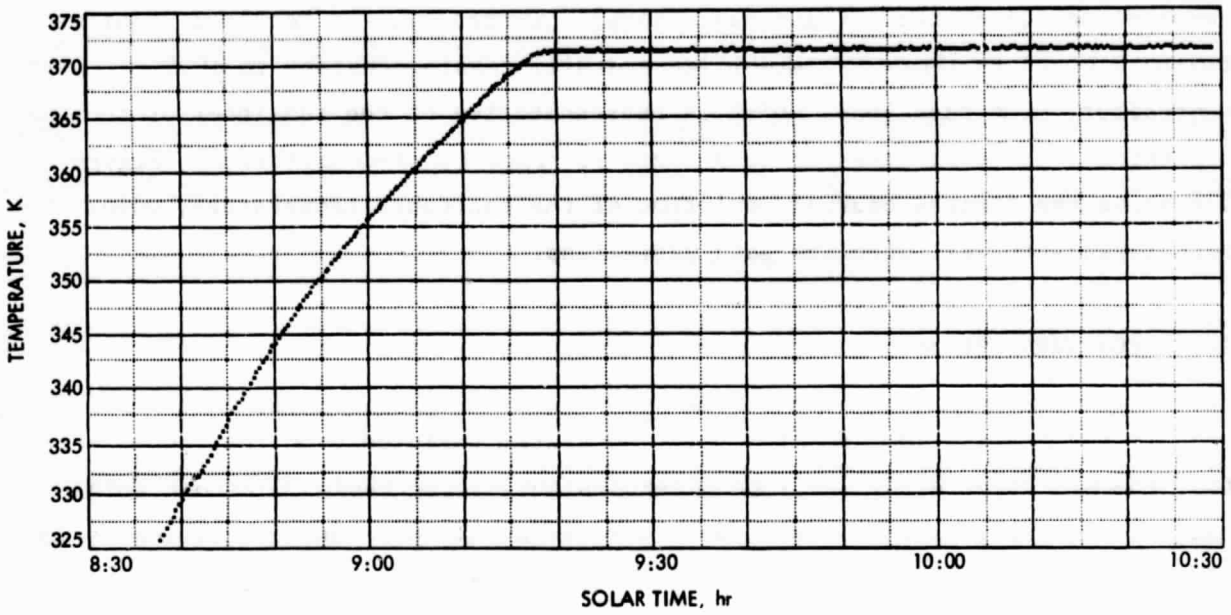

Figure 3-2. Hot Load Warmup Characteristics

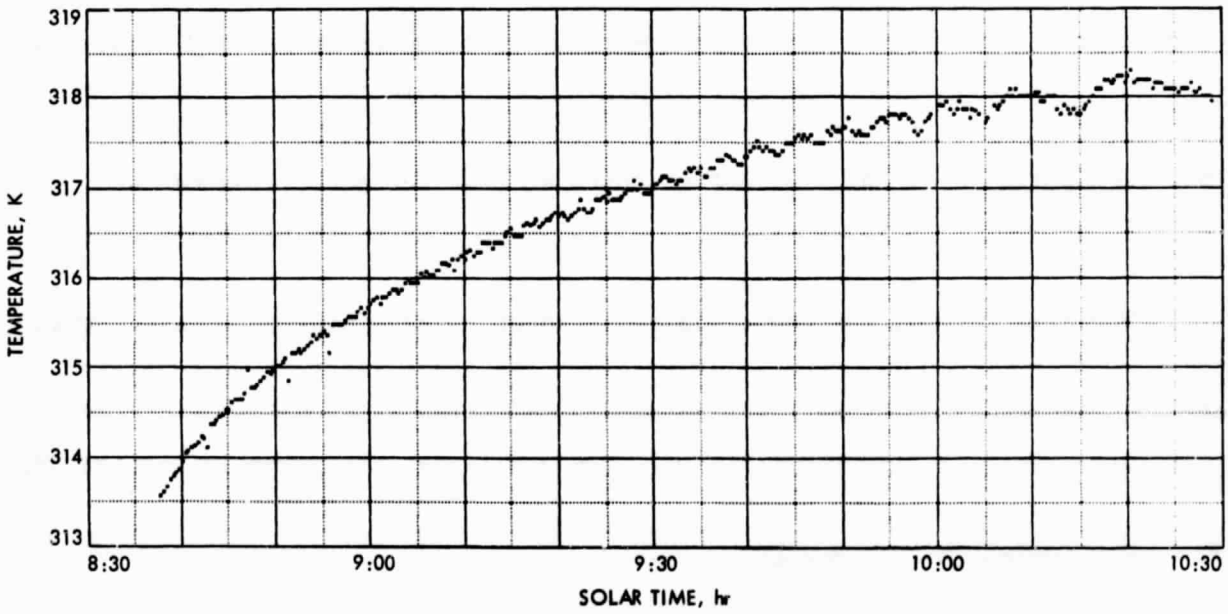

Figure 3-3. Base Load Warmup Characteristics

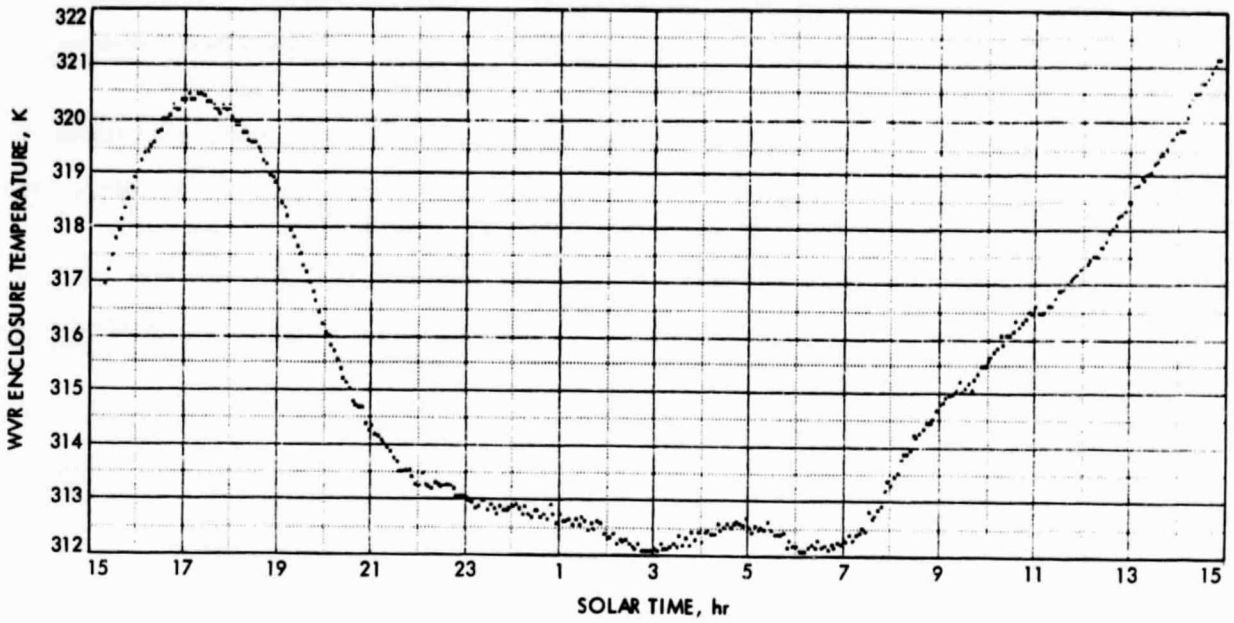

Figure 3-4. Enclosure Temperature vs. Time

planned control unit was the already-selected Data Acquisition Subsystem, developed by the MIT Haystack Observatory, which used a Hewlett-Packard HP1000 microprocessor. Initially, it was planned only to have a computer interface for automatic operation. However, the need to bench-test the microwave and positioner module interfaces resulted in the development of a local control panel, which subsequently turned out to be extremely useful for on-sight local control during field installation and on-sight troubleshooting. The design consideration for the control and interface software was to use a fairly general-purpose language that would automatically operate the WVR via the HP1000 microprocessor and that would also allow manual operation via a remote terminal.

In early talks with colleagues at Goddard Space Flight Center and at the Haystack Observatory, it was decided that the WVR would simply be treated as one of several devices on a daisy-chain type of serial interface. This interface has come to be known as the MAT (Microprocessor ASCII Transceiver) bus. Originally it was believed that the new RS422/423 interface standard would be necessary to implement the long lines to the WVR that were expected to be required at some installations. Unfortunately reliable components to implement the RS422/423 standard were not available in time to be implemented. A simple three-wire RS-232 is now in use with short-haul modems for the WVR interface lines.

The baud rate of the WVR is set to any standard rate from 75 to 19,200 baud by a combination of software and jumper changes on the microcomputer board. At the present time it is set to 9600 baud. Implementation of the operating modes and command/respond sequence is primarily a matter of sufficient software in the microprocessor. In the current version of this software only the OPERATE mode has been implemented along with a set of primitive commands. The microcomputer contains an analog I/O subsystem that is used to digitize the various analog signals from the microwave package and the positioner. The desire for 0.1 degree of position resolution dictated the choice of a 12-bit A/D converter (i.e. $2^{-11} > 0.1/360 > 2^{-12}$). Similarly, the quantization of the physical and brightness temperature measurements is

0.1 K. As indicated previously, the fluctuation level from the radiometer is on the order of 0.4 K. It is possible to reduce these fluctuations by averaging many samples. However, Clark (Reference 12), has pointed out that this must be done with caution if one attempts to reduce the fluctuations below the quantization level.

SECTION IV
WVR DESCRIPTION

A. GENERAL DESCRIPTION

A water vapor radiometer is an instrument for measuring sky brightness temperature at two frequencies on or near the spectral radiation emission line of the water vapor molecule, which is 22.235 GHz. The design basically incorporates two Dicke radiometers, one tuned to 20.7 GHz and the other tuned to 31.4 GHz. The WVR physically consists of three modules: (1) a microwave module, (2) a positioner, and (3) a controller/interface module. A block diagram of the WVR is shown in Figure 4-1. The microwave module contains the RF electronics, switching circuitry, and power supplies, and is mounted on the positioner, which points the unit in azimuth and elevation. The microwave package and positioner are connected to the controller/interface module, which consists of a microcomputer and control panel that allows the performance of the unit to be monitored and controlled locally, either for operation or troubleshooting. Under normal operating conditions, the controller automatically controls and acquires data from the microwave package and the positioner. The microcomputer can be connected to a host or main computer or to a remote terminal via an RS-232 serial interface.

B. MICROWAVE MODULE DESCRIPTION

The radiometer is a standard Dicke design (see Ref. 13 or 14 for principles of operation) and begins at the third waveguide switch, identified as C3 in Figure 4-1, which is called the "Dicke" switch. Switches C1 and C2 allow selection of the three possible inputs to the radiometer: base load, antenna, and hot load. The Dicke switch modulates the input signal at a 1 kHz rate. The mixer heterodynes the signal (double sideband) to an intermediate frequency (IF) range where it is amplified and fed to a square-law detector. After detection the signal is amplified again, synchronously demodulated with the switching signal, and low-pass filtered. The final stage of amplification also offsets the signal and outputs it to the control and interface module. This signal is digitized by the microprocessor and provided to the user as a number

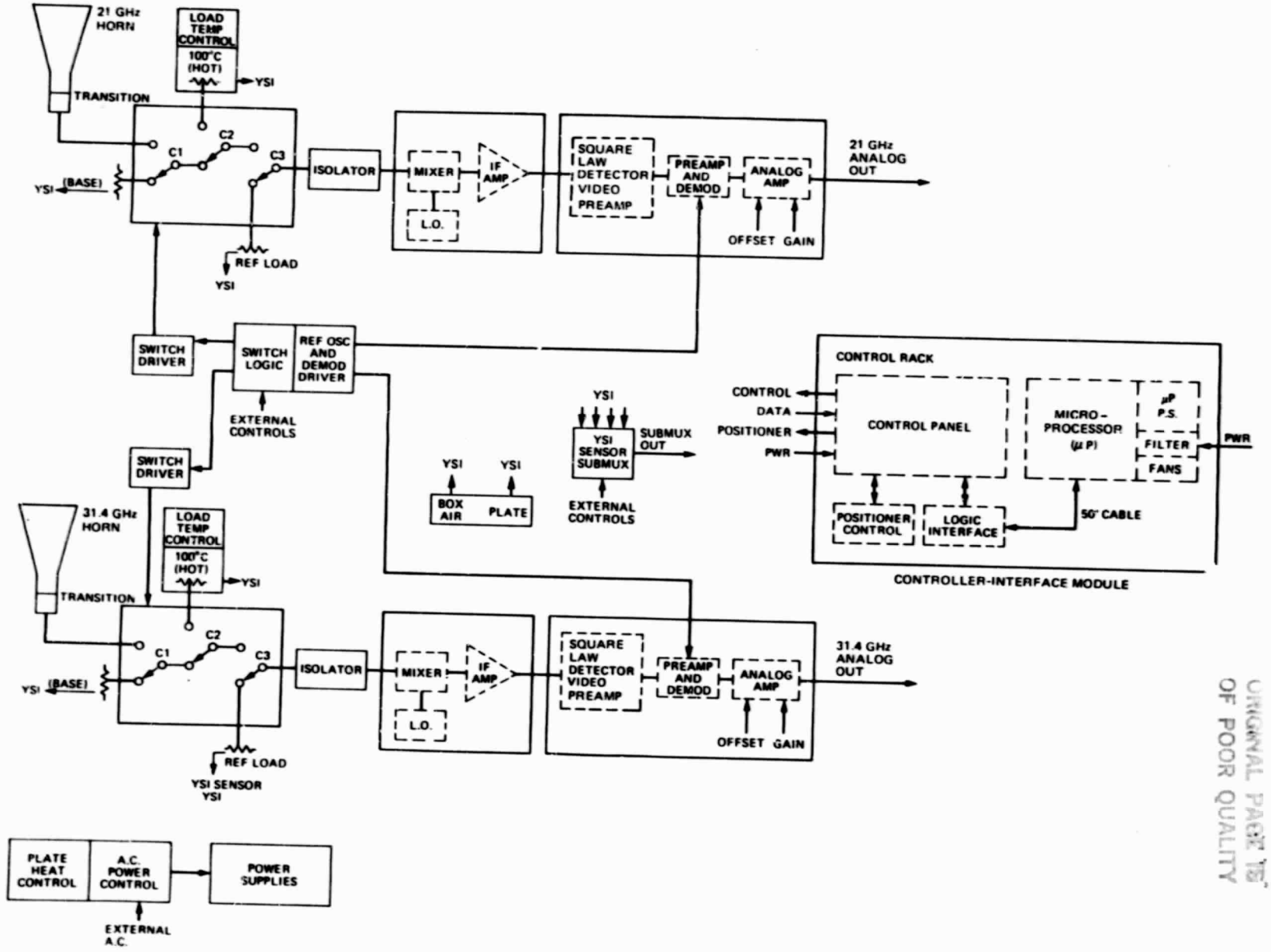

Figure 4-1. WVR Block Diagram

called "counts" corresponding to the three possible radiometer inputs, the antenna (NA), the base load (NB), or the hot load (NH). A typical plot of the output N versus the input temperature is shown in Figure 4-2.

The antenna is a corrugated conical feed horn and is described in Ref. 10. The beam pattern, shown in Figure 3-1, has a full width at half maximum of 7 deg (Ref. 15). The signal intercepted by the antenna represents the convolution integral (Ref. 13) of the beam pattern and the brightness distribution of the atmosphere. Neglecting background sources like the sun, the atmospheric brightness distribution represents the solution of the equation of radiative transfer. The equation of radiative transfer contains the density of water vapor (among several other atmospheric parameters) which allow us to relate the brightness temperature to the integrated vapor content or equivalent to the excess path delay. Since the signal entering the antenna is small, we need take care that the antenna beam avoid obstacles to ensure that the convolution integral is manageable and we can equate the antenna temperature to the brightness temperature.

The signal from the antenna is fed to the RF switches through a circular to rectangular transition and section of waveguide. The RF switches are three ferrite circulators contained in one package with a common heatsink in order to maintain the switches at the same temperature. The typical isolation is better then 25 dB and the insertion loss is typically 0.2 to 0.4 dB.

The three waveguide terminations connected to the circulators are used as blackbody microwave sources. Two are used for calibration. The calibration terminations are temperature controlled, one (hot load) is maintained at 100°C while the other (base load) is maintained at the temperature of the electronics mounting plate which is typically 45°C.

The signal from the antenna, hot load, or base load is modulated at a 1 kHz rate by circulator A, such that a constant comparison is made between the third termination (reference load) and the signal. The reference load is also maintained at the temperature of the plate. The modulated signal from the circulators is passed through an isolator and then mixed in a low-noise mixer with

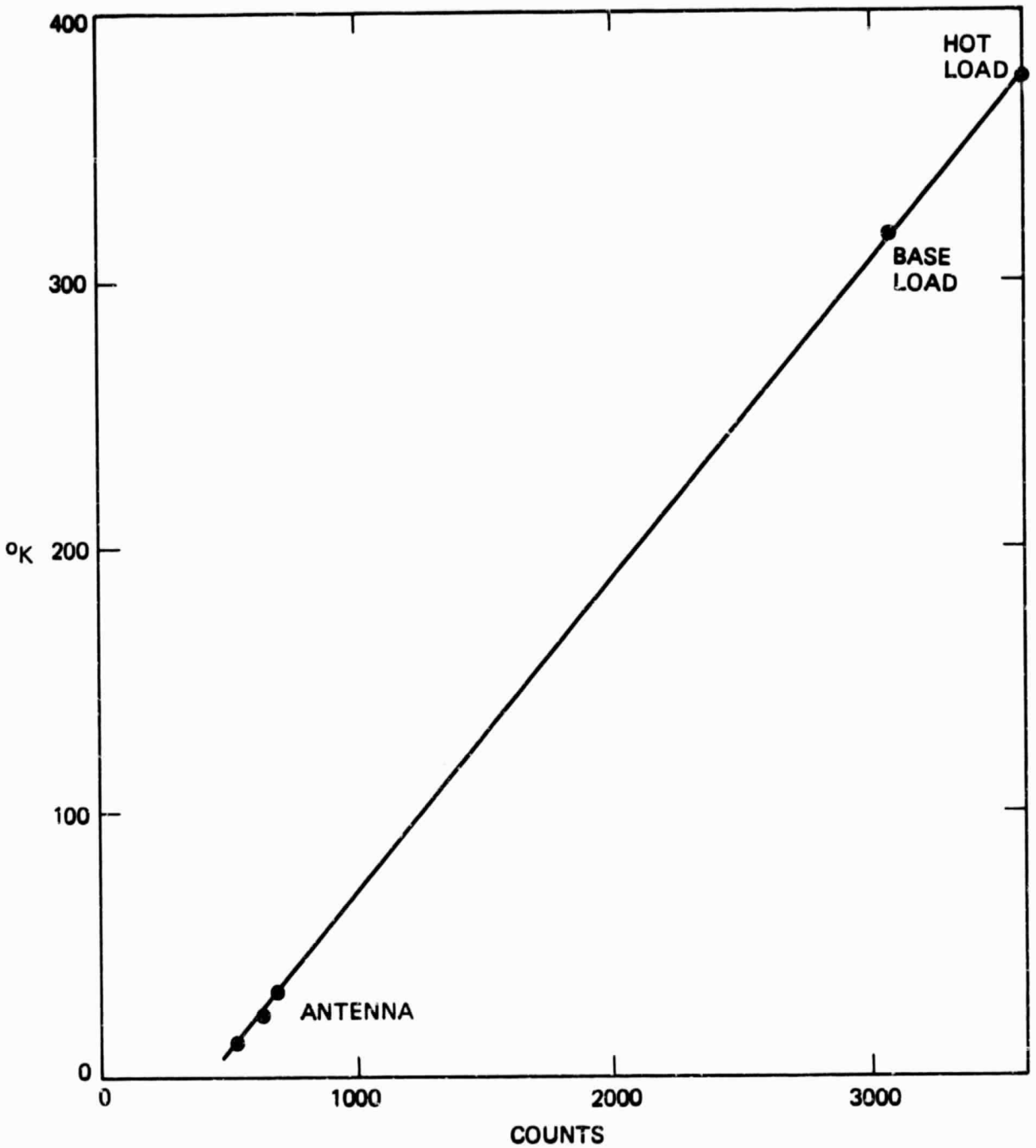

Figure 4-2. Typical Brightness Temperature vs. Counts

a local oscillator (LO) signal to produce an intermediate frequency (IF). The mixers are single balance Schottkey diode, double sideband mixers. The mixed signal is then amplified by the IF amplifier which has a typical gain of 70 dB. The mixer and IF amplifier have a combined bandwidth of 125 MHz. The mixer, LO and IF amplifier are assembled and tuned at the factory for maximum performance.

From the IF amplifier the signal passes through an RF attenuator and is then fed to a square law detector assembly. The attenuator adjusts the signal power level to operate the detector diode at least 5 dB below the point where the detector departs from square law operation. The square law detector assembly contains an impedance matching network, a zero bias Schottkey diode, and a video preamplifier. The matching network has an RF bandwidth of 10 to 110 MHz. The video preamplifier has a bandwidth of 7 kHz and an output that is a square wave video signal at a frequency of 1 kHz.

The signal from the square law detector assembly is amplified by the video amplifier and then synchronously demodulated. The output of the synchronous demodulator is proportional to the difference between the input signal and the reference load. The resultant dc signal is further amplified by a dc amplifier and is available as the analog output. The final dc amplifier has a typical time constant of 100 milliseconds and a typical offset of +7.0 volts.

1. Temperature Sensor Submux

Temperatures at 11 locations are sensed by precision thermistors manufactured by Yellow Springs Instruments (YSI). The temperature sensor submultiplexer selects one of the thermistors and supplies 0.25 mA d-c current. The voltage developed across the resistance load is amplified by a factor of four and sent to the microprocessor in the controller module for A-D conversion. Sixteen submux channels are available and can be selected either manually or by computer. Two calibration resistors accurate to $\pm$0.1% are located in submux channels 14 and 15 and provide a resistance measurement that is relatively independent of gain changes or drift in the submux constant current supply. The normalized value for the resistance is used with the appropriate set of thermistor constants to calculate the temperature.

2. Plate Heat Control and AC Power Control

The temperature of the electronic mounting plate is controlled by heater strips. A mercury thermostat, which is factory set at 45 degrees Celsius, controls a solid state relay which in turn switches power to the heater strips. A fan circulates the air inside the radiometer package to help reduce thermal gradients. Whenever the radiometer is not being operated, the temperature of the unit is maintained above 10 degrees Celsius in order to protect the electronics from low temperatures. There is also an overtemperature thermostat that will turn the instrument power off when the electronics mounting plate reaches 57^{o}C.

3. Radiometer Logic

The radiometer logic interfaces the mode control signals from the control panel to the various circulators of the radiometer. The 1 kHz Dicke drive to the circulator reference switch and the demodulator signal originate in this circuit.

4. Power Supplies

The power supplies provide 12 individual lines for the voltages required by the microwave package. They are located external to the microwave package for reasons of thermal isolation. The power supplies contain a heating circuit that switches on whenever the temperature drops below 10^{o}C.

5. RF Components

The reference and base loads are waveguide terminations. The hot load was constructed at JPL and is connected to the ferrite switch by a short section of stainless-steel silver-coated waveguide that acts as a thermal isolator. The hot load consists of the termination imbedded in a block of aluminum. The block is wrapped with a resistive strip heater and a mercury thermostat is imbedded in the block next to the heater strip. The thermostat controls a solid state relay which supplies power to the heater strip thus con-

trolling the temperature of the block and termination. The block and heaters are surrounded by insulating foam and fit into a metal cover. All other loads are thermally coupled to the mounting plate and thermistors are attached using high thermal conductive epoxy.

The three RF switches in each WVR channel are ferrite circulators that are factory tuned to the desired operating frequencies. The switch drivers drive the individual circulators. These drivers are located in a separate box connected to the switches by a short length of cable. The switch driver circuit is actuated by TTL signals from the local control panel or microprocessor through the switch logic circuit.

The final circulator (i.e. the Dicke switch) is connected to a 20 dB isolator that is used to reduce local oscillator (LO) leakage out of the horn. A short piece of waveguide connects the isolator to an assembly that consists of the LO, mixer, and IF amplifier. Frequency, LO power level, and LO to mixer coupling are all factory adjusted for minimum noise. The nominal noise equivalent receiver temperatures are 575 K at 20.7 GHz and 630 K at 31.4 GHz.

The output of the mixer/IF assembly is connected to a fixed attenuator which in turn is connected to the square law detector. The attenuator is used to adjust the IF signal level to the detector so as to ensure square law operation.

6. Synchronous Demodulator

From the detector assembly, the signal is routed to the synchronous demodulator. The circuits for both channels are identical and mounted on the same circuit card. The signal is amplified, inverted, and synchronously demodulated by a switching signal at the Dicke rate (1000 Hz). The switching signal is conditioned and divided. Part is fed to the switch driver for the Dicke circulator. The other part is optically coupled to the synchronous demodulator in each channel.

7. Power, Heating, and Protection Circuits

Two multiple voltage power supplies are used to provide all of the voltage levels required by the microwave package. Both supplies are packaged together but kept separate from the microwave module. The resistive strip heaters are located on the mounting plate/heat sink. Overcurrent protection is provided by a fuse that opens at a current of 15 amperes. If the temperature of the plate rises above 57°C the thermostat will open and cut all power until the temperature drops. The fan circulates air around the mounting plate/heat sink in an attempt to minimize thermal gradients between components.

8. Mechanical Description

Figure 4-3 shows the mechanical layout of the microwave module. Three aluminum plates are used to mount the various components. The base plate attaches directly to the positioner mounting table. The antenna mounting plate is positioned parallel to the base plate on four aluminum posts. Between these two plates, bolted directly to the antenna mounting plate, is the electronics mounting plate. This roughly rectangular package is enclosed on four sides by a sheet metal cover that screws into the base plate and is lined with styrofoam insulation. Another piece of styrofoam covers the horn antennas together with a thin (i.e., 0.127 mm) sheet of teflon. The foam insulation provides thermal isolation for the microwave electronics. Liquid water that precipitates on the WVR usually beads on the teflon cover (assuming the teflon is clean) and can be seen much more easily than on a styrofoam surface. When the WVR is removed from the zenith the liquid droplets slide off the teflon cover quite readily.

Primary temperature control occurs on the electronics mounting plate which is thermally isolated from both the base plate and the antenna mounting plate. Strip heaters cover most of the unused space on the electronics mounting plate which acts as the heat sink for all RF components. Typically, a change in the outside air temperature of 12°C will cause the temperature inside the enclosure to change by 3°C.

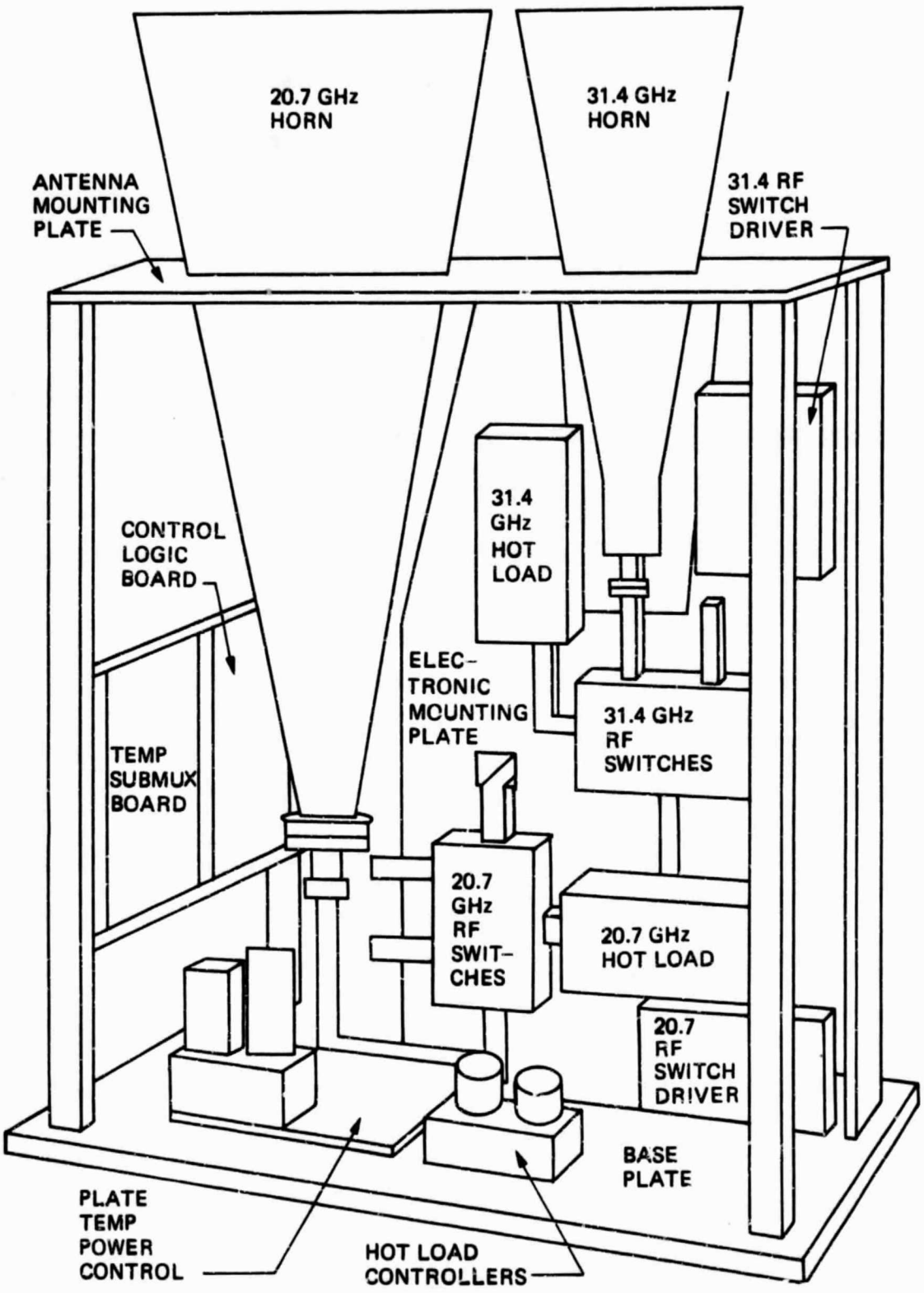

Figure 4-3. Microwave Module Mechanical Layout (Sheet 1 of 2)

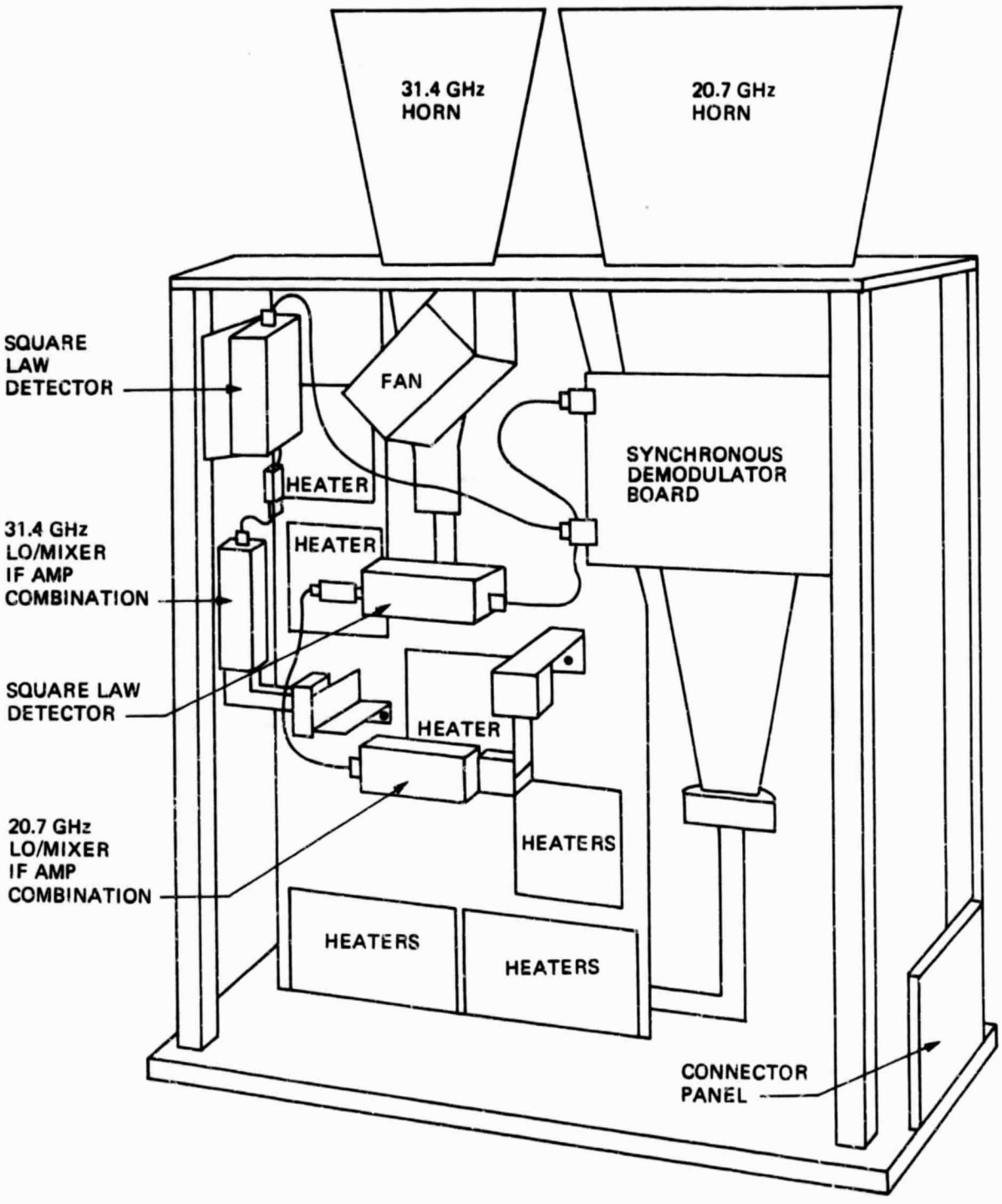

Figure 4-3. Microwave Module Mechanical Layout (Sheet 2 of 2)

The two power supplies are also mounted on one side of an aluminum plate with strip heaters on the other side of the plate and over/under temperature thermostats. These supplies are mounted in a small metal box separate from the microwave electronics.

C. DESCRIPTION OF WVR SERIAL NOS. R01, R02, AND R03 MICROWAVE MODULES

The purpose of this paragraph is to describe the differences in microwave modules used with WVR Serial No. R01, R02, and R03 from the preceding description. These differences primarily involve the hardware. Unit R01 was assembled using surplus parts from the NIMBUS E spacecraft radiometer program. Components for units R02 and R03 were purchased from Sense Systems, Inc., by Goddard Space Flight Center and provided to JPL.

1. RF Components

The port assignments in the RF switches of the 21 GHz channel in R02 and R03 are identical with the port assignments found in the 20.7 GHz channel of units R04 to R08. In the port assignments of the 31 GHz channel of R02 and R03, the calibration loads are reversed relative to the 21 GHz channel. In R01 there are three individual switches instead of the composite package found in the other WVRs, and the switch drivers are also different. Both channels of R01 have the same port assignments. The 31.4 GHz channel of R01 has a different mixer/LO/IF amplifier assembly. The second IF amplifier, square law detector, and video amplifier are from the original NIMBUS E design.

2. Synchronous Demodulator

The synchronous demodulator in units R02 and R03 is part of the commercial microwave module supplied by Goddard Space Flight Center. The demodulator for each channel is located on an individual circuit board and includes a blanking circuit. A unity gain, inverting amplifier with offset was added to each channel so as to provide an output voltage that varied between 0 and 10 volts. The demodulators for both channels of R01 are from the NIMBUS E unit and are enclosed in small boxes. They do not contain

blanking circuits - instead switch transients are tuned out with shim stock placed in the waveguide between the isolator and the mixer.

3. Switch Logic

The components that comprise the switch logic and the layout of these components in units R01, R02, and R03 are from the original designs.

4. Submultiplexer

The submultiplexers for units R02 to R08 are all identical. Unit R01 has a similar design but differs in that R01 uses platinum sensors to monitor the various physical temperatures.

5. Power, Heating, and Protection Circuits

The power to the heater strips for unit R01 is controlled by proportional controllers. The sensing element is a thermistor instead of a mercury thermostat used in all of the other radiometers. R01 does not have an extreme low-temperature protection circuit and should be protected whenever it is not being operated. The circuit still has overcurrent and high-temperature protection components. The hot load heater control and control sensing element are also of the proportional design.

The hot load temperature controllers for units R02 and R03 are the commercial manufacturer's design. They are proportional controllers with a thermistor as the control sensing element. There are no plate heaters in these units. The internal temperature is controlled by mercury thermostats. The heating elements are contained in a small rectangular tube placed in front of a fan.

6. Power Supplies

Each channel of units R02 and R03 contains its own separate power supply. The voltages for the submultiplexer are tapped from the 21 GHz power supply. The power supplies are located inside the microwave module.

The various voltages for unit R01 are supplied by a number of different power supplies. They are mounted external to the microwave module.

7. Mechanical Description

Unit R01 is similar to R04-R08 in mechanical layout. Each separate channel for units R02 and R03 with their antennas and waveguides is held to the base plate by two posts. The box heating apparatus is located between the two channels and is mechanically connected to one of the posts of the 21 GHz channel. The cover is different from R04 in order to accommodate the commercially supplied packages.

D. POSITIONER MODULE

The positioner module is an off-the-shelf unit, commercially manufactured by PELCO Inc., and modified by JPL. The positioner is inexpensive, reliable, and capable of pointing in azimuth (az) and elevation (el) with an accuracy of $\pm$1 deg. The pointing angle can be read with an accuracy better than 0.2 deg. Model PT2000 is used for WVR units R01 and R04 to R08 while Model PT2500 is used for units R02 and R03. Model PT2000 moves at a maximum rate of 8 deg/second while Model PT2500 has a maximum slew rate of 1.5 deg/second. The mounts are inscribed with serial numbers M01 through M08 and, except for unit M01, are interchangeable.

The positioner table is driven about two orthogonal axes by d-c motors. The direction of rotation is determined by the polarity of the drive voltage; the rotation rate is determined by the RMS voltage level as well as the gearing to the rotational axis. For positioner unit M01, variable rate drive circuits are contained in a separate box that was purchased with the mount. For units M02 through M08, circuits were added at JPL to control the polarity of the drive signal at a fixed voltage level. Consequently, units M02 through M08 always move at or near the maximum slew rate. JPL also added a thermostat and a strip heater that is energized when the ambient temperature falls below 0°C. Limit switches are provided to prevent damage to cabling.

The az and el angles for all positioners are determined by two precision potentiometers. The el potentiometer is driven by a chain and sprocket arrangement. The azimuth potentiometer is driven directly from a reducing gear connected to the azimuth shaft. The potentiometer excitation voltage for the units M04 through M08 is provided by an eight-volt regulator located in the positioner. For units M01, M02, and M03, the excitation voltage is provided by a five-volt power supply located in the controller module. The voltages from the wipers of the potentiometers are buffered by unity gain amplifiers whose outputs are the az and el signals.

Worst case errors due to pointing inaccuracy are on the order of 0.5 K in brightness temperature and 0.3 cm in path delay. At low elevation angles the indicated elevation requires correction to compensate for the finite width of the beam and the asymmetric brightness distribution of the atmosphere.

1. Elevation Pointing Error Effects

The full width at half power (FWHP) beam of the horn antennas used on the WVR is 7 deg at both frequencies. One might presume that the pointing requirements are then identical to the resolution of the instrument, i.e., 6 or 7 deg. While this is true of the azimuth coordinate, it is not true of the elevation coordinate because the atmospheric brightness temperature varies approximately as the cosecant of the elevation. At low elevation angles, a small error in the elevation can cause a measurable change in the WVR output. Errors in elevation can affect the measurement directly, i.e., an incorrect line of sight, or indirectly by introducing a bias in the tip-curve calibration.

Since the brightness temperature of the sky is a function of elevation, the quantization of elevation angle could introduce an error in the determination of T_b. We can evaluate the magnitude of this effect by noting that we can always write the brightness temperature of the sky as

$$T_b = T_c e^{-\tau} + T_m(1-e^{-\tau}) \qquad (4\text{-}1)$$

where T_c = 2.9 K is the cosmic blackbody background, T_m ~ 275 K is the mean radiating temperature of the atmosphere, and τ is the opacity along the line of sight of the WVR. If the atmosphere is stratified then the opacity is

$$\tau = \tau_o / \sin(E) \tag{4-2}$$

where E is the elevation angle and τ_o is the zenith opacity. The pointing sensitivity is then

$$(dT_b/dE) = -(T_c - T_m)e^{-\tau} \quad [\tau \operatorname{ctn}(E)] \tag{4-3}$$

and is shown in Figure 4-4 for several values of zenith opacity over an elevation angle range of zenith to 10 degrees. These curves are dominated by the τ term in Equation 4-3 for elevation angles near zenith, and by the ctn(E) term for intermediate elevation angles. However, as the opacity gets large the curve will peak and the $e^{-\tau}$ term will force the sensitivity to zero. Physically, this means that for large τ you cannot "see" through the entire atmosphere. The brightness temperature approaches the mean radiating temperature and is quite insensitive to small changes in pointing. The zenith opacity will typically range between 0.01 to 0.5 nepers at the frequencies used in the WVR for the sites that have been considered in the Crustal Dynamics Project. Inspection of Figure 4-4 shows that for an elevation angle of 15 deg and τ_o = 0.5 (worst case conditions) the sensitivity of the brightness temperature to small changes in the elevation angle is 5 K/degree. At our quantization level of 0.1^o this means there could be a maximum error of 0.5 K in T_b due simply to the coarseness of the elevation angle readout, i.e., a one bit error. However, note that this error is correlated in the two WVR channels and would tend to partially cancel in a common mode. Thus pointing errors are expected to contribute less than 3 mm errors in the determination of the path delay correction. Note that the WVR can be pointed with an accuracy of $\pm$1 deg, but the readout is accurate to $\pm$0.2 deg.

If we approximate the beam pattern as Gaussian with a 7 deg beam (full width-half maximum), the pattern is

$$P(\theta) \sim \exp[-(\theta/4.2)^2] \tag{4-4}$$

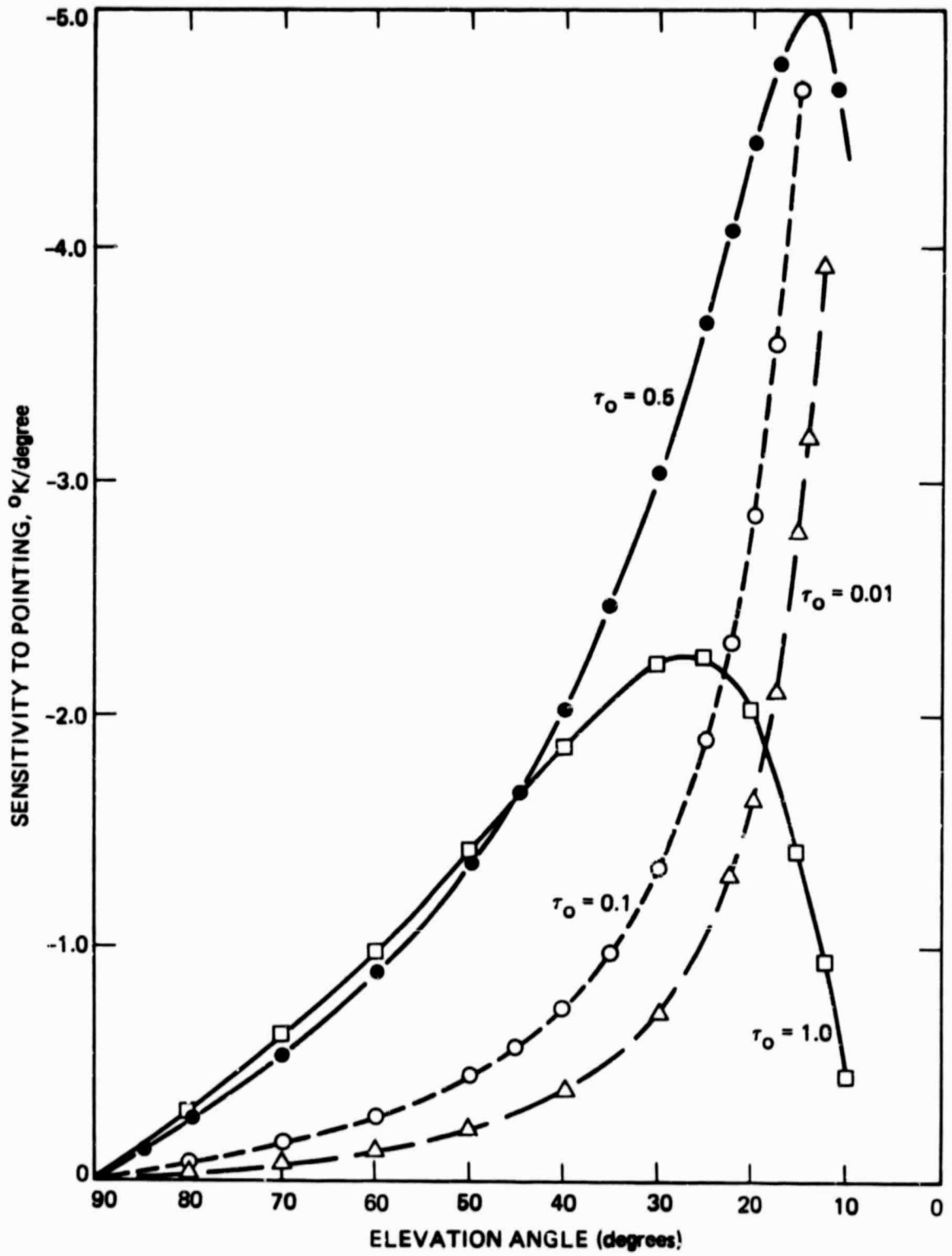

Figure 4-4. Pointing Sensitivity vs Elevation Angle

At a separation of 10^{o} from the beam center the response is down by 25 dB. An obstruction whose brightness temperature is on the order of 290 K would then contribute less than 0.9 K depending on the solid angle subtended by the obstruction. It is recommended that the WVR never be pointed closer than 10 deg to an obstruction (including the horizon).

2. Pointing Corrections

As we have noted in Equation 4-1, the brightness temperature is a strong function of elevation angle. If the atmosphere is homogeneous and stratified, then the brightness temperature T_b at some elevation E is just

$$T_b(E) = T_o/\sin(E) \tag{4-5}$$

where T_o is the zenith brightness. Since the antenna beam subtends a finite angle and is symmetric about the pointing direction E_x, this means there will be more power entering the lower portion of the beam ($E < E_x$) than through the upper portion of the beam (i.e., $E > E_x$). Under the assumptions previously cited this means that the observed brightness temperature in the direction E will be slightly larger than the value given by Equation 4-5 and the discrepancy will be a function of E. An equivalent way of viewing the problem is to note that since the observed brightness temperaure is a convolution between the distribution in Equation 4-5 and the antenna power pattern, the elevation angle of the beam averaged brightness distribution E_x' is always less than the geometrical pointing elevation E_x. This effect gives rise to a small bias in the observable (i.e., T_b), which can be removed by correcting either T_b or E.

When the WVR is pointing in the direction θ', ϕ' the observed brightness temperature $T_{obs}(\theta', \phi')$ is

$$T_{obs}(\theta', \phi') = \int T(\theta, \phi)\, P(\theta - \theta', \phi - \phi') \sin\theta\, d\theta\, d\phi \tag{4-6}$$

where $T(\theta, \phi)$ is the true brightness temperature distribution, $P(\theta, \phi)$ is the beam pattern, θ and ϕ, are spherical coordinates. For the WVR a reasonable approximation of the true brightness distribution of the sky is

$$T(o) = T_o/\sin(\chi/2-\theta) \tag{4-7}$$

The quantity $\chi/2 - \theta$ is just the elevation.

The effects of two dimensional antenna smoothing in terms of the sampling theorem are discussed in Ref. 16, where it is shown that for a Gaussian beam the observed brightness temperature is given by

$$T_{obs}(\theta, \phi) = T(\theta, \phi)/_2 + [T(\theta + \theta_1, \phi + \phi_1) + T(\theta - \theta_1, \phi + \phi_1) + T(\theta - \theta_1, \phi - \phi_1) + T(\theta + \theta_1, \phi - \phi_1)] \tag{4-8}$$

This is equivalent to replacing the integral in Equation 4-6 with a finite sum, i.e., imagine the beam to be the sum of segments - half the power originating from one segment around the beam center and the other half of the power from reduced segments around the half power points. Since the brightness distribution in Equation 4-7 does not depend on ϕ, $T(\theta, \phi + \phi_1) = T(\theta, \phi - \phi_1)$ so that Equation 4-8 reduces to

$$T_{obs}(\theta, \phi) = T_o/2\cos\theta) + T_o[1/\cos(\theta - \theta_1) + 1/\cos(\theta + \theta_1)]/4 \tag{4-9}$$

Thus, for a beam of finite size pointed in the direction θ, there will be a residual error in the observed brightness temperature given by

$$(T-T_{obs})/_T = 1/2 - (\cos\theta/4)[1/\cos(\theta - \theta_1) + 1/\cos(\theta + \theta_1)] \tag{4-10}$$

This residual is shown in Figure 4-5 for values of θ_1 equal to 7 deg, 3.5 deg, and 1.75 deg, and is the percent error in brightness temperature if we do <u>not</u> correct the pointing. The parameter θ_1 is the half-width at the half-power points of the antenna beam and is denoted in Figure 4-5 as HWHP. Even at 90 deg elevation there is power entering the beam from angles other than zenith so that the effect never goes to zero.

In practice, it is generally easier to compute a corrected pointing angle or air mass rather than correct the brightness temperature. If we expand the cosines and use the small angle approximation $\sin \theta_1 \sim \theta_1$, $\cos \theta_1 \tau 1$, then we obtain

$$T_{obs} = T_o(AM)/2 + [1 - 1/(1-x^2)] \qquad (4\text{-}11)$$

where $x = \theta \tan \theta$. In stratified conditions we would like the observed brightness temperature to vary as the corrected air mass AM´, i.e.,

$$T_{obs} = T_o\,(AM') \qquad (4\text{-}12)$$

which implies

$$AM' = AM[1+1/(1-x^2)]/2 \qquad (4\text{-}13)$$

If $x << 1$, this equation can be further simplified to

$$AM' = AM(1+x^2/2) \qquad (4\text{-}14)$$

The ratio AM´/AM calculated from Equations 4-13 and 4-14 is shown in Figure 4-6.

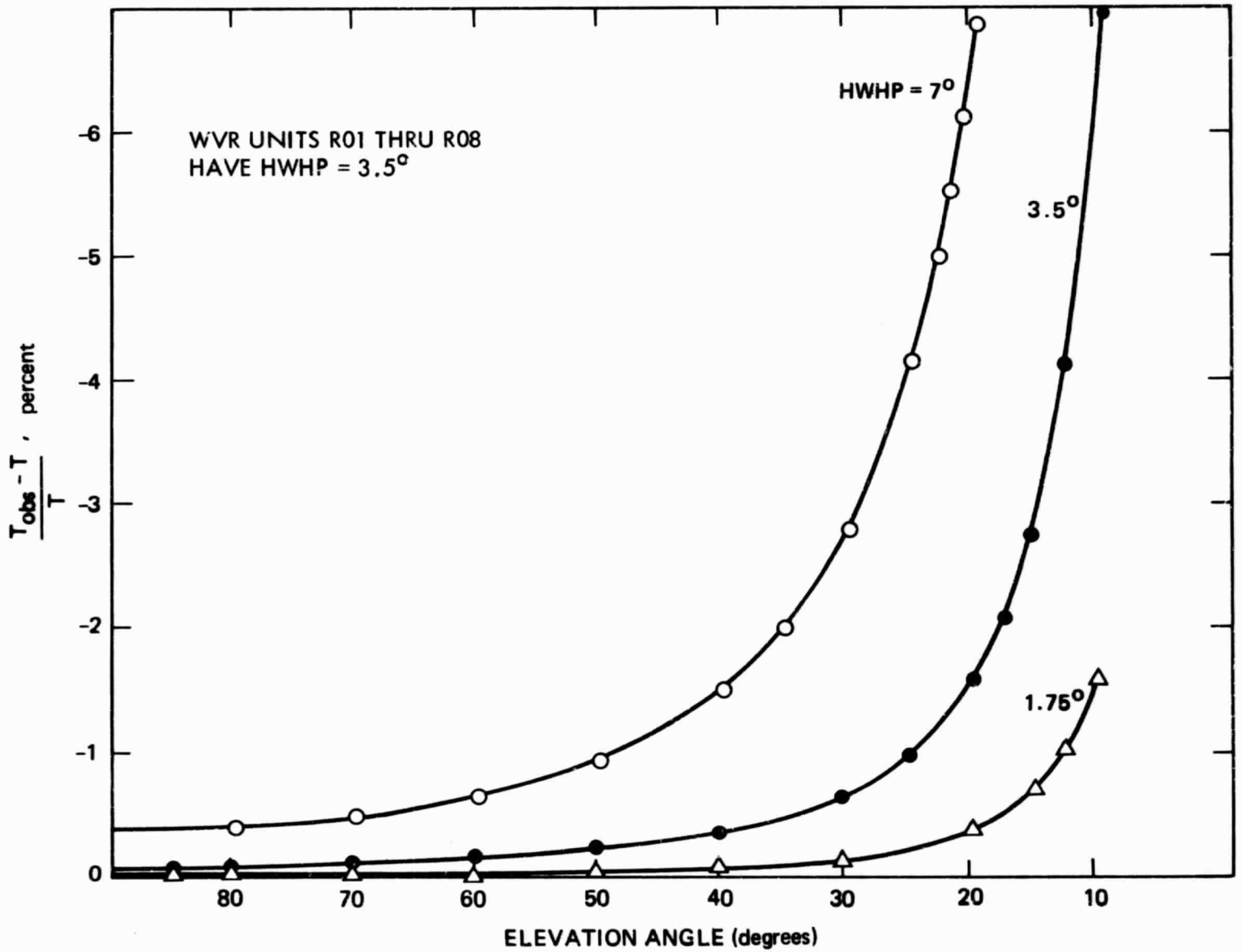

Figure 4-5. Residual Brightness Temperature Error Due to Finite Beam Size as a Function of Elevation

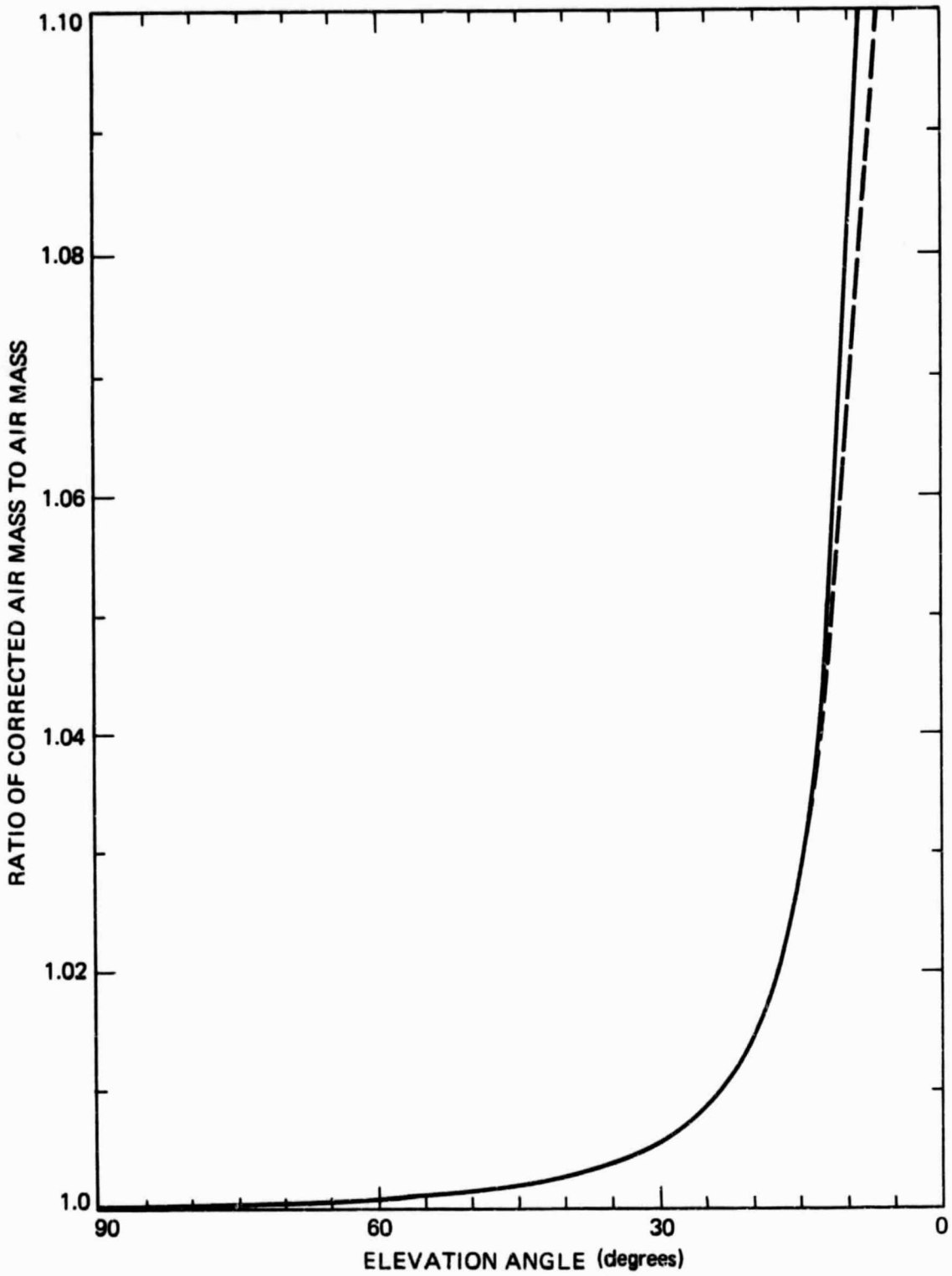

Figure 4-6. Ratios of Corrected Air Mass to Indicated Air Mass vs Elevation Angle For a Beam of 7 Degrees (Full Width at Half Maximum)

3. Positioner Coordinates A_i and E_i

As the positioner turns about a particular axis the potentiometer (i.e., the "pot") shaft also turns such that the resistance R_w, measured on the pot wiper, is linearly related to the angle turned by the mount; that is

$$R_w = a\theta + b \tag{4-15}$$

where a and b are constants. The most direct method of sensing this angle in the WVR controller is to measure a voltage with an analog-to-digital converter (ADC) by passing a current through the potentiometer and measuring V_w, the voltage on the wiper, so that Equation (4-15) becomes

$$\theta = a'V_w + b' \tag{4-16}$$

The voltage V_w is presented to the ADC whose output is a binary number N, which we will denote as counts, where

$$N = \alpha V_w + \beta \tag{4-17}$$

The constants α and β represent the gain and offset of the ADC circuitry. It is a trivial matter to relate N to θ or vice versa in an expression that involves a', b', α and β.

As a practical matter it is quite difficult to guarantee that the quantities a', b', α and β are truly constant. As the line voltage fluctuates, the power supply ages, or the temperature changes, the current through the pot may change and the gain and offset of the ADC may drift. In order to reduce or eliminate these effects, the voltage V_x, used to excite the pot, is sent back to the ADC. By measuring the ratio V_w/V_x (where V_w is the voltage on the wiper of the pot) we are relatively independent of current fluctuations. The voltage V_x is also used to drive a precision voltage divider that provides a voltage V_c, which provides a calibrating capability for the ADC.

The input to the ADC is through a 16-position switch called a multiplexer (MUX). The wiring assignments have been standardized so that the excitation voltage always appears when MUX channel 9 is selected*, the wiper arm voltage appears in channels 10 and 11 (az in channel 11, and el in channel 10), and the calibration voltage is in channel 12. Thus we observe the numbers

$$N_x = \alpha V_x + \beta \tag{4-18}$$

$$N_w = \alpha V_w + \beta \tag{4-19}$$

$$N_c = \alpha V_c + \beta \tag{4-20}$$

If, in Equation (4-15) we use the normalized pot voltage as a measure of position then

$$\theta = \theta' + m(V_w/V_x) \tag{4-21}$$

Using Equations (4-17) through (4-19) we then get

$$\theta = \theta' + m\,(N_w-b)/(N_x-b) \tag{4-22}$$

where

$$b = (N_c-N_x)[R_2/(R_1+R_2)]/[1-R_2/(R_1+R_2)] \tag{4-23}$$

In all of the WVRs, R_1 = 10 K ohms ($\pm$1%) and R_2 = 1 K ohm ($\pm$1%) is used. During calibration of the positioner, a precision multimeter is used to measure the ratio $R_2/(R_1 + R_2)$.

If the user wishes to know where the WVR is pointed, the procedure is to measure MUX channels 9, 10 (or 11), and 12 to get N_x N_w, and N_c, and use the following equations.

---

*Note that channel 0 is the first MUX address and channel 15 is the last.

$$Az = Az' + M_A(N11-b)/(N_x-b) \quad (4\text{-}24)$$

$$El = El' + M_E(N10-b)/(N_x-b) \quad (4\text{-}25)$$

Early versions of the WVR controller software require the user to point the device in counts. Thus, the host computer should use the expression

$$N_w = b + (\theta - \theta')(N_x-b)/M \quad (4\text{-}26)$$

N_w must be sent to the WVR as a four digit integer.

The overtravel limit switches restrict the azimuth range to approximately 350 deg. The actual azimuth range will vary from mount to mount, depending on how carefully the stops were located during checkout. Version 3.0 (and earlier) of the WVR controller software does not check the az or el limits. Thus, if the user commands the WVR into the limit, the limit switch will disconnect the drive power to the motors. The controller, however, has no way of knowing this has happened and will keep trying to drive past the limit. When this happens, recovery is accomplished by depressing the RESET button on the microprocessor and restarting the control program. The next version of the WVR control software will prevent this condition. The current Mk III WVR-Driver software simply checks the limits and does not issue any point command that takes the WVR into the dead zone. It is also possible to "go over the top", i.e., move the positioner through 180 deg about the horizontal axis. The elevation travel is limited to a nominal of 10 deg to 170 deg.

4. Calibration of the Positioner Constants

The constants for each positioner were measured by turning the positioner through several well-measured angles and noting the respective voltages V_w and V_x. These data were fitted in the least squares sense to determine the offset and slope constants. To calibrate the elevation angle, the positioner was mounted on a flat surface and the elevation of the mounting

table was measured using a clinometer with an accuracy of ± 1.5 arc minutes. The departure of the flat surface from level was measured and subtracted from the clinometer readings. For the azimuth angle calibration, a pen was firmly attached to the edge of the positioner with its tip in contact with a sheet of paper. As the mount rotated in azimuth, the pen scribed a circle on the paper. At various points on the circle, the voltages were noted as well as the length of the chords between marks. These data were used to calculate the azimuth angle corresponding to a particular azimuth voltage. In all cases the quality of the fit was very high and seemed to be dominated by the accuracy of the clinometer or measurement of chord length.

5. Pointing Offsets

The aperture of the horn antennas defines the WVR coordinate system. Some care has been taken to mount these horns precisely, so that the aperture plane is very nearly parallel to the baseplate of the microwave module. Since the baseplate is bolted directly to the positioner table it is sufficient (and more convenient) to measure az and el offsets directly from the table. In general, the positioner is never perfectly aligned with astronomical azimuth and elevation (i.e., true Az and El = A_t and E_t). The vertical axis of the positioner is offset from the true vertical by the angle ϕ_o. A plane drawn through both true vertical and the vertical axis of the positioner will intersect the horizontal plane of the positioner in a line that is described by $A_i = \phi_o$ and $A_i = \phi_o + 180^o$, where the i subscript denotes the internal coordinate system of the positioner.

Normally, the positioner is mounted on a pedestal and the internal coordinate system is commanded to $A_i = 0^o$ and $E_i = 90^o$. Large departures from vertical, e.g., greater than 1^o, are usually removed by placing shims under the bolts that hold the positioner to the pedestal. Once the coarse alignment to vertical is completed, the offsets θ_o and ϕ_o are measured with a clinometer. This device is essentially a bubble level with a vernier readout that is accurate to ± 1 minute of arc. The clinometer is placed on the table in the direction $A_i = 0$ and the reading noted. The positioner is then turned to the angles, $A_i = 90^o$, $A_i = 180^o$ and $A_i = 270^o$, and the clinometer reading is noted at each position. The elevation angle offset is

$$\sin E_o = \sin \theta_o \sin (A_i + \phi_o) \qquad (4\text{-}27)$$

So when we plot the clinometer reading versus A_i we observe a sine function whose amplitude is sin θ_o and phase is ϕ_o, both of which can be determined by a least squares fit to the data.

The true elevation is just $E_t = E_i + E_o$, or

$$E_t = E_i + \theta_o \sin (A_i + \phi_o) \qquad (4\text{-}28)$$

using the small angle approximation.

The azimuth offset is most easily determined by observing a source. At night in the northern hemisphere, the positioner table can be pointed so that it is possible to sight Polaris along the side edge of the table. The azimuth offset is then $\phi_o = -A_i$. It is only slightly more complicated to use the sun instead of Polaris, either optically or radiometrically. If the optical metnod is used, a shadow can be observed rather than sighting the sun directly. To obtain a shadow, use a carpenter`s square to scribe a line on the positioner table perpendicular to the leading edge of the table. Rest the handle of the carpenter`s square on the table so that the line is centered along the handle and the ruler is extended upwards. Move the positioner until the shadow of the ruler lies along the scribed line and note the time and indicated azimuth. Given the time, latitude, longitude, and an almanac, the true azimuth of the sun can be calculated and the offset is $\phi_o = A_t - A_i$. Alternately, one can utilize the fact that the sun is a radio source that will increase the antenna temperature by approximately 25 K at both frequencies. The WVR can be manually pointed in the approximate solar direction until a peak reading is found from either the 21 or 31 GHz channel. Again note the time and indicated azimuth, calculate the true azimuth of the sun and solve for the azimuth offset as previously described.

E. CONTROLLER/INTERFACE MODULE DESCRIPTION

The controller/interface module consists of a LOCAL/REMOTE control panel and a microprocessor. The control panel is used primarily during installation and checkout. Any signal from either the microwave module or positioner can be selected and the voltage displayed on a 3-digit voltmeter built into the panel. Signal output ports are available to drive a chart recorder if desired. Toggle switches are provided to move the positioner in azimuth and elevation. Under normal operating conditions the control panel is switched to the REMOTE position, which connects all signals to the microprocessor. The microprocessor outputs signals that move the positioner, and actuate waveguide switches in the microwave module. Signals are input via an analog-to-digital (A/D) converter. Communications to a user terminal or host computer are made over an RS 232 serial interface.

1. Commands

The controller will accept commands for immediate execution, store commands for later execution, and/or will send a command receipt confirmation message before execution, when requested. There are five basic commands:

(1) Abort Pointing or Taking Data - Aborts pointing or taking data when the controlling computer (host) or operator determines that an operation has not been executed within the allotted time.

(2) Set Radiometer Mode to X - Sets waveguide switches in the microwave module so that the WVR "sees" one of the following:

X = 1: Hot load
X = 2: Base load
X = 3: Antenna

(3) Point to Azimuth = aaaa, Elevation = eeee - Initiates pointing the positioner module. The four-digit values for az and el are in counts. Calibration data stored in the controller convert these angles into the required counts, which are then included in the commands.

(4) Set Submultiplexer to Channel XX - Analog water vapor data received by the microwave module is returned through a 16-channel multiplexer. One channel is dedicated to a submultiplexer, which provides access to 16 additional analog data channels.

(5) Exit to WVRMON - Aborts any incomplete operation and calls the WVR monitor program (WVRMON), which troubleshoots malfunctions.

2. WVR Data

Water vapor data are delivered by the controller in response to one of the data prompts listed below.

(1) Display Calibration Data - The controller responds with a block of calibration data stored in the controller when the WVR was calibrated as a unit. The calibration data includes values for converting counts to temperatures for the microwave module, counts to angles for the positioner, and counts to voltages for the controller. Calibration data formats are listed in Appendix A.

(2) Return All Radiometer Data - Returns the following data:

- Pointing status
- Data taking status
- Last submux channel selected
- Current WVR mode; e.g., hot load, base load, antenna

(3) Return Voltage Data - Returns the output of the A/D converter 16-channel multiplexer in 4-digit numbers, representing the A/D output (voltage) in counts.

(4) Return Temperature Data - Returns 16 channels of temperature sensor data through the submultiplexer

(5) Return One Mux Channel - Returns a single reading for mux channel XX, where XX ranges from 0 to 15.

(6) Return One Submux Channel - Same as above for submux channels.

(7) Fast Sampled Data - Used primarily for testing and calibration.

3. Controller Hardware Description

Figure 4-7 shows schematically the relation between the three WVR modules and the host computer. The controller module serves as the local control and monitor point for troubleshooting diagnostics and to transfer control to the microprocessor in the REMOTE position. Refer to Figure 4-1 for a block diagram of the controller.

Figure 4-8 is a drawing of the control panel. The function of each item on the control panel is as follows:

(1) POWER - Power on/off for all components except the microprocessor.

(2) DIGITAL PANEL METER (DPM) - Digitizes and displays the various voltages from the microwave and positioner modules.

(3) METER SELECT - Manual selection of the voltage to be displayed by the digital panel meter. The various positions are listed in Table 4-1 along with nominal values.

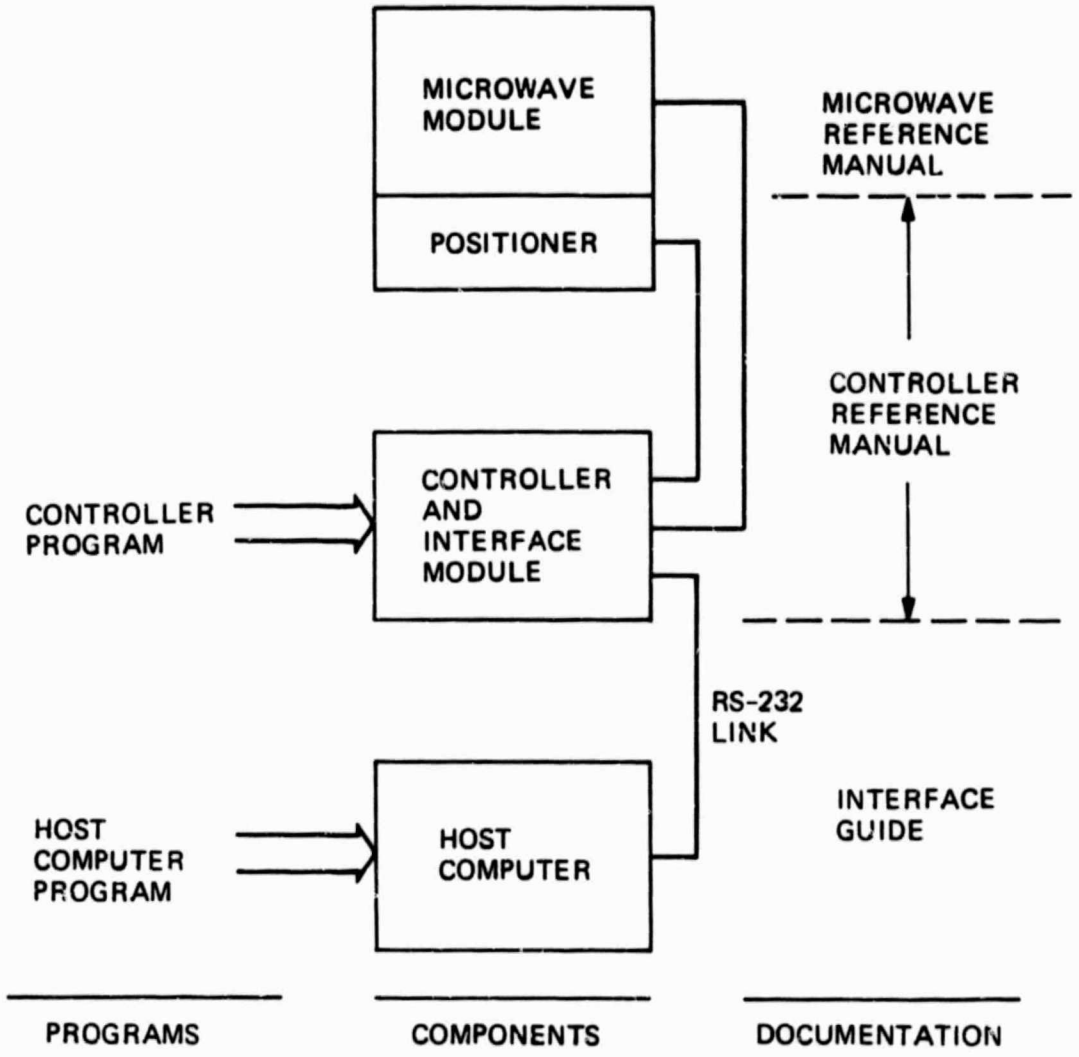

Figure 4-7. Water Vapor Radiometer Software and Component Interfaces, and Related Documentation

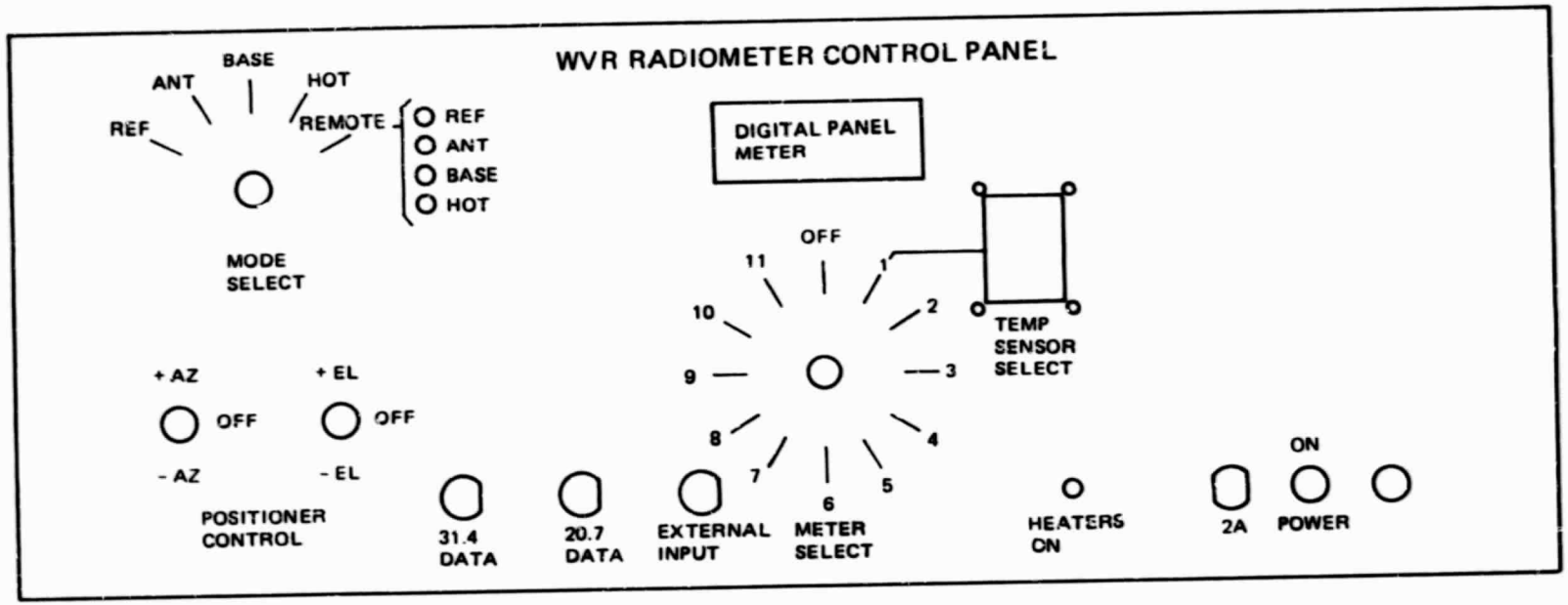

Figure 4-8. WVR Local Control Panel

(4) TEMPERATURE SENSOR SELECT - Manually addresses the physical temperature sensors via the submultiplexer. The correspondence between the sensor select switch and the physical placement of the sensors is given in Table 4-1.

(5) HEATERS ON/OFF - A single light emitting diode (LED) is provided to indicate whether the heaters in the microwave module are on or off.

(6) EXTERNAL INPUT - A BNC jack is provided so that an external voltage can be displayed on the DPM. This is useful to check the meter calibration.

(7) MODE SELECT SWITCH - Manual selection of radiometer mode. Both channels are switched to hot load, base load, reference load, antenna, or REMOTE. In the REMOTE position the mode select is controlled by the microprocessor.

(8) MODE INDICATOR - A set of LEDs that indicate which radiometer mode is selected. Indicates in both LOCAL and REMOTE positions.

(9) POSITIONER CONTROL - Bi-directional toggle switches that provide manual control of the azimuth and elevation of the positioner. Figure 4-9 illustrates the positioner movement with respect to these switches.

(10) DATA JACKS - BNC jacks that provide the analog output voltages from the 20.7 and 31.4 GHz synchronous detectors.

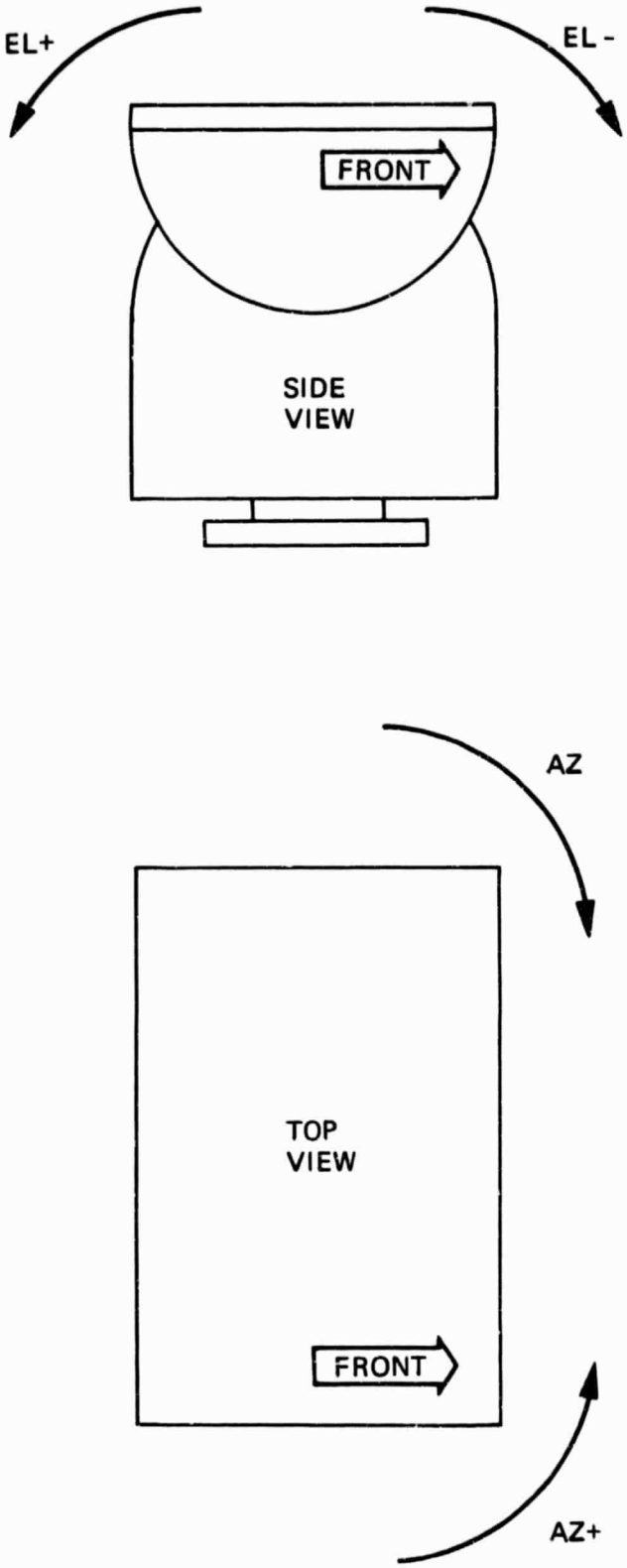

Figure 4-9. Positioner Movement Directions

Table 4-1. Meter Select Switch Positions and Nominal Voltage Values

Meter Select Switch Position	Temp. Sensor Select Switch	Nominal Voltage*	Display
1	0	2.2	Hot load 21 GHz
	1	1.4	Base load 21 GHz
	2	1.4	Ref load 21 GHz
	3	2.3	Hot load 31 GHz
	4	1.4	Base load 31 GHz
	5	1.4	Ref load 31 GHz
	6	1.4	Mounting plate
	7	11.2 (Open)	Spare
	8	1.9	Horn ant 21 GHz
	9	1.9	Horn ant 31 GHz
	10	11.2	Spare
	11	11.2	Spare
	12	1.7	Enclosure air temp
	13	2.0	5 kΩ resistor (2 kΩ on ant R04)
	14	1.0	1 kΩ calibration resistor
	15	9.6	9.5 kΩ calibration resistor

*May vary ±10% between WVR units

The microprocessor consists of three circuit boards, a four-slot card cage, power supply, and front panel containing a power ON/OFF and RESET switch. The three circuit boards are: 1) a single board computer, 2) an expansion memory board, and 3) an analog INPUT/OUTPUT board. All boards are MULTIBUS*

*MULTIBUS is a registered trademark of the Intel Corp.

Table 4-1. Meter Select Positions and Nominal Values (Contd)

Meter Select Switch Position	Nominal Voltage	Display
2	9.0	Hot)
	7.8	Base) 21 GHz
	9.0	Ref) Analog output
	1.5 to 5.0	Ant)
3	9.1	Hot)
	7.8	Base) 31 GHz
	7.9	Ref) Analog output
	1.2 to 6.0	Ant)
4	1.7	Hot)
	3.3	Base) 21 GHz
	4.9	Ant) Mode control voltage
	1.5	Ref)
5	1.7	Hot)
	3.3	Base) 31 GHz
	4.9	Ant) Mode control voltage
	1.5	Ref)
6	1 to 7*	Azimuth
7	1 to 7*	Elevation
8	0 to 11	External input
9	-	Spare (N.C.)
10	-	Spare (N.C.)
11	-	Spare (N.C.)

* The azimuth and elevation signals are voltages read from the wipers of the potentiometers that are connected to the azimuth and elevation axis. Changes in the gain and excitation voltage will affect the particular value. Compensation is made for these changes in software residing in the Host computer.

compatible. Manufacturer's documentation for all microprocessor components is supplied with each WVR. The single board computer is one of the 80/10 series from National Semiconductor Corp and is built around the 8080 microcomputer. All boards have at least 4 kbytes of space for programmable read-only memory (PROM) and 1 kbyte to 4 kbytes of random access memory (RAM). In addition, there is a serial I/O port that is jumpered for RS-232 operation. The baud rate can be set with jumpers and is set up for delivery at 9600 baud. The expansion memory board is from Monolithic Systems Inc. and contains 8 kbytes of RAM and sockets for up to 8 kbytes of PROM. The analog I/O board is from Analog Devices Inc. and contains: 1) a 12-bit A/D converter with sample and hold circuitry, 2) a programmable gain amplifier, 3) a 16-channel (double ended) input multiplexer, 4) dual 12-bit digital-to-analog (D/A) converters, 5) a pacer clock and 6) a socket for 1 kbyte of PROM. In the current configuration of the controller hardware the analog I/O board operations are memory mapped and the board requires 4 kbytes of address space.

4. Controller Software Description

The software installed in May 1981 in the microprocessor controller for WVR units R01 through R08 is referred to as "WVR-V3.0". This set of programs has been extensively upgraded from previously issued versions to provide enhanced operation of the monitor program and compatibility with the Mark III Microprocessor ASCII Transceiver (MAT), while preserving compatibility with existing host computer programs (see Ref. 17 for a definition of the MAT interface and functions).

The program WVR-V3.0 (as well as its predecessors) was created on an INTEL microcomputer development system using a CP/M* (vers. 1.4) operating system. Program segments are compiled, assembled, linked, and loaded on the development system and then "burned" into PROMs. The PROMs are then plugged into the 3 WVR microprocessor boards and tested under operating conditions. Once the program has been debugged, it can be burned into a set of PROMs which are then sent to each WVR location and installed in the field.

*CP/M is a trademark of Digital Research Inc.

5. MAT Compatibility

WVR3 is fully compatible with the MAT although the nature of the radiometer does not permit an exact emulation of the host computer to MAT interface. Some of the responses, while meaningful, will not be exact duplicates of the responses given by the MAT. These differences are due to the nature of the WVR and should not interfere with the operation of the WVR or MATs when they are combined on a single RS-232 daisy chain. The user should note that the WVR microprocessor does not have two serial I/O ports. Thus if the WVR is used on the MAT daisy chain it must be the very last device on the chain.

WVR3 has no alarm state implemented as yet, but will accept certain control characters as command terminations to provide normal operation under either HP/MAT or existing host computer conventions.

6. Start Up

Refer to Figure 4-10, the simplified flowchart of WVR3, for the following discussion. WVR3 is installed in PROMs on the BLC80/xx CPU board (PROMs 00, 04, and 08) and the memory expansion board (PROMs 60, 68, and 70). The CPU board PROMs contain initialization and monitor programs written in assembly language. The expansion board PROMs contain the WVR3 main program and subroutines, written in Fortran-80 and the M80 relocating macro assembler.

Upon application of power or the pressing of the RESET switch, the CPU begins operation at location 0 (MEMBASE:). There a jump instruction jumps the program counter past the interrupt vectors and enters the initialization routine at INIT:. This routine sets up the USART for 9600 baud, 7 data bits, even parity, and two stop bits. It then sets up vectors and the stack using RAM memory on the CPU board. It then verifies the existance of the first instruction in PROM 08, and if it is there, program execution is passed to PROM 08 to initialize the WVR program.

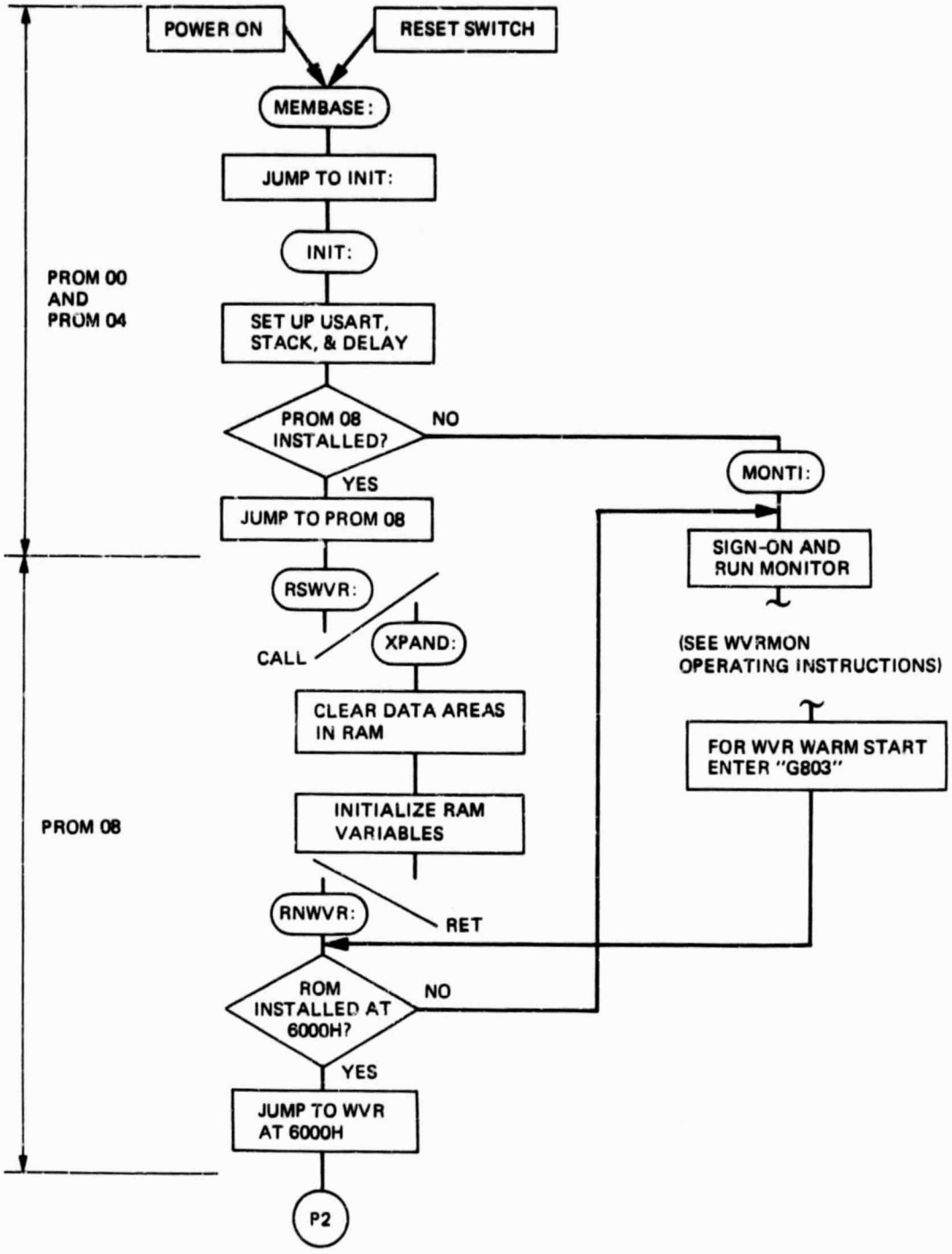

Figure 4-10. WVR3 Simplified Flowchart (Sheet 1 of 2)

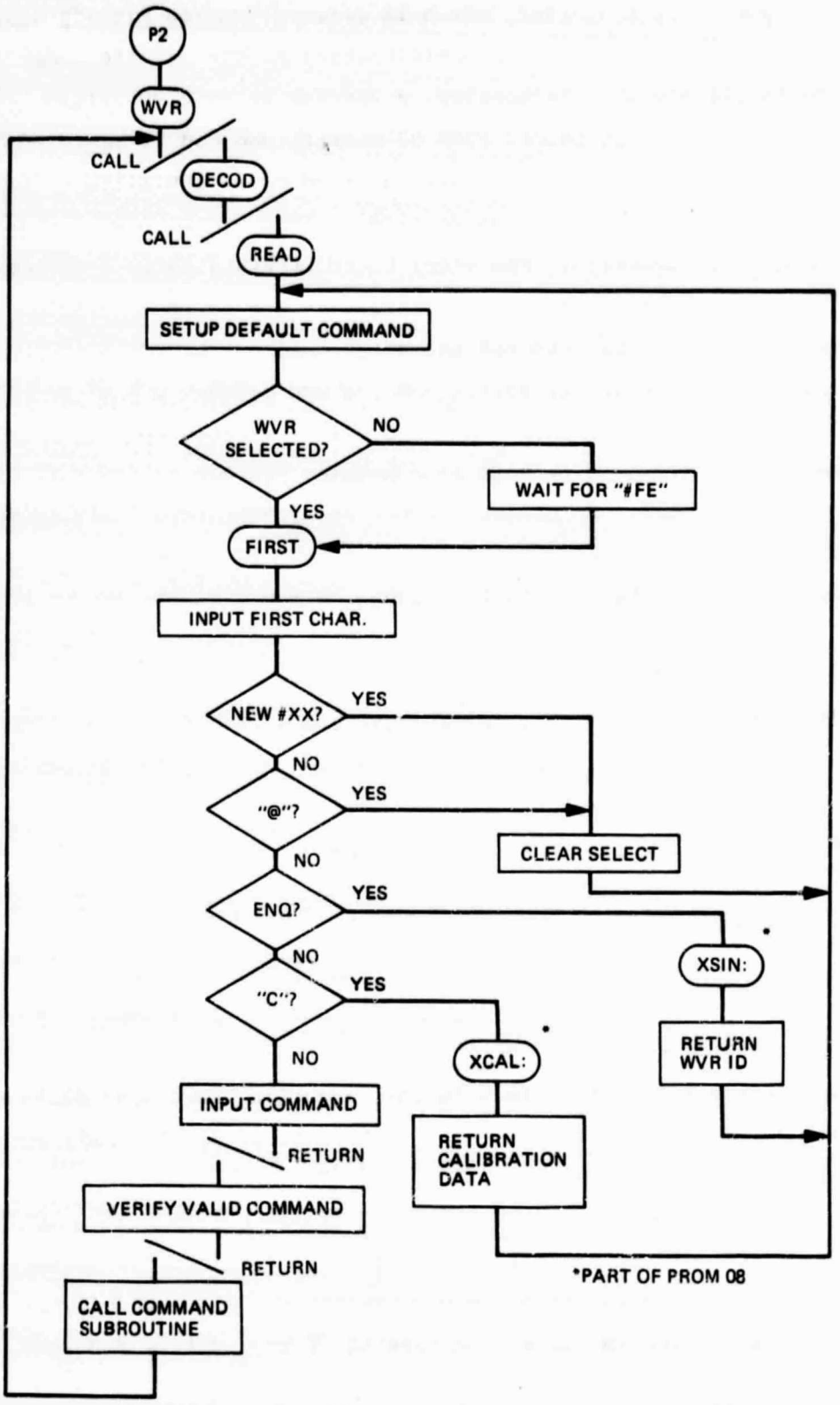

Figure 4-10. WVR3 Simplified Flowchart (Sheet 2 of 2)

If no PROM 08 is installed, WVROM is entered instead and signs on with the message "WVROM..." to permit troubleshooting at the machine language level. (To facilitate troubleshooting, a version of PROM 00 marked "NO AUTO START" is installed in the unused PROM 0C socket, and can be moved to PROM 00 socket to force execution of WVROM, whether PROM 08 is installed or not).

If PROM 08 is installed, the entry to it (RSWVR:) calls a subroutine that performs the initialization of RAM areas on the memory expansion board. These areas contain the buffers and variables used by the WVR 3 program. This initialization is necessary as Fortran-80 and M80 produce a load module that expects to be loaded into an all-RAM computer. Constants and variables with initialized values are part of that load module, but can not be part of a PROMmed version of WVR3. These data values were compressed (only non-zero values recorded) into a table that is part of PROM 08. The PROM 08 XPAND: subroutine expands the table into the expansion board RAM to permit proper execution of WVR3.

XPAND: returns to RNWVR:, and a quick check is made of the PROM starting address of WVR3 to see if the expansion board is installed. If not, WVRMON is entered. Otherwise a jump is made to the WVR3 start address at 6000H (PROM 60).

7. WVR3 Operation

Refer to sheet two of Figure 4-10 for the following. The WVR3 main program is entered at address 6000H, and after some initialization (including establishing a new stack in the expansion board RAM) calls subroutine DECOD. DECOD immediately calls READ (part of module RDWT) for the input of a command line.

READ includes all the code that is responsible for making the radiometer compatible with the MAT bus conventions. READ establishes the radiometer in the selected state upon receipt of the address #FE, and

maintains it until receipt of any other address or the ASCII reset character @. Turn-around delays for MAT are included in READ. A default command is established to return the radiometer status line in response to the MAT ? inquiry. Controls are included to permit pending of commands and/or data requests and echoing command line inputs. READ also includes the responses to ENQ and C requests for radiometer identification and calibration data.

If none of these special inputs are received, READ inputs a command line or data request and returns to DECOD. This subroutine analyzes the input line for valid commands and the correct number and format of operational parameters. DECOD then returns to the WVR3 main program.

8. Command Data Request Execution

The main program calls a subroutine depending on the command or data request character(s) in the input line. Each command or request has its own subroutine call. All of these are not included in the flowchart since operation at this level is straightforward. One subroutine is called, it executes the command or data request, then returns to the main program, error checks are made, and the operation loops back as shown on sheet two of Figure 4-10. The one exception is the abort command A, which is executed within the main program.

Command	Subroutine called
A (Abort)	none
M (Mode)	SMODE
P (Point)	POINT
S (Submultiplexer)	SUBMUX
X (Monitor)	MONITR
Data request	
D (Data)	ODATA
FS (Fast sample data)	DATAI

Descriptions of each of these subroutines are given in Appendix B. The program listings themselves will also have to be consulted for additional information.

SECTION V
TESTING AND CALIBRATION

A. TEST PHILOSOPHY

The test philosophy was consistent with the research and development nature of the WVR implementation task. The primary test objective was to determine if the WVR could pass a larger test: Does the instrument really calibrate water vapor effects in radio interferometric data? Testing for component failures or determining the mean time to failure was not rigorously pursued. In general, testing took place in parallel with fabrication and assembly. Some purchased parts and some parts fabricated at JPL were simply tested for conformance with procurement and performance specifications. The operating characteristics of critical components, such as the hot loads and detectors, were tested in detail. The results were documented and cataloged for future reference, as were the results of the full-up system tests for the individual modules.

B. TEST PROCEDURES

A total of 15 test procedures were developed to test the various assemblies of the WVR. These tests varied in complexity, generally required a test jig, and culminated in a 30-hour performance test of the instrument. For testing purposes the differences between the various WVR models designated R01 through R08, are described as follows. All test procedures apply to WVR units R04 through R08. Test procedures 1, 2, 7, 8, 11, 12, 13, 14, and 15 apply to units R02 and R03. Procedures 2, 5, 8, 10, 12, 13, 14, and 15, apply to unit R01.

Procedure 1 - Using a test jig, verify correct operation of the board containing the positioner control electronics.

Procedure 2 - Using a test jig, verify correct operation of the board containing the temperature sensor multiplexer electronics. Check temperature scale calibration to better than 1%.

Procedure 3 - Using a test jig, verify the mode control logic board operation.

Procedure 4 - Using a test jig, verify the correct operation of the video demodulator terminal board.

Procedure 5 - Using a test jig, exercise and calibrate the hot load assembly.

Procedure 6 - Using a calibrated power meter, attenuators, and signal generator, verify the amplitude and frequency response of the detector-video amplifier assembly.

Procedure 7 - Using appropriate test equipment, exercise, test, and calibrate the power, heat, and over-temperature control assembly.

Procedure 8 - Using a test jig, verify correct operation of the Local/Remote switch logic.

Procedure 9 - Using a test jig and spray coolant, test the power supply assembly. Verify operation as various components are heated or cooled to operating temperature limits.

Procedure 10 - Using appropriate test equipment, exercise the control panel assembly in all possible switch positions and verify correct control logic.

Procedure 11 - Using various test equipment, bench test the entire radiometer electronics assembly. Check all dc voltages, coaxial connectors, overheating, total power consumption. Verify operation of over- and under-temperature protection circuits. Adjust local oscillator voltages as needed. Exercise and verify all logic modes. Verify Dicke switch levels and freqencies. Check all components for abnormal temperature sensitivity. Adjust power level to detectors as needed. Check and verify linearity of entire operating assembly.

Procedure 12 - Using appropriate test equipment, measure and adjust the time constant (integration time) of the low-pass filter on the output of each WVR channel.

Procedure 13 - Using a sweep signal generator, harmonic mixer, and standard gain horn, check the operation and frequency response of the microwave components. Verify correct frequency, sideband response, and impedance matching between components.

Procedure 14 - Connect microwave module to positioner and to the controller microprocessor. Load test program that exercises all functions. Run for 24 hours and check for failures.

Procedure 15 - This was in reality a series of tests combined in one 30-hour session and performed after each WVR passed all bench tests. The unit was placed outdoors with a temperature-stabilized absorber over the aperture of the horn antennas. The microprocessor was connected to a host computer and test software commanded the WVR through a measurement cycle every minute for the entire test. Warmup characteristics from all temperature sensors were measured and documented as well as the response to diurnal variations of temperature. For a 26-hour period after warmup, the measured brightness temperature from the WVR was compared to the measured temperature of the aperture load. Residuals were plotted and analyzed to verify a noise-like distribution whose width conformed to the measured bandwidth and integration time of the radiometer.

In addition to the above procedures, several WVRs were subjected to additional testing when rather subtle variations were found in the temperature scale calibration. These additional tests included hot and cold aperture load tests in which the effective system noise temperature was remeasured and the switch isolation was verified. Other tests revealed that power from the local oscillator was leaking into the microwave enclosure, which was acting like a resonant cavity. The enclosure deformed as the WVR was pointed at different elevation angles and the resulting change in resonance led to a small change in gain. Unfortunately, most of the WVRs had been delivered by the time this was discovered. Modification kits were prepared and sent to the various WVR field locations.

C. CALIBRATION

Two types of calibration are required for the WVR. First, a frequent calibration of the relative gain of the instrument, and secondly a less frequent calibration of the absolute gain. The reference load of the Dicke switch is kept at the same temperature as the rest of the electronics. This means that the Dicke receiver is not fully stabilized (e.g., see Ref. 11) and susceptible to gain changes. Determination of the relative gain is accomplished by setting internal switches in the WVR so the the input of the Dicke receiver is connected to either of two waveguide terminations. One termination is kept at an elevated temperature (100^{o}C) and is called the hot load while the other is kept at the same temperature as the rest of the electronics (43^{o}C) and is called the base load. The physical temperature of these loads is measured with thermistors and denoted by TH and TB respectively. The output of the receiver is digitized and presented to the user as a number N that we shall term "counts". In order to determine an unknown antenna temperature TA we can (in principle) go through the observing sequences-hot load, base load, antenna, and observe the outputs TH, TB, NH, NB and NA. For an ideal radiometer the antenna temperature is simply

$$TA = TB + [(TH-TB)/(NH-NB)]\ (NA - NB) \qquad (5\text{-}1)$$

where the quantity in square brackets is called the relative gain or simply the gain of the instrument and is expressed in units of kelvin/count. For all of the WVRs, the value of the gain is approximately 0.1 K/count, and is determined by the product of the gains from all circuit elements extending from the Dicke switch to the analog-to-digital converter. Figure 5-1 illustrates the typical fluctuations in the gain from one of the WVR channels. We plot the relative gain, i.e. by subtracting out the average, versus time for a 40-hour period. A diurnal variation of $\pm$4% is quite obvious and is due primarily to temperature changes inside the microwave package. Superimposed on the diurnal variation are short term fluctuations due primarily to radiometer noise which can be reduced by averaging or smoothing.

Equation (5-1) describes an ideal radiometer. A real instrument suffers various shortcomings such as attenuation, less than perfect switch isolation,

Figure 5-1. Gain of One WVR Channel vs Time

reflections, etc. The calibration of absolute gain involves finding the correction factor that puts Eq. (5-1) closer to the absolute temperature scale. One of the procedures that can be used to find the instrumental correction factor is called a "tip-curve" and it is used to derive a correction to the hot load. Let us assume that we can rewrite Eq. (5-1) for a real radiometer as

$$TA = TB + [TH-TB+\Delta TH]\ N' \tag{5-2}$$

where $N'=(NA-NB)/(NH-NB)$ is the normalized count in the antenna mode, and TH is the hot load correction. The brightness temperature of the sky can be written

$$T_b = T_c e^{-\tau} + T_m(1-e^{-\tau}) \tag{5-3}$$

where T_c=2.9 K is the cosmic blackbody background, T_m is the mean radiating temperature of the atmosphere, and τ is the opacity. The mean radiating temperature exhibits some seasonal and site variations but with a reasonable degree of approximation we can assume that it is constant and equal to 275 K. For a stratified atmosphere the opacity can be expressed as

$$\tau = \tau_o(AM) \tag{5-4}$$

where τ_o is the zenith opacity and AM = 1/sin(elevation) is the air mass. Suppose we make a series of observations, first observing the internal loads to get TB, TH, NB, and NH, and then moving to different elevation angles to get NA_1, NA_2, ...etc., at positions AM_1, AM_2, ... etc., and assume that $TA=T_b$ Eq. (5-2), (5-3), and (5-4) can be combined to give

$$N_i' = [T_M + T_B + (T_c-T_m)\exp(-\tau_o AM_i)]/(TH-TB+\Delta TH) \tag{5-5}$$

Thus we have expressed the observable from the WVR as the dependent variable in terms of the independent variable AM_i, and the two parameters τ_o, and ΔTH. Given two or more observations at different AM_i, it is straightforward to solve for τ_o and ΔTH that are "best" in the least squares sense. Figure 5-2 shows tip curve data taken with WVR-R07 (31.4 GHz) located at Goldstone in May of 1981. All WVRs are calibrated in this manner prior to

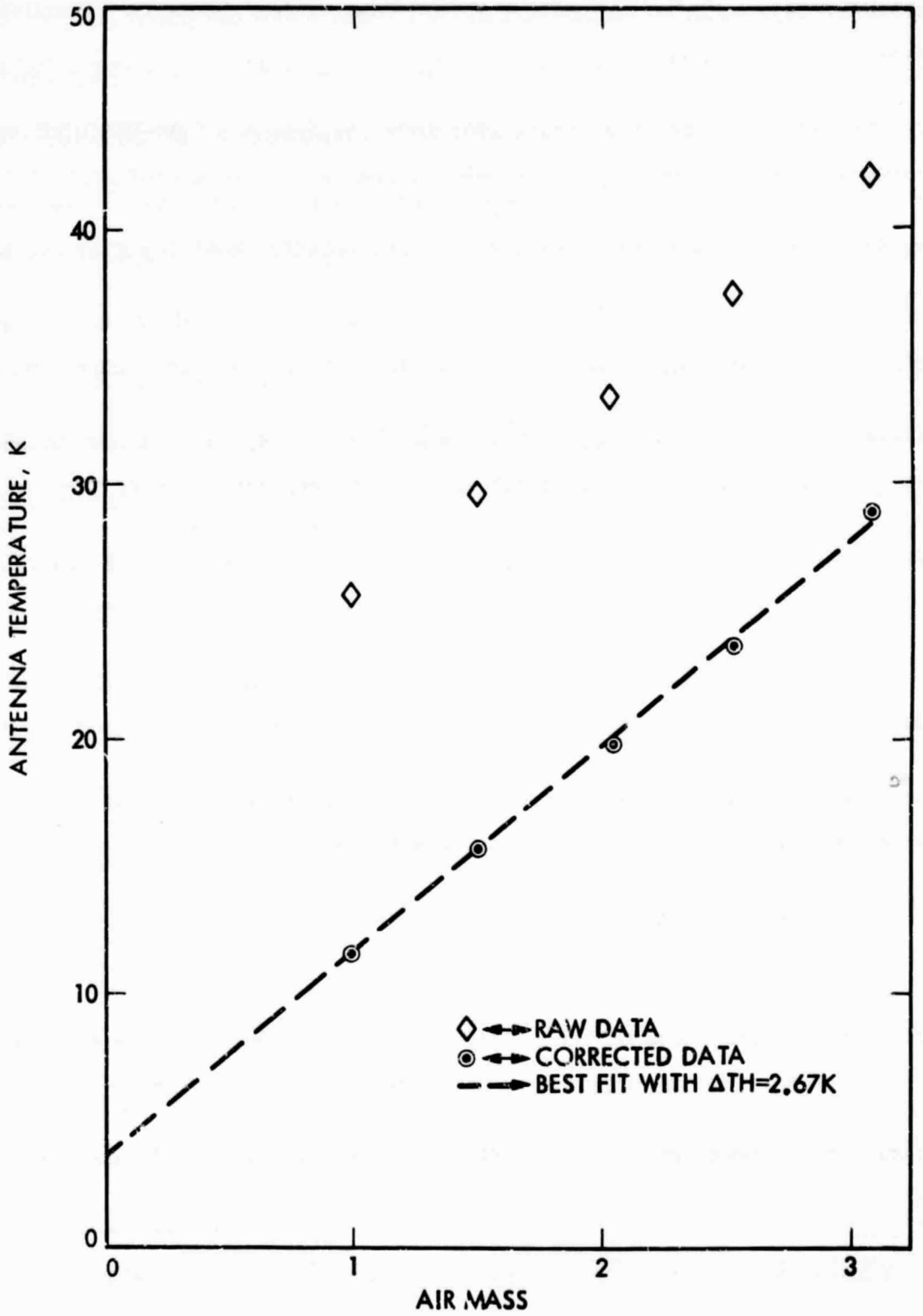

Figure 5-2. Tip Curve Determination of Hot Load Correction

shipment. In addition, the temperature scale of each radiometer channel is checked by observing hot and cold aperture loads which serves as a consistency check.

The proof of WVR performance lies in a comparison of the WVR with some independent (and hopefully more accurate) technique of measuring vapor path delay. The most convenient comparison technique is to use a radiosonde to provide a vertical profile of temperature and relative humidity that can be integrated to give an estimate of the zenith path delay which we then compare with the delay estimate from the WVR that is observing at the zenith. Figure 5-3 shows two such comparisons, the first made in May 1974 and the second in May 1975, which was reported in Ref. 5. Figure 5-4 shows previously unpublished data that was taken at Pt. Mugu, California in 1976 and Figure 5-5 shows the histogram of the residuals for this experiment. During the Pt. Mugu experiment an instrumented aircraft flew various slant paths up to a maximum altitude of 3 km which provided a larger range of path delay estimates than are normally obtained from radiosondes. These data are shown in Figure 5-6.

The rms residuals from these comparisons are, 1.6 cm from 1974, 1.1 cm from 1975, 1.5 cm from 1976 WVR/radiosonde, and 1.4 cm from 1976 WVR/aircraft (excluding data at 10 deg elevation). If the two techniques are truly independent, then we expect the rms residual to be the root-sum-square of the error from each technique. If we take the average rms residual to be 1.5 cm, assume that the radiosonde has a 10% accuracy, and the average path delay to be 1.0 cm, then we infer the accuracy of the WVR to be 1.1 cm.

The WVR used in the experiments just described operated at 22.2 and 31.4 GHz. Unfortunately none of the newer WVRs has undergone such comparison. If anything, the older radiometers should be noisier due to the greater sensitivity to the vertical distribution of vapor. Guiraud et. al., in Ref. 11, report a radiosonde comparison with a WVR that operates at 20.6 and 31.6 GHz and infer a WVR accuracy of 0.5 cm. The newer WVRs are expected to demonstate comparable performance.

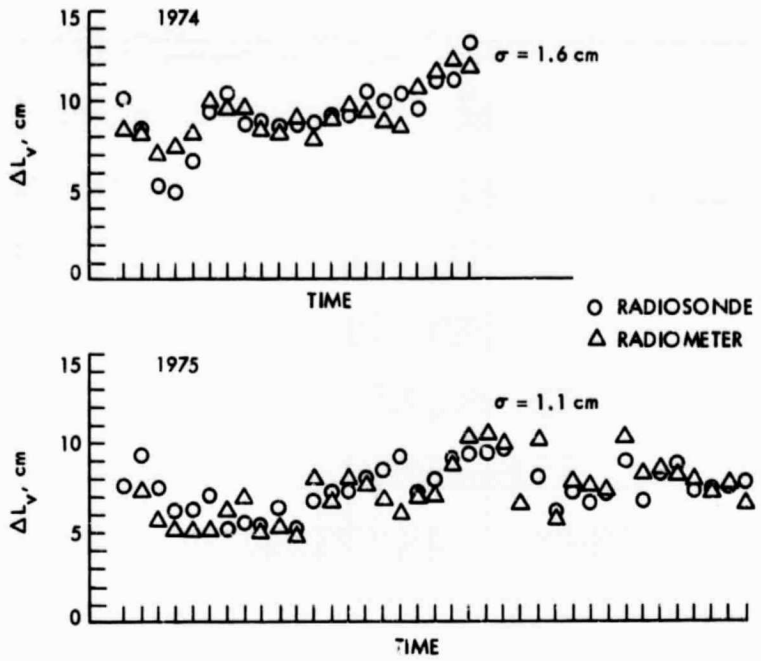

Figure 5-3. Comparison of Path Delay Determined by Radiosonde and WVR at El Monte, California, 1974 and 1975

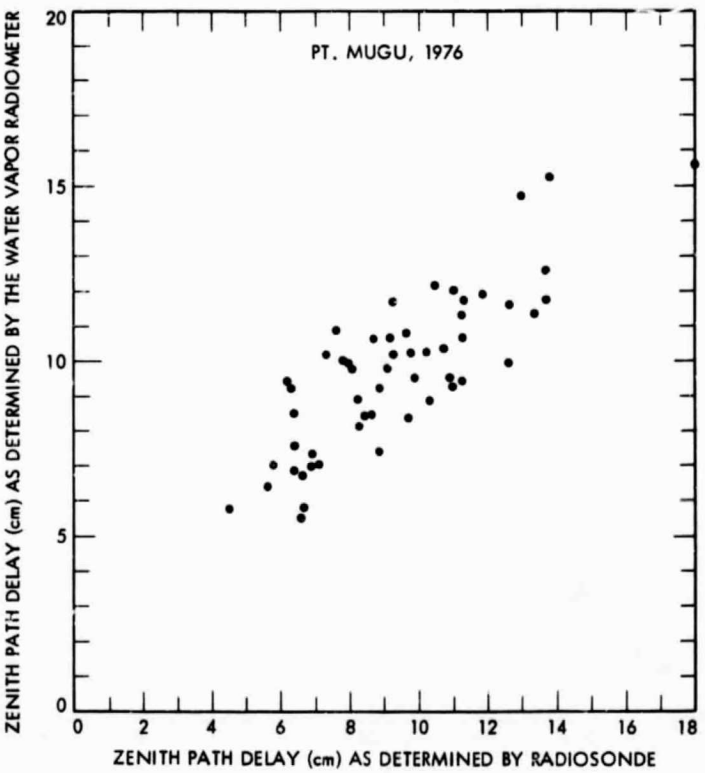

Figure 5-4. Comparison of Path Delay Determined by Radiosonde and WVR at Pt. Mugu, California, 1976

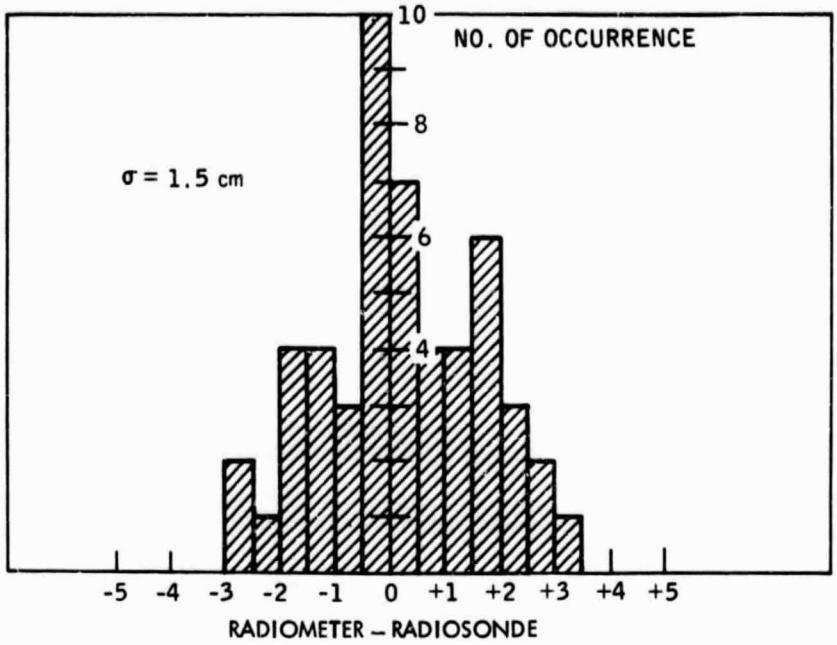

Figure 5-5. Histogram of Path Delay Residuals From Pt. Mugu Data

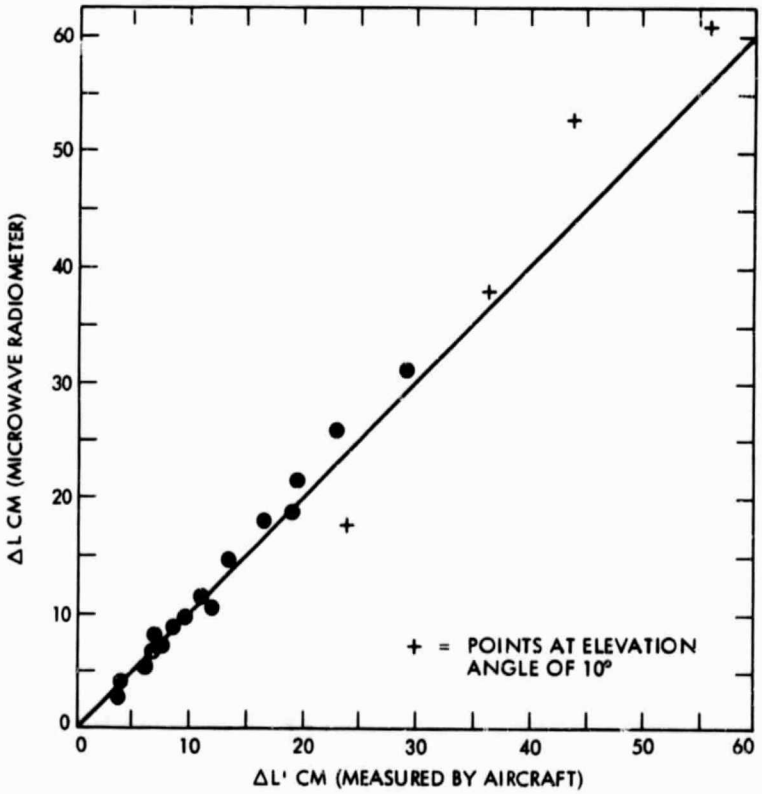

Figure 5-6. Comparison of Path Delay, Instrumented Aircraft vs WVR at Pt. Mugu

The instrumental correction factor should be constant for long periods of time (e.g., years). There are circumstances that could cause it to change slowly or dramatically. For instance, it is possible that the waveguide walls could deteriorate slowly in time due to atmospheric constituents. If the enclosure is leaking and there is a sudden change from warm damp conditions to cold conditions then liquid water or ice could form in the waveguide or switches or on the cover of the horn antenna. In either case the performance of the instrument will change and the pre-determined value of ΔTH will not be valid. It is recommended that tip-curves be performed periodically and the results kept as a history of the instrumental performance.

SECTION VI
INVERSION ALGORITHMS

A. INTRODUCTION

Water vapor radiometers will be operated under a wide variety of meteorological conditions. Several algorithms can be used to estimate the signal time delay from the observed microwave brightness temperature and to account for systematic effects due to site and seasonal variations. The excess path length can be expressed as an integral of the vapor density divided by the temperature integrated along the line of sight. The accuracy of the estimated delay, as indicated by a simulation calculation, is approximately 0.3 cm for a noiseless WVR in clear or moderately cloudy weather. With a realistic noise model of WVR behavior, the inversion accuracy is approximately 0.6 cm.

B. REFRACTION

The primary atmospheric propagation effect that concerns the geodesist or navigator is refraction. The apparent or electrical path length L_e, along some atmospheric path L, is defined as

$$L_e = \int_L n(s)ds \tag{6-1}$$

where n(s) is the refractive index at the position s.

As a matter of convenience we will work with the excess path length $\Delta L = L_e - L$ or

$$\Delta L = \int_L (n-1)ds \tag{6-2}$$

Since the refractive index of the atmosphere departs from unity by only a few parts per ten thousand (or less), it is customary to use the refractivity N, defined as

$$N = (n-1)10^6 \tag{6-3}$$

so that the refractivity of a unit volume is characterized by this number of N units, typically on the order of 320 at sea level. Bean and Dutton (Ref. 18) discuss several formulations of N as a function of atmospheric parameters. Used here is the form given by Smith and Weintraub (Ref. 4);

$$N = 77.6 \left(\frac{P}{T}\right) + 3.73 \times 10^5 \left(\frac{e}{T^2}\right) \tag{6-4}$$

where P = total pressure (mb), T = temperature (K), and e = partial pressure of water vapor (mb). This expression is considered accurate to 0.5% for frequencies less than 30 GHz in normal ranges of temperature, pressure, and relative humidity. Note that the total refractivity can be written as the sum of a "dry" term $N_d = 77.6\ (P/T)$ and a "wet" term $N_v = 3.73 \times 10^5\ (e/T^2)$ that yields both a dry ΔL_d, and wet ΔL_v, path delay correction:

$$\Delta L_d = 77.6 \times 10\text{-}6 \int \frac{P}{T}\, ds \tag{6-5}$$

$$\Delta L_v = 3.73 \times 10^{-1} \int \frac{e}{T^2}\, ds \tag{6-6}$$

The concern here is with the wet term. Using elementary definitions, (e.g., see Ref. 19), Equation 6-6 can be rewritten as

$$\Delta L_v\ (cm) = 1.723 \times 10^{-3} \int_L \frac{\rho_v}{T}\, ds \tag{6-7}$$

where ρ_v is measured in units g/m^3, s is in meters, and a line-of-sight through the entire atmosphere is assumed. Since water vapor is not a well mixed constituent of the atmosphere, ΔL_v will vary according to site, season, and local meteorological conditions. Both the point value of the vapor density and its distribution vertically and horizontally will vary on a variety of time and spatial scales. Zenith values of ΔL_v vary from 3 to

20 cm and scale approximately as the cosecant of the elevation angle for other line-of-sight paths. In applications, observations are not usually made at the zenith but over a wide range of elevation angles for which El = 30° might be an average value. The path delay might therefore vary between 3 and 40 cm as extremes. Clearly, if accuracy goals are on the order of 3 m, water vapor effects can be ignored. If the accuracy goal is 30 cm, somehow the water vapor must be estimated, but the estimate of ΔL_v does not have to be very good, e.g., if Eq. (6-7) could be estimated with an accuracy of 50%, the system accuracy requirement might well be satisfied. In order to make this estimate a nominal model of the vapor distribution, $\rho_v(s)$ might be used and vertical and horizontal fluctuations might simply be ignored. If the goal is a 3 cm system accuracy, then the temporal and spatial variation of ρ_v along the line-of-sight cannot be ignored. The integral in Eq. (6-7) must be estimated while observing with the geodetic system. Accurate estimates of the line-of-sight path delay must be made from direct measurements or by use of the techniques of remote sensing.

C. FORMULATION OF THE ALGORITHM

Paragraph B established the problem as the estimation of the integral quantity,

$$\Delta L_v = 1.723 \times 10^{-3} \int \frac{\rho_v}{T} \, ds$$

A suggestion of how this quantity might be estimated can be gotten from consideration of Fig. 6-1. In this figure is plotted the calculated brightness temperature of a model atmosphere in the frequency range 10 to 40 GHz for three cases. The first case is for a standard atmosphere containing no water, i.e., $M_v = M_L = 0$ where M_v and M_L are the precipitable vapor and liquid, respectively, in units of g/cm^2. The precipitable vapor or liquid is defined as that mass of vapor or liquid that would be precipitated from a column extending through the entire atmosphere with a cross section of 1 cm^2. The second case shows the spectrum of an atmosphere containing M_v = 2 g/cm^2 distributed exponentially with a scale height of 2 km. The third case shows the same atmosphere with an additional liquid M_L = 0.1 g/cm^2

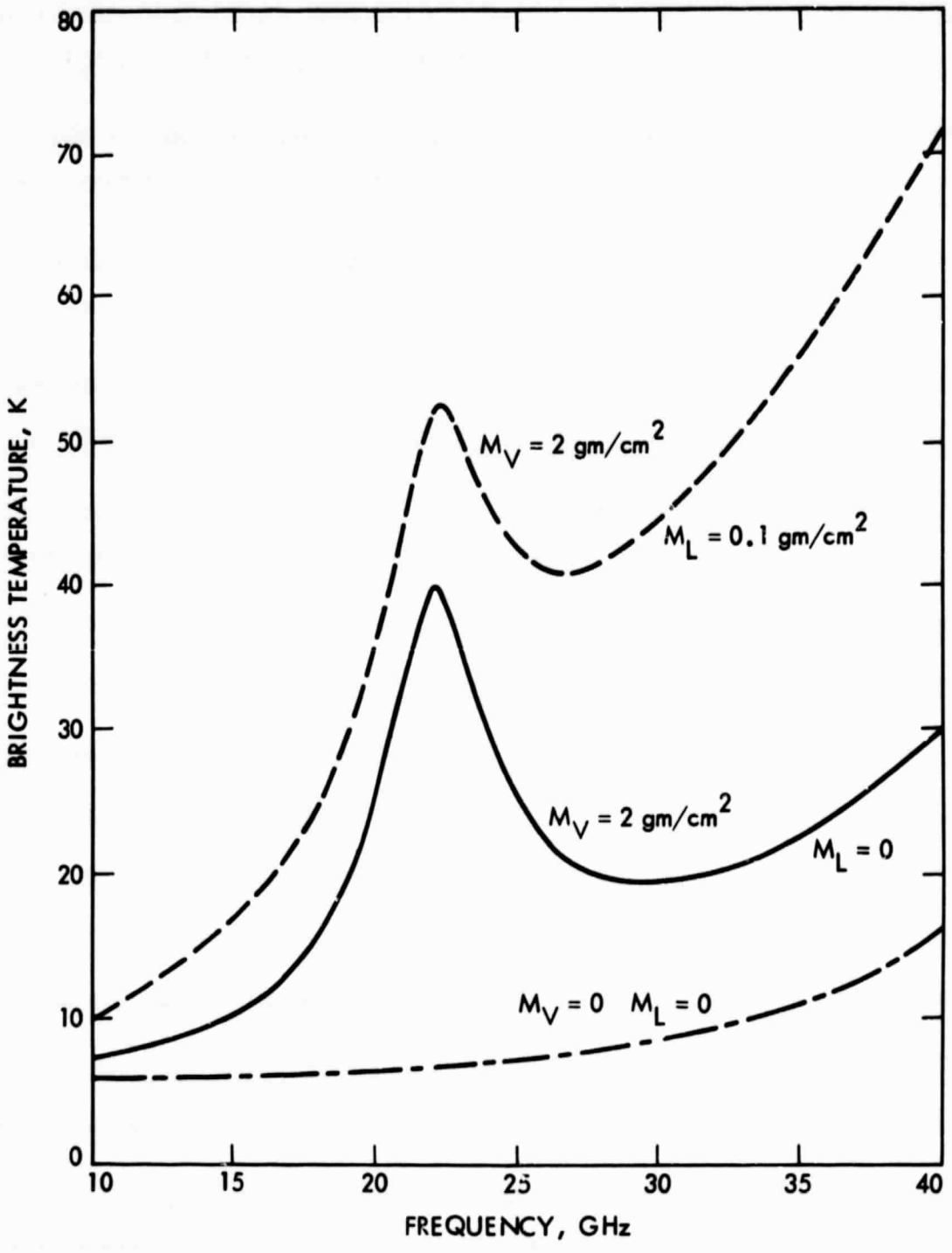

Figure 6-1. The zenith brightness temperature of a standard atmosphere for three cases: (1) no water vapor and no liquid water, (2) 2 g/cm^2 of vapor and no liquid, and (3) 2 g/cm^2 of vapor and 0.1 g/cm^2 of liquid

that is assumed to exist in small droplets. The "bump" in the curves for cases (2) and (3) is due to emission from the water vapor molecule, and it is apparent that the brightness temperature is a strong function of the amount of water vapor. Thus, a measurement of the brightness temperature is effectively an estimate of the integrated vapor density which constitutes a major portion of the integral in Eq. (6-7). The problem then is to find the explicit form of the relationship between brightness temperature and vapor path delay and to subtract out the effect of liquid water. In order to do this, the techniques of passive remote sensing will be used.

We will consider the emission and absorption properties of the atmosphere in terms of a gaseous medium in local thermodynamic equilibrium. For a nonscattering, nonrefractive medium, the equation of radiative transfer given by Chandrasekhar (Ref. 20) can be transformed using the Rayleigh-Jeans approximation of Planck's law of radiation to the form,

$$T_b(s) = T_b(0)\exp\left[-\tau(s, 0)\right] + \int T(s)\alpha(f, s)\exp\left[-\tau(s, s')\right] ds \qquad (6\text{-}8)$$

which is shown schematically in Fig. 6-2. Radiation at a frequency f of apparent blackbody temperature $T_b(s)$ is detected at position s from a medium that both emits and absorbs. Radiation $T_b(0)$ is incident on the medium at s = 0 and is attenuated by the factor exp $[-\tau(s, 0)]$. A unit volume of the medium at a physical temperature T(s), characterized by an absorption coefficient $\alpha(f,s)$, will emit radiation at frequency f, which is attenuated by the factor exp $[-\tau(s, s')]$. The optical thickness τ (or opacity), is defined as

$$\tau(s, s') = \int_s^{s'} \alpha(f, s'')\, ds'' \qquad (6\text{-}9)$$

By the mean value theorem of integral calculus the integral in Eq. (6-8) can be written

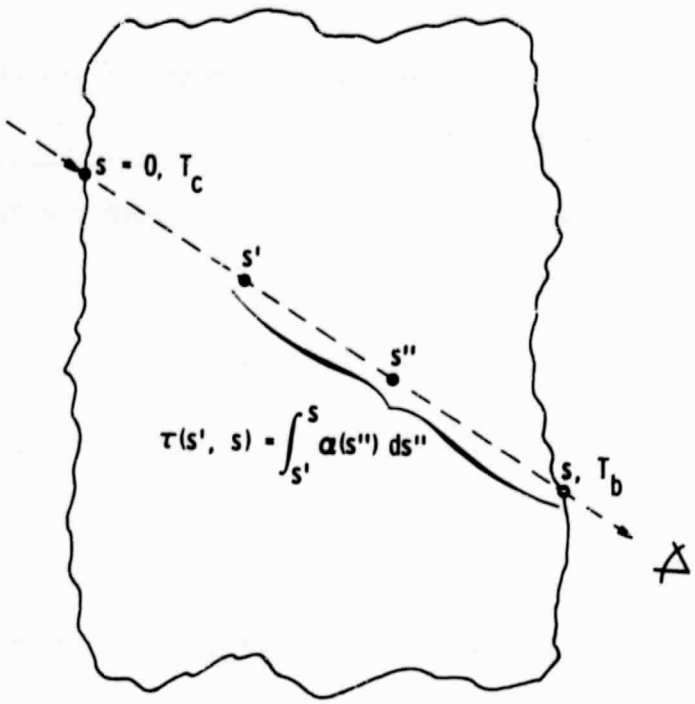

Figure 6-2. Schematic representation of the equation of radiative transfer

$$T \alpha \exp(-\tau)ds = T_M \int \alpha \exp(-\tau)ds \qquad (6\text{-}10)$$

where T_M is termed the mean radiating temperature of the atmosphere. Using this definition the solution to Eq. (6-8) is

$$T_b = T_c \exp(-\tau) + T_M [1 - \exp(-\tau)] \qquad (6\text{-}11)$$

For low values of the opacity ($\tau << 1$) $T_b \sim T_c$, i.e., the medium is transparent and we simply "see" the incident radiation which in this case is T_c, the cosmic blackbody background at an apparent temperature of 2.9 K.

For large values of the opacity ($\tau >> 1$) $T_b \sim T_M$, the medium is opaque and we "see" the gas radiating at its effective temperature. It is convenient to solve Eq. (6-11) for the opacity in the form,

$$\tau = -\log_e \left(\frac{T_M - T_b}{T_M - T_c} \right) \qquad (6\text{-}12)$$

We can express the total atmospheric absorption in Eq. (6-9) as the sum of its three primary contributors, a water vapor term α_v, a liquid term, α_L, and a "dry" term, α_d, that describes the background radiation primarily from the wings of a series of oxygen resonance lines near 60 GHz,

$$\tau = \int (\alpha_v + \alpha_L + \alpha_d)ds \qquad (6\text{-}13)$$

$$= \tau_v + \tau_L + \tau_d$$

Explicit formulations of the absorption coefficients can be found in the literature. This study uses Waters' form of the water vapor absorption coefficient (Ref. 21), Snider and Westwater's form for oxygen (Ref. 22), and Staelin's form for liquid water (Ref. 23). Since the water vapor absorption is a linear function of the vapor density we can write the vapor opacity term as

$$\tau_v = \int \left(\frac{\rho_v}{T} \right) \left(\frac{\alpha_v T}{\rho_v} \right) ds \qquad (6\text{-}14)$$

Thus, the opacity due to water vapor can be expressed in a form that contains the functional form (i.e., Eq. [6-7]) of the path delay integral.

To express the vapor opacity as a linear function of the path delay, $\tau_v = G(\Delta L_v)$ where G should be constant with respect to s but may be a function of frequency f, implies

$$G(f, s) = (5.803 \times 10^2) \left(\frac{\alpha_v T}{\rho_v}\right) \tag{6-15}$$

Let us suppose that we measure the brightness temperature at two frequencies f_1 and f_2 and transform the observables T_{b1}, T_{b2} using Eq. (6-12) to estimate the total opacity. At each frequency Eq. (6-12) can be written

$$\tau_1 = G_1 (\Delta L_v) + \tau_{L1} + \tau_{d1} \tag{6-16}$$

$$\tau_2 = G_2 (\Delta L_v) + \tau_{L2} + \tau_{d2} \tag{6-17}$$

Staelin (Ref. 23) has given an expression for the absorption coefficient for liquid water which varies as frequency squared so that $\tau_L = kf^2$, or $\tau_{L2} = (f_2/f_1)^2 \tau_{L1}$. In a similar manner the dry opacities scale by frequency according to $\tau_{d2} = \beta(f_2/f_1)^2 \tau_{d1}$, where the parameter β depends on f_1 and f_2. Thus, Eq. (6-17) is transformed to

$$\tau_2 = G_2 (\Delta L_v) + \left(\frac{f_2}{f_1}\right)^2 \left(\tau_{L1} + \beta \tau_{d1}\right) \tag{6-18}$$

which, together with Eq. (6-16), can be solved to give,

$$\Delta L_v = \left[G_1 - \left(\frac{f_1}{f_2}\right)^2 G_2\right]^{-1}$$

$$X \left[\tau_1 - \left(\frac{f_1}{f_2}\right)^2 \tau_2 - (1 - \beta)\tau_{d1}\right] \tag{6-19}$$

C-2

$$\tau_{L1} = \left[G_2 - \left(\frac{f_2}{f_1} \right)^2 G_1 \right]^{-1}$$

$$X \left[G_2 \tau_1 - G_1 \tau_2 - \left(G_2 - \beta \left[\frac{f_2}{f_1} \right]^2 G_1 \right) \tau_{d1} \right] \qquad (6\text{-}20)$$

As we did with the vapor term, we can assume that $\tau_L = Z_L M_L$, where Z_L is is the weighting function for liquid water, and M_L is the precipitable liquid. Thus,

$$M_L = \left[G_2 - \left(\frac{f_2}{f_1} \right)^2 G_1 \right]^{-1}$$

$$X \left[G_2 \tau_1 - G_1 \tau_2 - \left(G_2 - \beta \left[\frac{f_2}{f_1} \right]^2 G_1 \right) \tau_{d1} \right] Z_L \qquad (6\text{-}21)$$

Equations (6-19) and (6-21) represent the formal solutions for the excess path delay due to water vapor ΔL_v, and the integrated liquid content M_L, in terms of the transformed observables τ_1 and τ_2 defined by Eq. (6-12).

If we are able to measure the brightness temperatures T_{b1} and T_{b2}, then in principle we can estimate the vapor path delay ΔL_v and integrated liquid content M_L. The accuracy of these estimates is limited by our ability to measure the brightness temperatures and the quality of our assumptions, namely (1) that the quantities T_M, G_1, G_2, τ_{d1}, and Z_1 are constant and (2) that the radiation from liquid water varies as f^2. Accurate measurement of T_b is primarily an instrumental calibration problem.

D. DETERMINATION OF CONSTANTS IN THE ALGORITHM

In order to use the inversion algorithms given in Eqs. (6-19) and (6-21), we must determine the mean radiating temperature of the atmosphere, the vapor weighting functions, the liquid weighting function, and the opacity due to the dry component of the atmosphere. These quantities have been assumed to be constant in the derivation of the algorithm, but in a real atmosphere they exhibit variation and correlation with other atmospheric parameters. While these variations are not so large as to invalidate the basic assumptions, they clearly indicate some level of error in the algorithm. This implies that we must always expect some level of "algorithm noise," and our efforts must be directed towards its reduction. Furthermore, some fraction of this algorithm noise is likely to represent systematic variations that are a function of site and season. If we were given a meteorological history of each WVR site, we might be able to develop the constants in our algorithms in such a way that would be optimized for that site and hopefully reduce the seasonal variations. However, this procedure presents potential operational problems: (1) The meteorological history may not be available or easy to obtain; (2) it is a fair amount of work if there are many sites (e.g., as with mobile VLBI); and (3) someone must keep careful track of which algorithm goes with a particular site, and if that someone mixes the algorithms, the error could be compounded. A far simpler procedure would be to derive a single formulation of the algorithm in which the "constants" were no longer constant but instead some simple function of site and seasonal parameters, i.e., in effect we would use a model to reduce the site and seasonal systematic errors in the algorithm. Any WVR user must decide on which approach to use based on his accuracy requirements as well as cost and operational reliability. The interpretation adopted here is to use a single algorithm for all sites and to demonstrate that the residual site and seasonal dependencies are less than the currently required level of accuracy.

We can best evaluate the level of algorithm noise as well as site and seasonal variations by determining the constants in a given formulation of the algorithm using a regression analysis. That is, we will use meteorological data (e.g., radiosonde data) to compute the path delay and to solve the equation of radiative transfer for the associated brightness temperatures at

20.7 and 31.4 GHz for a relatively large number of cases. This data base will then be used to determine the value of the constants in an inversion algorithm that will minimize the residuals in a least squares sense. Of course, as a practical matter, we will still be left with the problem of relating the temperature scale of our WVRs to the temperature scale defined in Eq. (6-8). Since our knowledge of fundamental quantities like the absorption coefficients as well as our calibration of the radiometers will always be less than perfect, we must accept the fact that ultimately the WVRs must be compared directly with some independent method of measuring path delay if we wish an absolute calibration.

A data base of radiosonde data was assembled from five sites in the United States during the year 1976. The sites - Portland, Maine; Pittsburgh, Pennsylvania; El Paso, Texas; San Diego, California; and Oakland, California - were chosen to represent a cross-section of meteorological conditions. Each radiosonde launch provides an approximately vertical profile of pressure, temperature, and relative humidity that is used to calculate the vapor path delay and to numerically solve the equation of radiative transfer for the brightness temperature, mean radiating temperature, and the opacity. One launch out of eight was selected from each site so as to obtain equal amounts of data from both 0 and 12 hours Universal Time and to cover seasonal trends in the data. Thus, for each radiosonde site we have 92 values of the vapor path delay ΔL_{vi} and 92 pairs of brightness temperatures $T1_i$ (20.7 GHz) and $T2_i$ (31.4 GHz). We use the latter to estimate the path delay $\langle \Delta L_v \rangle_i = f(T1_i, T2_i)$ and in a straightforward manner solve for the constants in any given functional form $f(T1_i, T2_i)$ that minimizes the difference $\Delta L_{vi} - \langle \Delta L_v \rangle_i$, in a least squares sense.

The radiosonde data does not provide any direct indication of the presence or amount of liquid water. As we noted previously, the presence of even small amounts of liquid (as in clouds) has a pronounced effect on the brightness temperatures measured by the WVR. Hence, it is essential that we evaluate the performance of the vapor retrieval algorithm in the presence of liquid. In order to simulate the presence of clouds the data from each radiosonde launch are scanned for an indication that the relative humidity is greater than 95%, which we assume indicates an equilibrium condition with

liquid. The points at which the relative humidity falls below 94% define the top and bottom of the cloud, and the altitude of these points is calculated by simple linear interpolation. Given the cloud thickness and altitude, we use all three of the models for the cloud liquid density given by Decker et al. (Ref. 24) which we denote by CMODEL = 1, 2, or 3 (CMODEL = 0 denotes no liquid). The temperature of the liquid was taken to be the interpolated temperature of the radiosonde in the cloud, and the absorption coefficient of liquid water given by Staelin (Ref. 23) is used to calculate the brightness temperature. Using this criterion, a total of 121 radiosonde launches from the 5 sites was found that suggests the presence of liquid water. Thus, for each cloud model there were 121 values of the precipitable liquid M_{Li}, and 121 pairs of observables $T1_i$ and $T2_i$. The regression analysis for the liquid water retrieval then proceeds in a manner that is completely analogous to analysis used for the vapor algorithm. For the vapor algorithm, the constants are derived in the regression analysis using clear sky data and tested with the cloud data. For the liquid algorithm, the constants are derived with the cloud data and tested with the clear-sky data.

Generally, the zenith brightness temperature in clear-sky conditions at both of our frequencies will be less than 50 K and the corresponding opacity less than 0.2 neper. This suggests that we could expand the logarithm in Eq. (6-20) and keep only the first order term in T_b, i.e., a low opacity approximation. The estimated path delay would then be of the form

$$(\Delta L_v)_i = A_o + A_1 \, [T1 - 0.4346 \times T2]_i \qquad (6\text{-}22)$$

where T1 and T2 are the brightness temperatures at 20.7 and 31.4 GHz respectively. Table 6-1 summarizes the best fit parameters for this estimate. First, note that since we are using noise free data, the RMS of the fit represents the quality of the assumptions that have gone into the estimate, i.e., "algorithm noise". We would expect a larger RMS than shown if we actually compared WVR data with real radiosondes for in that case we would be comparing two noisy observables and the RMS would represent the quadratic sum of the radiosonde error and WVR error. Second, note that the values of the "constants" A_o and A_1 vary from site to site by more than their standard errors, clearly indicating systematic effects are present in the data. This

Table 6-1. Summary of Best Fit Parameters for a Vapor Algorithm Involving Brightness Temperature

$$\langle \Delta L_v \rangle = A_o + A_1 \{T1 - 0.4346\ T2\}$$

(no measurement noise)

Cloud Model = 0

Site	A_o	σ	A_1	σ	RMS, cm
Portland	-1.57	0.05	0.662	0.003	0.28
Pittsburgh	-1.45	0.05	0.649	0.003	0.25
El Paso	-1.39	0.06	0.610	0.004	0.26
San Diego	-1.71	0.13	0.642	0.007	0.38
Oakland	-1.63	0.13	0.644	0.007	0.35
All sites	-1.62	0.05	0.646	0.002	0.41

Cloud Model	Average Residual	RMS
1	0.29	0.45
2	0.20	0.58
3	-0.26	1.55

is further emphasized by the fact that the RMS of the fit for all sites is larger than the RMS from any single site. Progressive degradation of the algorithm can be seen in the increasing RMS under cloudy conditions, i.e., increasing opacity. Analysis of the residuals indicates that they correlate with surface values of the pressure, temperature, and the opacity. Of these correlations the opacity is by far the most important. Since our data base represents only zenith values, both the variation and the absolute values of the opacity tend to be small. In a real experiment, the WVR may be pointed down to an elevation angle of $\sim 15^{\circ}$ and the range of opacities will vary accordingly. Still, the RMS of the fit for all sites is not too bad so that Eq. (6-22), since it is particularly simple, is adequate for a quick estimate of the delay.

In order to obtain some idea as to the performance of our algorithms in actual operation we must know the instrumental noise spectrum imposed on the observables, and include an estimate of its magnitude in the regression analysis. One method that can be used to estimate the instrumental stability is to have two side-by-side radiometers observe the same target, e.g., the sky, and note the difference between the two brightness temperatures. In principal, this difference should appear to be Gaussian noise with an RMS equal to $\sqrt{2}$ times the RMS fluctuations of a single radiometer and can be reduced by simply increasing the integration time. In reality, the integration time can only be increased to the point where the inevitable systematic errors begin to predominate. Data taken during the testing and calibration of the WVRs indicate that the noise spectrum is "white" on time scales less than ~3 h and therefore can be reduced by averaging. For time scales greater than 3 h, flicker noise seems to predominate and appears as a slow drift of the antenna temperature about some nominal value with an amplitude of ± 1 K. Since the geodetic experiments that we expect to support are normally longer than 3 h, we will model the radiometer noise with a uniformly distributed random variable drawn from the interval ± 1 K, added to the brightness temperature. The regression analysis then proceeds as in the noise-free case. Differences in the RMS of the fit between the noisy and noise-free data indicate the relative importance of instrumental noise and systematics in the algorithm.

The simple formulation in Eq. (6-22) does not take into account that radiation from distant vapor along the line-of-sight is attenuated by intervening vapor. This correction is done explicitly by using the opacity as the transformed observable. Table 6-2 summarizes the best fit parameters for the path delay estimate that now includes the transformation to opacity given by Eq. (6-12) (where T_M = 275 K). Except for the El Paso data set, we see that the constants are reasonably consistent from site to site. Although there is a small bias for the cloud liquid data, the RMS of the estimate in the presence of liquid is consistent with the clear sky data - a definite improvement over the previous algorithm. When a uniformly distributed $\pm$1 K of noise is added to the brightness temperatures, the RMS for all sites rises to 0.55 cm, indicating roughly equal contributions from algorithm noise and instrumental systematics. This form of the algorithm is useful in circumstances where measurements of surface temperature and pressure are not readily available.

When values of the surface pressure and temperature are available, we can use them to further refine our algorithm. The next most obvious parameter to model is the mean radiating temperature T_M. Figure 6-3 illustrates the frequency dependence of T_M in a plot of T_M versus frequency for a standard atmosphere containing an exponential distribution of water vapor with total columnar content M_v = 2 g/cm^2. Figure 6-4 shows how T_M varies as a function of M_v, again in a standard atmosphere. The mean radiating temperature is also a function of the physical temperature distribution in the atmosphere and will exhibit site and seasonal variation. Figure 6-5 illustrates this variation for the Portland, Maine, data for the year 1976, and Table 6-3 summarizes the statistics of both T_M and the surface temperature T_S. The RMS variations in T_M indicated in Table 6-3 suggest that this could be a significant error source in the inversion algorithm and some effort is warranted to reduce this variation. If we assume a simple linear relationship between T_M and the surface temperature T_s, then the estimates

$$T_{M1} = 50.3 + 0.786\ T_s \qquad (f = 20.7\ \text{GHz}) \qquad (6\text{-}23)$$

$$T_{M2} = T_{M1} + 3.4 \qquad (f = 31.4\ \text{GHz}) \qquad (6\text{-}24)$$

Table 6-2. Summary of Best Fit Parameters for a Vapor Algorithm Involving the Opacities

$$\langle \Delta L_v \rangle = A_o + A_1 \{\tau_1 - 0.4346\ \tau_2\}$$

$$\tau_i = -\log_e \left(\frac{275 - TA_i}{272} \right)$$

Cloud Model = 0

Site	A_o	σ	A_1	σ	RMS[a], cm
Portland	0.01	0.04	160.5	0.6	0.24 (.49)
Pittsburgh	0.08	0.05	158.3	0.7	0.24 (.45)
El Paso	-0.03	0.05	151.4	0.9	0.25 (.45)
San Diego	-0.07	0.11	156.9	1.6	0.37 (.54)
Oakland	-0.07	0.10	158.6	1.7	0.32 (.53)
All sites	-0.06	0.03	157.9	0.5	0.36 (.55)

Cloud Model	Average Residual	RMS[a]
1	0.18	0.35 (.56)
2	0.17	0.35 (.51)
3	0.14	0.37 (.60)

[a]Numbers in parenthesis indicate the RMS with an added noise of ± 1 K in each channel.

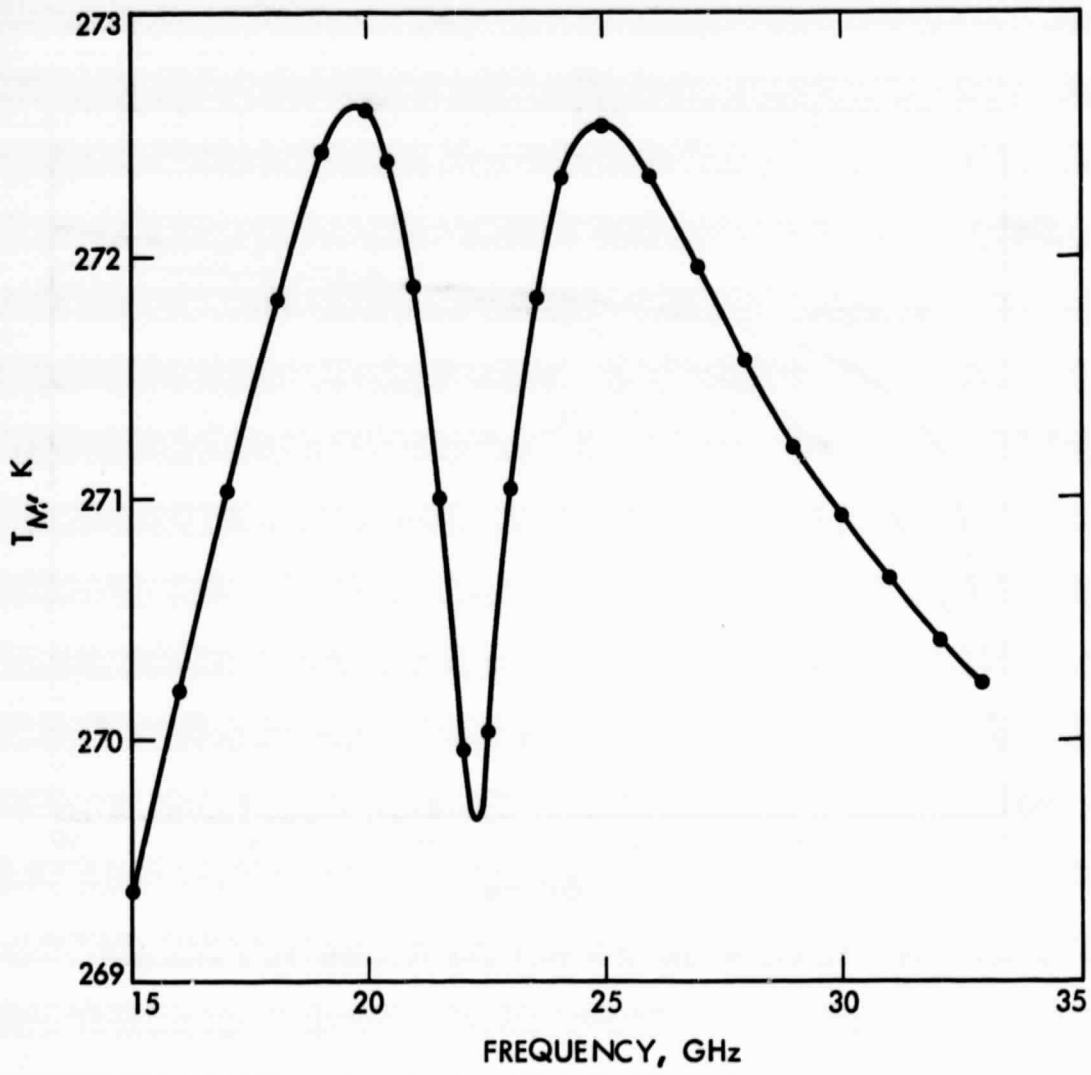

Figure 6-3. The mean radiating temperature of a standard atmosphere T_M vs. frequency for M_v = 2 g/cm^2 exponentially distributed in a standard atmosphere

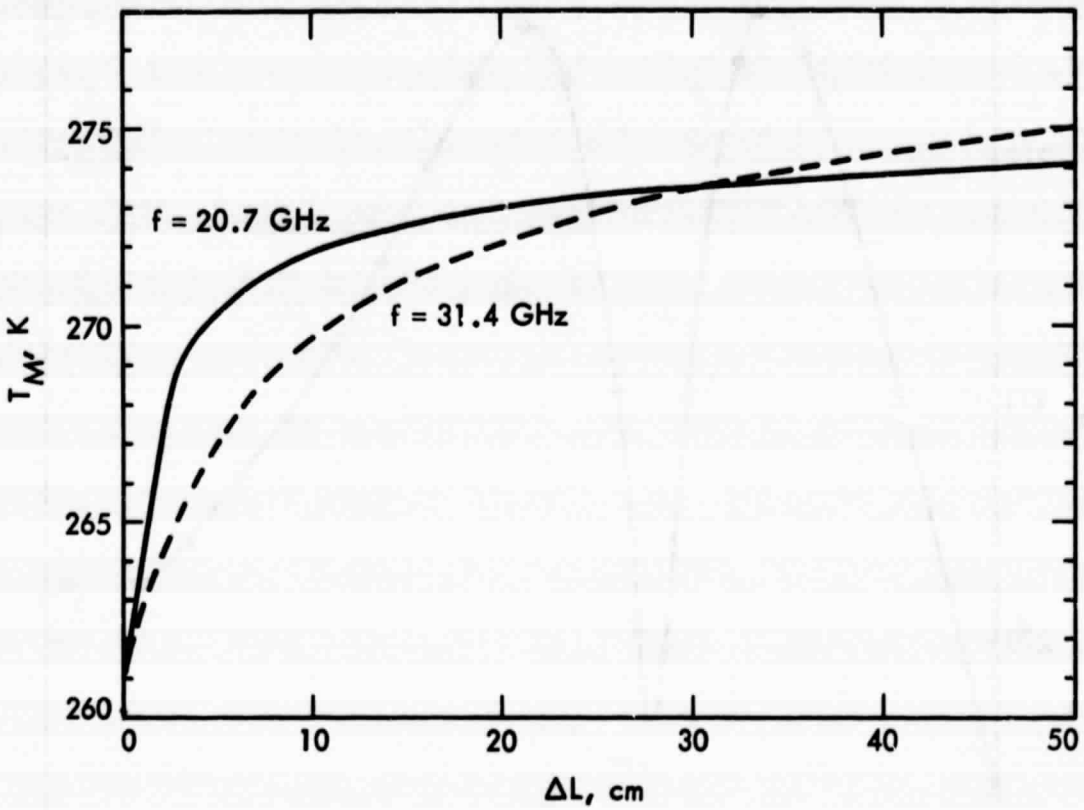

Figure 6-4. T_M vs. M_V for f = 20.7 and 31.4 GHz in a standard atmosphere

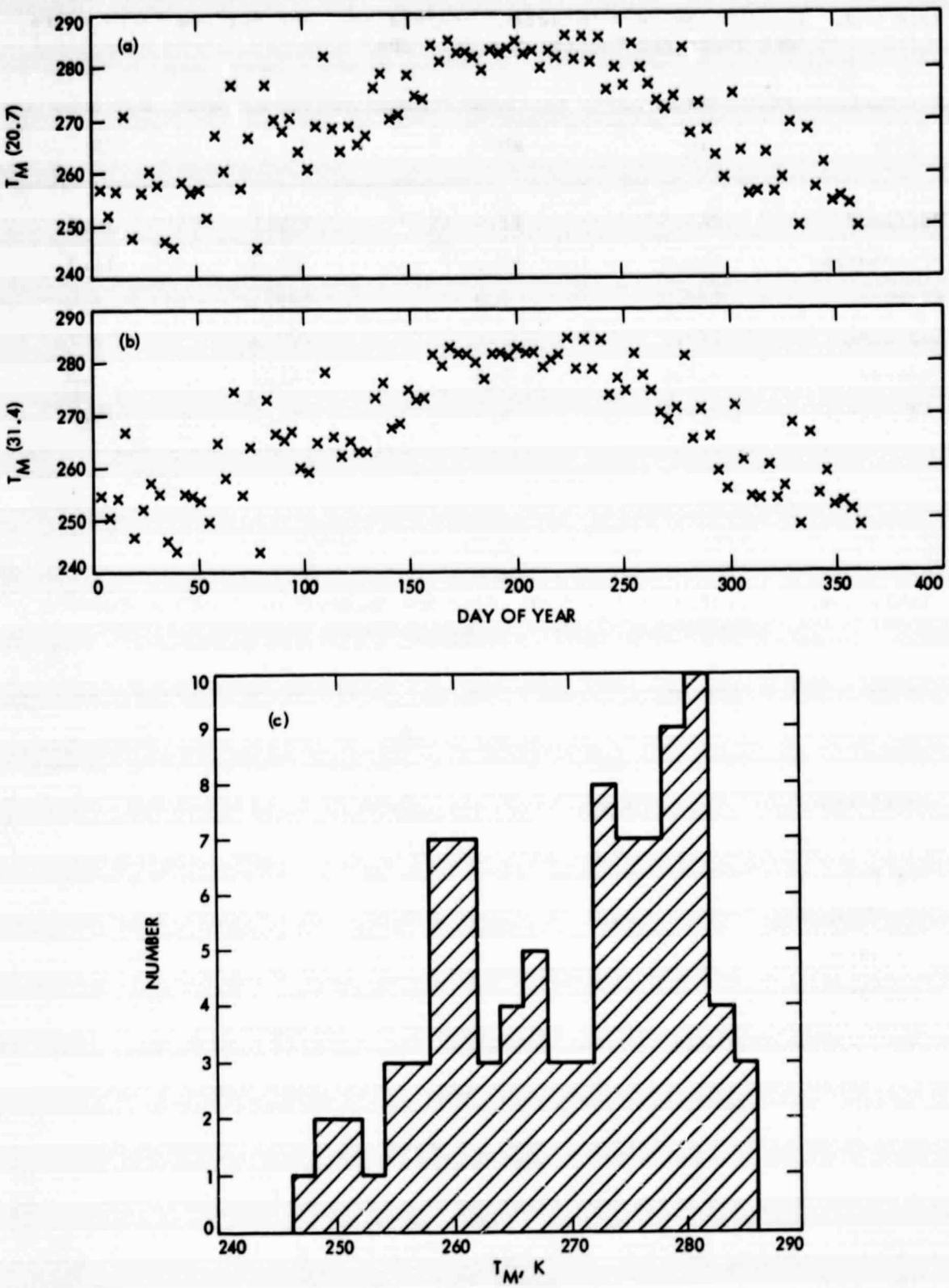

Figure 6-5. Portland, Maine, radiosonde data showing (a) T_M vs. time at f = 20.7 GHz; (b) T_M vs. time at f = 31.4 GHz; and (c) the histogram of T_M at 20.7 GHz

Table 6-3. The Average Mean Radiating Temperature, the Surface Temperature, and Their RMS Values (f = 20.7 GHz)

SITE	T_M	RMS	T_S	RMS
Portland	269.4	11.4	279.1	10.8
Pittsburgh	270.3	10.9	281.5	11.3
El Paso	275.2	7.0	289.5	6.0
San Diego	280.1	5.1	290.6	5.7
Oakland	278.0	5.3	287.7	6.0
All Sites	274.7	9.4	285.7	10.5

Table 6-4. Estimates of the Mean Radiating Temperature From the Surface Temperature ($T_{M1} = A_o + A_1 T_S$, f = 20.7 GHz)

SITE	A_o	A_1	RMS
Portland	6.6	0.94	4.2
Pittsburgh	15.3	0.91	3.7
El Paso	121.8	0.53	3.9
San Diego	86.1	0.67	3.4
Oakland	110.7	0.58	3.9
All Sites	50.2	0.786	4.5

reduce the RMS variation of T_M from all sites by a factor of two. Table 6-4 summarizes the best linear fit between T_M and the surface temperature T_S for each site. Note that the RMS for all sites in Table 6-4 is larger than the RMS for any individual site. This strongly suggests that this simple linear fit does not completely remove all site-to-site and/or seasonal variations. However, these equations do reduce the RMS to an acceptable level and have the virtue of being simple to use - a significant consideration if one must deal with data from many sites.

For the next formulation of an algorithm we will model the mean radiating temperatures T_{M1} and T_{M2} and assume that the dry opacity scales as the surface pressure squared times the surface temperature to the -2.86 power. The multiplier of the dry opacity term will be chosen to force the bias term, i.e., A_o, to be zero. The algorithm that we shall now fit then takes the form

$$(\Delta L_v) = A_o + A_1 \left[\tau_1 - 0.4346\ \tau_2 - \left(\frac{A_2}{A_1}\right)\left(\frac{P_s}{1013}\right)^2 \right.$$

$$\left. X \left(\frac{293}{T_s}\right)^{2.86} AM \right] \qquad (6\text{-}25)$$

where we have included the air mass scaling for the dry term, i.e., AM = cosecant (elevation). The opacity at frequency f_i is

$$\tau_i = -\log_e \left(\frac{T_{Mi} - T_{bi}}{T_{Mi} - T_e}\right) \qquad (6\text{-}12)$$

where T_{M1} is given by Eq. (6-23) and T_{M2} by Eq. (6-24). Table 6-5 summarizes the regression analysis for this algorithm. We see that the RMS and the site-to-site consistency is a bit better than the previous algorithm and the performance in the presence of liquid is about as good. If surface measurements are available, we would prefer this algorithm to the previous formulation, but note that the accuracy of either meets the calibration

Table 6-5. Summary of Best Fit Parameters for a Vapor Algorithm Involving Opacities and Surface Data

$$\langle \Delta L_v \rangle = A_o + A_1 \{\tau_1 - 0.4346\ \tau_2 - 0.0016\ \tau_d\}$$

where

$$\tau_i = -\log_e \left(\frac{T_M - TA_i}{T_M - T_c} \right)$$

$$T_{M1} = 50.3 + 0.786 \times T_s$$

$$T_{M2} = T_{M1} - 3.4$$

$$\tau_d = \left(\frac{P_s}{1013} \right)^2 \left(\frac{293}{T_s} \right)^{2.86}$$

Cloud Model = 0

Site	A_o	σ	A_1	σ	RMS[a], (cm)
Portland	0.07	0.03	165.4	0.5	0.18 (.45)
Pittsburgh	0.11	0.03	165.1	0.5	0.16 (.44)
El Paso	-0.05	0.03	159.4	0.5	0.14 (.39)
San Diego	-0.03	0.09	163.7	1.3	0.30 (.47)
Oakland	0.05	0.09	163.9	1.5	0.27 (.44)
All sites	-0.001	0.03	163.9	0.4	0.28 (.48)

Cloud Model	Average Residual	RMS[a]
1	0.13	0.30 (.46)
2	0.19	0.34 (.54)
3	0.29	0.50 (.63)

[a]Numbers in parenthesis indicate RMS with an added noise of ±1 K to each channel.

requirements of the Crustal Dynamics Project. When noise is added to the RMS, the fit for all sites rises to 0.48 cm and the small site-to-site differences are blurred by larger sigmas on each of the constants.

Since the path delay due to liquid is $\Delta L_L \sim 1.6 M_L$ (for both ΔL_L and M_L in cm) and M_L is rarely larger than a few millimeters, we see that the liquid delay is considerably smaller than the errors in the vapor estimate. The primary reason for a liquid estimate is not for direct geodetic calibration so much as it is an indicator of WVR performance. We can rewrite Eq. (6-21) in the form

$$M_L = A_o + A_1 \left[\tau_2 + \left(\frac{A_2}{A_1} \right) \tau_1 + \left(\frac{A_3}{A_1} \right) \tau_d \right] \qquad (6\text{-}26)$$

The value of (A_2/A_1) is found either from calculation of the weighting functions or a multiple regression analysis on the radiosonde data base to be $(A_2/A_1) = -0.366$. We will use the same functional dependence for the dry term as we used in the vapor algorithm and require the value of (A_3/A_1) to be such as to minimize the value of A_o, i.e., we will minimize the bias term. Table 6-6 shows the parameters for the best fit solution for this formulation. As we required, the bias term A_o is less than its standard error for each cloud model and can be taken as effectively zero. When this is done and the liquid water algorithm is used with the main radiosonde data base (where we assumed there was no liquid water), the average residual at each site is comfortably small with an RMS value comparable to the retrieval accuracy in the liquid data set. Note that units have switched to micrometers for the liquid measure. The increasing RMS of the retrieval with cloud model suggests that the accuracy of the liquid retrieval is a function of the liquid density. Figure 6-6 shows the average precipitable liquid versus the RMS of the retrieval for each site and each cloud model. The error in the liquid water estimate suggested by this data is

$$\mathrm{RMS}(M_L) = 0.32 \times M_L \qquad (6\text{-}27)$$

Table 6-6. Summary of Best Fit Parameters (μm) for a Liquid Water Algorithm

$$\langle M_L \rangle = A_o + A_1 (\tau_2 - 0.366, \tau_1 - 0.022 \tau_d)$$

All Sites Cloud Model	A_o	σ	A_1	σ	RMS[a]
1	-0.3	2.8	5368	107	24 (26)
2	+8.4	12.1	5352	119	105 (108)
3	+26.7	25.7	5279	125	224 (223)

Cloud Model = 0 (no liquid)

Site	Average Residual	RMS*
Portland	0.6	33 (34)
Pittsburgh	0.3	25 (34)
El Paso	11.8	9.6 (15)
San Diego	-7.2	15.6 (22)
Oakland	-3.6	12.7 (17)
All sites	0.3	21.8 (25)

[a]Numbers in parenthesis indicate rms with an added noise of ±1 K to each channel.

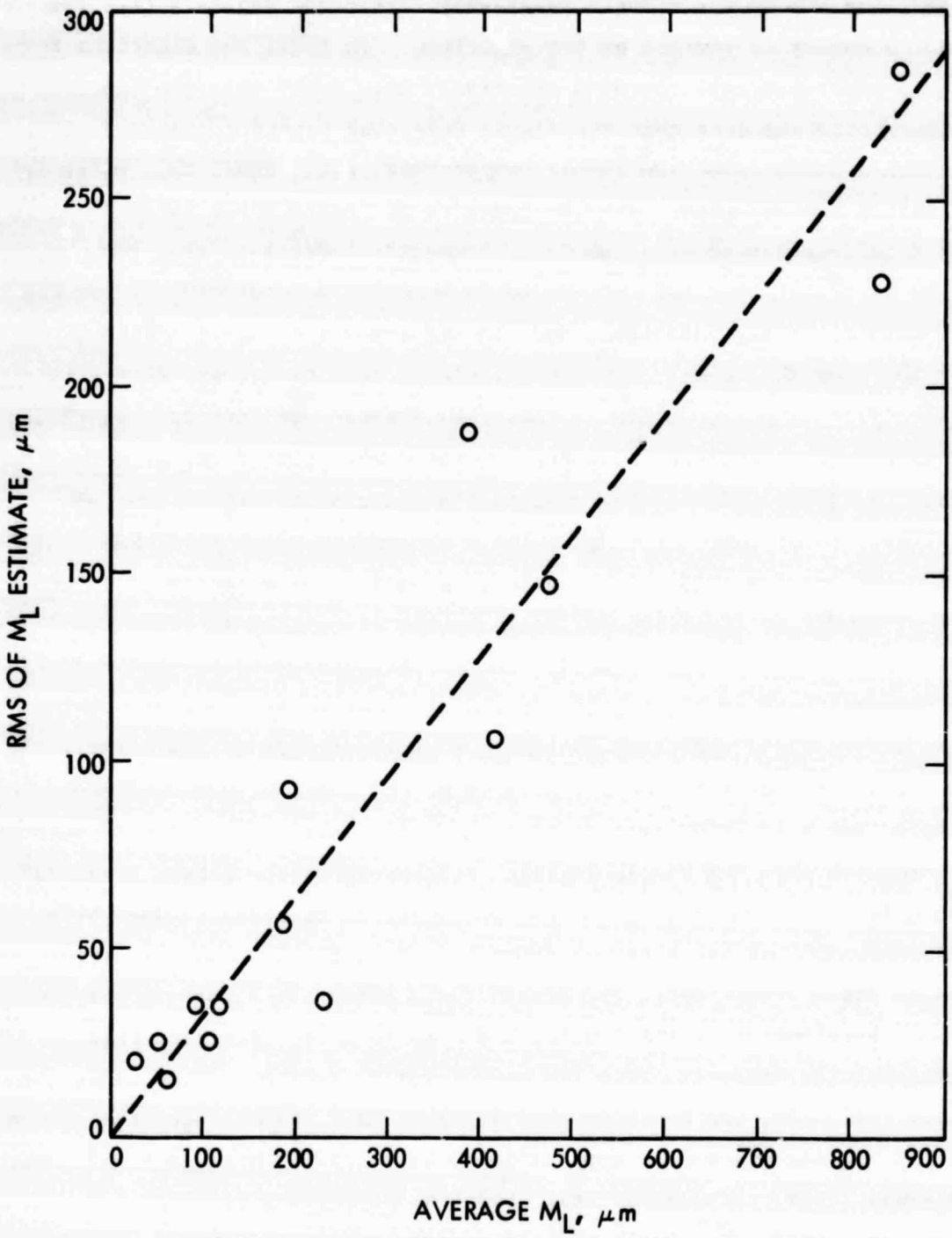

Figure 6-6. The RMS of the liquid water retrieval vs. M_L, the precipitable liquid along the line-of-sight.

When we include the WVR error model in the regression analysis for liquid retrieval, the RMS of fit changes relatively little and suggests that the retrieval accuracy is limited by the algorithm. In fact, the algorithm for the liquid water estimate contains relatively more error than the vapor algorithm due to the fact that the liquid weighting function contains an exponential dependence on the liquid temperature, e.g., (Ref. 23), which is not an easily modeled quantity. The presence of liquid water during a tip-curve calibration observation is an immediate indication that the tip-curve data will be noisy and should be weighted accordingly. If we are observing in clear sky conditions and the WVR reports a non-zero (i.e., greater than the RMS value) amount of liquid water, it suggests that either the radiometric temperature scales need recalibration or the vapor weighting functions are very different than the "average" weighting function determined by earlier analysis. The latter possibility could be due to an unusual vertical profile of vapor although we have chosen the vapor sensitive frequency to minimize this type of error. Finally, the presence of large amounts of liquid or equivalently, large values of opacity at 31.4 GHz, indicate that an important assumption in our derivation may be violated. In large concentrations of liquid, the drop size tends to grow and scattering plays an increasingly important part in the apparent radiation spectrum. When the effective diameter of the drop is on the order of the observing wavelength, the scattering process is termed Mie scattering, and the spectrum is more complex than the simple Rayleigh scattering which we have assumed. The radiation spectrum of large drops can no longer be characterized by a simple power-law type behavior, which means that both our vapor and liquid algorithms break down. Since the breakdown is primarily a function of the drop size distribution of the liquid, there is no clear criterion that distinguishes the operating from the non-operating regimes of the algorithm. Westwater (Ref. 25), and Westwater and Guiraud (Ref. 26) estimate that these remote sensing techniques are applicable up to opacities of 3 dB = 0.7 neper (at 31 GHz). Given the considerable observing experience of these experimenters, this is probably the best operating/non-operating criterion that can presently be stated.

E. SUMMARY

Several reasonably simple algorithms have been derived that relate observables, i.e., the brightness temperatures measured with a two-channel WVR, to the line-of-sight path delay that is required to correct various types of radiometric data for the effects of atmospheric water vapor. The three formulations that can be used to estimate the excess path delay due to atmospheric water vapor ΔL_v, are

$$\langle \Delta L_v \rangle = -1.6 + 0.65 \, (T_1 - 0.435 \, T_2) \tag{6-28}$$

for convenience. A better algorithm, if no surface measurements are available, would be

$$\langle \Delta L_v \rangle = 158 \, (\tau_1 + 0.435 \, \tau_2) \tag{6-29}$$

where the opacity τ, is

$$\tau_i = -\log_e \left[\frac{275 - T_i}{272} \right] \tag{6-30}$$

When surface measurements are available, use

$$\langle \Delta L_v \rangle = 164 \left[\tau_1 - 0.435 \, \tau_2 - 0.0016 \right.$$

$$\left. \times \left(\frac{P_s}{1013} \right)^2 \left(\frac{293}{T_s} \right)^{2.86} \right] \tag{6-31}$$

where the opacity is now

$$\tau_i = -\log_e \left[\frac{T_{Mi} - T_i}{T_{Mi} - T_c} \right] \tag{6-32}$$

and the quantities T_{Mi} are given in Eq. (6-23) and (6-24).

The regression analysis indicates that the ultimate accuracy of the two-channel technique is about 0.2 to 0.3 cm, and with a realistic noise model of the current generation of instruments, a 0.5 cm accuracy is possible. Note that the question of radiosonde accuracy is irrelevant in this analysis; it simply represents the "truth". However, if the WVRs are to be compared directly to radiosondes, then the question of radiosonde accuracy is crucially important. Indeed, the WVRs must eventually be calibrated on an absolute scale, and radiosondes seem to be the most cost-effective way to accomplish this at the present time. Consider that such a direct comparison is made at each of the radiosonde launch sites that were used in this analysis. If we assume an average zenith path delay of 10 cm and the measurement accuracy of the radiosonde is 10%, then the RMS of the radiosonde/WVR comparison would be

$$(1.0)^2 + (0.5)^2 = 1.12 \text{ cm}$$

While it is important to make such a comparison to investigate the possibility of a bias term in the inversion, the analysis suggests that the WVR is more accurate than the radiosonde. Hence, the comparison must be done with great caution when attempting improvements in the WVR instrumentation or refinements in the algorithm. We are faced with a recurring problem -- how to demonstrate that a new measurement technique is superior to any existing technique, including those that would be used for calibration.

REFERENCES

1. Gold, T. (1967) "Radio Method for the Precise Measurement of the Rotation Period of the Earth", Science, V167, p 302.

2. Shapiro, I. I., and C. A. Knight (1970) "Geophysical Applications of Long Baseline Interferometry", in Earthquake Displacement Fields and the Rotation of the Earth (Mansinha, Smylie, & Beck, eds), Reidel Publ., Holland, pp 284-301.

3. Ong, K. M., P. F. MacDoran, J. B. Thomas, H. F. Fliegel, L. J. Skjerve, D. J. Spitzmesser, P. D. Batelaan, and S. R. Paine (1976) "A Demonstration of a Transportable Radio Interferometric Surveying System with 3-cm Accuracy on a 307-m Baseline", J. Geophys. Res., V81, pp 3587-3593.

4. Smith, E. K., and Weintraub, S., (1953) "The Constants in the Equation for Atmospheric Refractive Index at Radio Frequencies", Proc. IRE, V41, 1035-1057.

5. Winn, F. B., S. C. Wu, G. M. Resch, C. C. Chao, O. H. vonRoos, and H. Lau (1976) "Atmospheric Water Vapor Calibrations: Radiometer Technique", DSN Prog. Repts. 42:32, pp 38-49.

6. Moran, J. M., and H. Penfield, (1976) "Test and Evaluation of Water Vapor Radiometers and Determination of their Capability to Measure Tropospheric Propagation Path Length", SAO final report on Contract NAS5-20975 (June 1976) available from National Technical Info Service, Springfield, VA.

7. Resch, G. M., (1980) "Water Vapor - The Wet Blanket of Microwave Interferometry", in Atmospheric Water Vapor (Deepak, Wilkerson, and Ruhnke, eds), pp 265-282 Academic Press, New York.

8. Westwater, E. R., (1967) "An Analysis of the Correction of Range Errors due to Atmospheric Refraction by Microwave Radiometric Techniques", ESSA

Tech. Rept. IER 30-ITSA30 available from National Technical Into. Service, Springfield, VA.

9. Wu, S. C., (1979) "Optimum Frequencies of a Passive Microwave Radiometer for Tropospheric Pathlength Correction", IEEE Trans. Ant. & Prop., AP-27, pp 233-239.

10. Janssen, M. A., S. M. Bednarczek, S. Gulkis, H. W. Marlin, and G. F. Smoot, (1979) "Pattern Measurements of a Low-Sidelobe Horn Antenna", IEEE Trans. Ant. & Prop., AP-27, pp 551-555.

11. Guiraud, F. O., J. Howard, and D. C. Hogg, (1979) "A Dual-Channel Microwave Radiometer for Measurement of Precipitable Water Vapor and Liquid", IEEE Trans. Geoscience Elect., GE-17, pp 129-136.

12. Clark, B. G. (1973) "The Effect of Digitization Errors on Detection of Weak Signals in Noise", Proc. IEEE, V61, 1654-1655.

13. Kraus, J. D., Radio Astronomy, McGraw-Hill Book Co., New York (1966), pp 233-239.

14. Price, R. M., "Radiometer Fundamentals", in Methods of Experimental Physics, Vol. 12-Part B, ed. M. L. Meeks, Academic Press, New York, 1976.

15. Franco, M., S. D. Slobin, and C. Stelzried, "20.7/31.4 GHz Solar Disk Temperature Measurements", JPL IOM 3333-81-032, April 27, 1981.

16. Bracewell, R. N. (1956) "Two Dimensional Aerial Smoothing in Radio Astronomy", Aust. J. Phys., Volume 3, 297-314.

17. "Manual for Mark III Microprocessor ASCII Transceiver", author unknown, 1 Apr. 81 (available from T. A. Clark, Goddard Space Flight Center, Greenbelt, MD. 20771).

18. Bean, b. R., and E. J. Dutton (1968), Radio Meteorology, Dover Publ., New York, NY.

19. Hess, S. L. (1959), Introduction to Theoretical Meterorology, Holt, Rinehard & Winston, New York.

20. Chandrasekhar, S. (1950), Radiative Transfer, Oxford Univ. Press, New Jersey.

21. Waters, J. W. (1976), "Absorption and emission by atmospheric gases," ed., M. L. Meeks. Methods of Experimental Physics: Astrophys., Part B, 12, pp. 142-175.

22. Snider, J. B., and E. R. Westwater (1969), "Atmospheric attenuation at 15, 31, and 53 GHz," ESSA Tech. Reprt. eRL 156-WPL 11, Dec. 1969.

23. Staelin, D. H. (1966), "Measurements and interpretation of the microwave spectrum of the terrestrial atmosphere near 1-cm wavelength," J. Geophys. Res., 71, pp. 2875-2882.

24. Decker, M. T., E. R. Westwater, and F. O. Guiraud (1978), "Experimental evaluation of ground-based microwave radiometric sensing of atmospheric temperature and water vapor profiles," J. Appl. Meteor., 17, pp. 1788-1795.

25. Westwater, E. R. (1978), "The accuracy of water vapor and cloud liquid determinations by dual-frequency ground based microwave radiometry," Radio Science, 13, pp. 677-685.

26. Westwater, E. R., and F. O. Guiraud (1980), "Ground-based microwave radiometric retrieval of precipitable water vapor in the presence of clouds with high liquid content," Radio science, 15, pp. 947-957.

APPENDIX A

CALIBRATION DATA FORMATS

In response to a data prompt "#FE C" the radiometer controller will return a block of calibration data in the format shown in the left column below, except that the values will be returned on a single line, separated by spaces. The meanings and uses of the constants are shown to the right.

DATA	FUNCTION
0328 1795	AZ scaling, in counts, AZ = 0, AZ = 360 degrees
0176 1008	EL scaling, in counts, EL = 0, EL = 90 degrees
1000 to 9500	Calibration resistors R2 & R2, in ohms
1.40423E-3	Temperature sensor thermistor constant G1
2.37076E-4	" " " " G2
1.00062E-7	" " " " G3
9.40946E-4	Hot load thermistor constant G1
2.20236E-4	" " " " G2
1.31748E-7	" " " " G3

APPENDIX B
WVR3 SOFTWARE MODULE DESCRIPTIONS

Modules are written in Fortran-80 (.FOR), Microsoft Macro Assembler Language (.MAC) or CP/M Assembly Language (.ASM). The modules are listed below in the order in which they are encountered, as much as is possible.

WVRMON.ASM

WVRMON is an expansion of the National BLC 80P Monitor supplied with the National BLC 80 CPU board. WVRMON includes new commands to make it easier to troubleshoot new programs downloaded into WVR RAM for debugging, as well as providing facilities for downloading.

When power is first applied to the WVR, or the controller RESET switch is pressed, CPU execution begins at location zero in CPU PROM 00. This first location includes a jump instruction to the initialization routine INIT:. In 8080 family CPUs this location zero is one of eight hardware interrupt vectors that can also be accessed through software interrupts RST0 through RST7. The original BLC 80P Monitor used these vectors to provide access to subroutines within the monitor program. WVRMON includes software-equivalent routines compatible with the original BLC 80P routines, but now only three-byte jump instructions are located at each of the eight interrupt vectors. All of the code for the subroutines is included within WVRMON above address 40H, as was not the case with the original BLC 80P Monitor.

Another difference is that WVRMON uses only the vectors at location 0 (jump to INIT) and location 8 (jump to breakpoint entry). WVR3 uses the vector at location 38H for the hardware interrupt PACER clock. The other vectors, RST2 through RST6, will still access internal subroutines in WVRMON equivalent to those in the BLC 80P Monitor, but are not currently used. These other vectors are not used so that WVRMON can be included in future controllers requiring a larger number of functional hardware interrupts.

Upon entry through the RST0 vector, WVRMON initializes the serial communications USART, initializes functions used internally, and looks at memory location 0800H. If a jump instruction (0C3H) is found at this location, WVRMON decides that a functional controller program is installed and jumps to that entry point at location 0800H. A test version of WVRMON, labeled "No Auto Start" is available with this function inhibited to provide debugging of new programs.

If no jump instruction is found at 0800H, the monitor program itself is entered, signs on with its own revision date, and displays a list of available commands. See the operating instructions for details.

PROM.ASM

This set of radiometer-specific routines and calibration data is burned into the PROM installed on the CPU board in address space 0800H up. For compatibility with WVRMON auto-start, PROM08 begins with a jump instruction to RSWVR: which will Reset and run WVR3. Before execution of WVR3, data areas in RAM have to be initialized, which is accomplished by subroutine XPAND:. Following this expansion, (at RNWVR:, RuN WVR) a check is made for the existance of a PROM at the start address of WVR. If no PROM is found, execution is aborted to WVRMON. If a PROM exists at the starting address defined as WVR, a jump is made to that address.

Other routines within PROM08 include WVR sign-on and calibration message subroutines, entered through vectors at addresses 0809H and 080CH, respectively.

WVR.FOR

This is the main program within WVR3. The .ASM modules discussed above are assembled and burned into PROM separately from WVR.FOR and the following modules. These following modules are compiled as relocatable (.REL) files and linked by L80 before being burned into PROMs located on the memory expansion board within the WVR controller.

WVR.FOR provides the definition of all COMMON memory, initializes some variables, and calls subroutine DECOD.FOR to get a command or data request from the host computer. WVR.FOR then provides for the execution of the command or data request, by calling the appropriate subroutine.

SUBROUTINES:

The following modules are written as subroutines. They are listed along with the calling convention (samples from actual calling programs are shown) and the program(s) and/or subroutines that call them. Where more than one entry exists into a module, entry lables, calling conventions, and callers are also given. Some modules contain subroutines that are only used internally. These are not listed.

Module	Calling Convention	Called By
DECOD.FOR	CALL DECODE	WVR

This subroutine reads in a command or data request from the host computer by calling subroutine READ (part of RDWT.MAC). It then verifies the format and contents of the input line. A check is made for the proper device address (#FE). The alphabetic opcode field is decoded and stored as a numeric value in ICOM. Numeric arguments following the opcode are converted to integer values and stored in COMMON for use by other modules. Illegal formats are flagged in IBAD.

Module	Calling Convention	Called By
RDWT.MAC	not called, see entries below	
READ	CALL READ(IBUF,NC)	DECOD, DATA1
WRITE	CALL WRITE(OBUF,NC)	WVR, ODATA, DATA1
LFCR	CALL LFCR	WVR, ODATA, DATA1

RDWT includes subroutines WRITE:, LFCR:, and ALFCR: for writing (outputting to the host computer) the contents of a buffer (OBOF), a line feed/carriage return, or an "ACK" followed by line feed/carriage return.

The READ subroutine entry provides for reading a command or data request from the host computer, and includes all of the code necessary to provide the dual personality WVR3: the compatibility with both the MAT and pre-existing Host computer conventions.

READ establishes a default data request (#FE D 1) in the input buffer (IBUF), and waits for the receipt from the host of the proper WVR address, #FE. Following receipt of this address, READ establishes the WVR in the selected mode, and accepts and passes on to DECOD all valid commands or data requests. Receipt of any other device address or the reset character @ causes READ to reset to the non-selected mode.

All MAT control compatibility is provided within READ, and only those commands and data requests with formats compatible with WVR software versions 2B and earlier are passed back to DECOD.

Module	Calling Convention	Called By
POINT.MAC	CALL POINT	WVR

This subroutine handles the servos whenever a pointing command is decoded. The elevation and azimuth angles in counts are checked to see if the pointing command is reasonable. If the command is out of limits, an error code of 14 is returned to the caller. The current positions (channel 10 for elevation, 11 for azimuth) are compared to the commanded positions. If the elevation position is higher than the command, the elevation motor is started with a positive voltage. The same sense applies to azimuth. When the pointing command is active, interrupts occur every 1 millisecond.* Only every

* Pacer Clock Interrupt Handling. Two subroutines, POINT and DSAMP make use of the 1 ms clock interrupt provided by the RTI-1200 board. When interrupts are enabled and the PACER clock is activted, a hardware interrupt (RST7) occurs. This interrupt is vectored through the WVRMON prom to the user`s vector UVECT set up in CPU board RAM at location 3C3DH. POINT and DSAMP set up jump instruction in UVECT before enablng interrupts or the clock. The clock is enabled by storing the value 2 in RTI-1200 location SETUP. A zero stored in SETUP tops the clock.

fourth interrupt results in a comparison between command and present position. Pointing is stopped when the command and present position counts agree within the limits set by constants TOLAZ and TOLEL. Pointing can also be stopped by an abort command setting flag PA to non-zero. When pointing is terminated, the interrupting PACER clock is stopped and a return to the caller is made with interrupts disabled.

Module	Calling Convention	Called By
MODATA.FOR	CALL ODATA	WVR

This subroutine is called when a `D` data request has been received. ODATA tests for a valid data request parameter (0 through 5) in the not-busy condition, or (1) if data taking or pointing is active. The first input argument (IA1) is used to direct control to one of six statement numbers. If IA1 is zero, the effect is the same as if 1, 2, and 3 were used in succession. The block of code from statement 70 to just before statement 205 is used as an internal subroutine, where variable K1 is used to return to the caller via the assigned GO TOs. Statement 40 handles the requests for a single voltage channel, and statement 50 for a single temperature channel. Any temperature channel data request will result in a change in the submultiplex channel. This should be reset to an unused channel to prevent sensor self-heating effects. It is up to the host computer program to insure that this is done.

Module	Calling Convention	Called By
DATA1.FOR	CALL DATA1	WVR

This subroutine handles requests for fast sampled data. The first argument (IA1) determines the type of fast sampling. If IA1 = 0, the data sampling strategy number is given by IA2. Data strategies are extracted from COMMON block /STRING/ and have to be moved into /STRING/ after XPAND: has been called (see PROM08.ASM).

Non-zero values of IA1 determine what data is to be returned from the fast sampling process. If IA1 = 1 or 2 a summary is returned. If IA1 = 3 the

data is returned by bins, i.e., separated and converted to ASCII. If IA1 = 4 the data is all returned in raw binary format, where each two-byte quantity contains the four-bit bin number and the 12-bit contents.

Module	Calling Convention	Called By
DTA.FOR	CALL DTA(IMAGE,OBUF(I))	WVR, ODATA, DATA1

This subroutine converts a two-byte integer into a four-byte ASCII string and stores the string in consecutive locations in OBUF. The integer is assumed to be unsigned with a range of from 0 to 9999. Values outside that range will be converted into a garbled string.

Module	Calling Convention	Called By
DSAMP.MAC	CALL DSAMP	DATA1

This subroutine handles the data taking following a data request of `FS` for fast sampling. Since the WVR must be able to communicate with the host computer while data taking is in progress, this routine is also interrupt driven by the 1 ms clock.* The calling program sends the starting address of a string of command bytes (the data strategy). Each command is a one-byte opcode followed by 0, 1, or 2 bytes of operand. The opcodes and operand sizes are given below:

Opcode	Operand Size	Function
`M`	1	set mode
`S`	1	set submux channel
`R`	2	read channel m into bin n
`(`	1	repeat m times
`)`	0	end repeat
`A`	1	command azimuth motor
`D`	2	delay m milliseconds
`E`	1	command elevation motor
[CR]	0	end of data strategy

*See footnote, Page B-4

DSAMP has several flags and counters that are used to keep track of the data taking sequency. NREAD is the number of points stored. TIME is the number of seconds elapsed since the data taking started. DA is a flag that can be set by an external routine that will cause the data taking to be aborted. The data taking will also abort itself if an unrecognized opcode is encountered in the data strategy string, or if the data buffer is overflowing. Currently, 1008 points can be stored without an abort.

Each data item read is caused by an opcode of `R`, and consists of two bytes (16 bits) stored as follows:

bbbbmmmmllllllll

where bbbb is a four-bit bin number, mmmm is the most significant four bits of the reading, and llllllll is the least significant eight bits of the reading. For instance, a reading of 1000 into bin five would be (in hex): 53E8 since 3E8 is hex for 1000 decimal.

The flags and data read are stored in COMMOM block /FS/.

ROM.MAC

ROM is a collection of the following short miscellaneous subroutines.

Module	Calling Convention	Called By
$INIT	CALL $INIT	WVR

$INIT replaces the FORLIB routine of the same name, which is called automatically at the beginning of every FORTRAN 80 program. $INIT sets the stack pointer. Since the FORLIB version of $INIT assumes both program and data areas are in RAM, it will not set the stack pointer properly for the ROM based WVR software. Therefore the ROM.MAC version of $INIT must be linked before FORLIB is searched. This will prevent the FORLIB version from missetting the stack pointer.

Module	Calling Convention	Called By
MONITR	CALL MONITR	WVR

This is a sample jump to WVRMON, invoked by the `X` command.

Module	Calling Convention	Called By
INIT	CALL INIT	WVR

This initializes the parallel I/O ports on the CPU board and sets up the RTI-1200 A/D board. INIT is called only once, at the beginning of WVR.

Module	Calling Convention	Called By
ICHAN	J = ICHAN(K)	POINT, DSAMP

This is a function call that returns the reading of an A/D input channel in counts, where K is the input channel number (0 to 15).

Module	Calling Convention	Called By
SUBMUX	CALL SUBMUX(K)	WVR, ODATA, DSAMP

This subroutine sets the submultiplexer to a temperature channel, where K = channel number from 0 to 15.

Module	Calling Convention	Called By
DRIVER	???	???

No invocation of this subroutine has been found. It is identified in the source program as an external ENTRY. It may be a leftover from ancient days.

Module	Calling Convention	Called By
SMODE	CALL SMODE(K)	WVR, DSAMP

This subroutine sets the mode of the radiometer to hot load, base load, antenna, or reference load, where K is an integer from 0 to 3.

Module	Calling Convention	Called By
DAC1	CALL DAC1(K)	POINT

This subroutine sets a voltage on D/A output channel one to turn on/off the elevation drive motor. The voltage output will be -10 V for K = 0, 0 V for K = 2048; and 9.9952 V for K = 4095.

Module	Calling Convention	Called By
DAC2	CALL DAC2(K)	POINT

This is the same as DAC1, except for the azimuth drive motor.

Module	Calling Convention	Called By
FDLY	CALL FDLY(K)	WVR, ODTA, DATA1

This causes a software timing loop to delay 16 times K microseconds.

TECHNICAL REPORT STANDARD TITLE PAGE

1. Report No. JPL Publication 85-14	2. Government Accession No.	3. Recipient's Catalog No.
4. Title and Subtitle Water Vapor Radiometry Research and Development Phase Final Report		5. Report Date April 1, 1985 6. Performing Organization Code
7. Author(s) G. M. Resch, M. C. Chavez, N. I. Yamane, K. M. Barbier, and R. C. Chandlee		8. Performing Organization Report No.
9. Performing Organization Name and Address JET PROPULSION LABORATORY California Institute of Technology 4800 Oak Grove Drive Pasadena, California 91109		10. Work Unit No. 11. Contract or Grant No. NAS7-918 13. Type of Report and Period Covered JPL Publication
12. Sponsoring Agency Name and Address NATIONAL AERONAUTICS AND SPACE ADMINISTRATION Washington, D.C. 20546		14. Sponsoring Agency Code FJ-692-40-01-00-01

15. Supplementary Notes

16. Abstract

This report describes the research and development phase for eight dual-channel water vapor radiometers constructed for the Crustal Dynamics Project at the Goddard Space Flight Center, Greenbelt, Maryland, and for the NASA Deep Space Network.

These instruments were developed to demonstrate that the variable path delay imposed on microwave radio transmissions by atmospheric water vapor can be calibrated, particularly as this phenomenon affects very long baseline interferometry measurement systems. Water vapor radiometry technology can also be used in systems that involve moist air meteorology and propagation studies.

17. Key Words (Selected by Author(s))	18. Distribution Statement
Spacecraft Communications, Command, and Tracking Geodesy Meteorology and Climatology Astronomy	Unclassified - Unlimited

19. Security Classif. (of this report)	20. Security Classif. (of this page)	21. No. of Pages	22. Price
Unclassified	Unclassified	131	

JPL 0184 R 9/83